WIND PRESSURES ON FLAT ROOF EDGES AND CORNERS OF LARGE LOW BUILDINGS

Hatem Alrawashdeh

A Thesis
In
The Department
of
Building, Civil and Environmental Engineering

Presented in Partial Fulfillment of the Requirements
for the Degree of Master of Applied Science (Building Engineering)
at
Concordia University
Montréal, Quebec, Canada

September 2015

CONCORDIA UNIVERSITY

School of Graduate Studies

This is to certify that this thesis prepared

By: Hatem Alrawashdeh

Entitled: Wind Pressures on Flat Roof Edges and Corners of Large Low Buildings

and submitted in partial fulfillment the requirements for the degree of

Master of Applied Science (Building Engineering)

complies with the regulations of the University and meets the accepted standards with respect to originality and quality.

Signed by the final Examining Committee:

Dr. R. Zmeureanu	Chair
Dr. L. Kadem	Examiner External (to program)
Dr. K. Galal	Examiner
Dr. T. Stathopoulos	Supervisor

Approved by Dr. Fariborz Haghighat, GPD
Department of Building, Civil and Environmental Engineering

Dr. Amir Asif, Dean
Faculty of Engineering and Computer Science

Date

ABSTRACT

WIND PRESSURES ON FLAT ROOF EDGES AND CORNERS OF LARGE LOW BUILDINGS

Hatem Alrawashdeh

The present wind tunnel study examines the suitability of the current wind provisions in wind codes and standards for the design of roof zones of flat-roofed low-rise buildings with large dimensions. Current wind codes and standards have load provisions dealing with low buildings of common configurations. Large buildings, say 100 m long, have not been considered when these provisions were established. As a result, the interaction between wind and buildings of such geometries should be investigated for the assessment of current wind provisions in terms of their applicability to such configurations.

Nine large low-rise buildings of 5, 7.5 and 10 m high with flat roofs have been tested in a typical open country exposure in the Boundary Layer Wind Tunnel of Concordia University. The models have been tested for wind directions ranging from 0° to 90° at increments of 15°. The buildings have large square plan with equivalent full-scale horizontal dimensions ranging from 60 to 180 m.

Local roof pressure coefficients have been obtained from the wind tunnel measurements. Moreover, area-averaged negative peak pressure coefficients have been established using numerical integration of individual pressure coefficients. The effects of building dimensions on the generated roof pressures have been addressed in this study.

This thesis presents a comparative study based on code provisions and experimental results. The first part compares the application of the current code roof zone systems and the design

wind pressures specified in codes and standards. The second part of the study compares the experimental results with the respective values specified in code/standard provisions in terms of wind pressures and roof zone sizes to assess the suitability of these provisions. These comparisons show significant differences in the patterns of the design pressure coefficients among the current wind codes and standards.

Application of the current provisions of ASCE 7-10 and NBCC 2010 on building geometries of large roofs and low height may lead to considerably conservative and uneconomic roof design. An exception for very long low buildings, as far as the determination of the sizes of roof edge and corner zones is concerned, has been recommended to rectify the deficiency of wind codes and standards for these building geometries.

ACKNOWLEDGMENTS

This work would not have been possible without the support of my family, supervisor and friends.

It has been my privilege and the honor of my academic life to work closely with Dr. Theodore Stathopoulos, I have learned a lot from his knowledge and experience. His frequent insights and patience with me are always appreciated. I am very proud of what we have achieved together.

I would like to thank my family for their encouragement in all of my pursuits to follow my dreams. I am especially grateful to my mother Aida, my father Salem, brothers and sister. Also, I must thank in particular Dr. Khairedin Abdalla at Jordan University of Science and Technology, who has introduced me to Dr. Stathopoulos two years ago.

Finally, I would like to thank my friends and colleagues from Jordan, Greece and Canada for their support. Special thanks are due to Dr. Mohamed Elsharawy for his help with the wind tunnel tests.

Dedicated to

My Beloved Mother, Father, Brothers

and to My Sweet Sister Wafa'

TABLE OF CONTENTS

LIST OF FIGURES

LIST OF TABLES

LIST OF SYMBOLS

A_i	Contributing area to the i^{th} pressure tap
B	Building plan width
C_{dir}, K_d	Directionality factor
C_e, C_r	Terrain factor
C_e^*, C_o	Topographic factor
C_g, G	Gust effect factor
C_p, $C_{p,e}$	External pressure coefficient
$C_{p,A}(t)$	Instantaneous area-averaged pressure coefficients at measurement pressure tap (i)
C_pC_g, GC_p	Peak pressure coefficient
$C_{Pi}(t)$	Instantaneous wind pressure coefficient at pressure tap (i)
C_{seas}	Seasonal factor
Ds	Least horizontal plan dimension
H	Eave height
h	Mean roof height
$I_u(Z)$, I, I_V	Longitudinal turbulence intensity
K_a	Area reduction factor.
$K_{c,e}$	Combination factor for external pressures.
M_d	Directionality factor
K_l	Local pressure factor.
K_p	Porous cladding reduction factor.
M_s	Shielding multiplier.
K_z	Terrain factor
K_{zt}	Topographic factor
L	Building plan length

L_b	Characteristic length of the building
L_u^x	Longitudinal integral length scale
M_t, $M_{z,cat}$	Terrain factor
n	Frequency
N	Number of pressure taps in the specified area
P_i	Wind pressure at instrument tap (i)
P_s	Static pressure at reference location
$\overline{q_z}$	Mean value of the dynamic pressure at reference height
Re_b	Reynolds number
$R_{e,r}$	Roughness Reynolds number
$Re_{r,crit}$	Critical roughness Reynolds number.
$R_u(\tau)$	Auto-covariance function
U_*	Friction velocity
$\overline{V}$	Mean wind speed
V'	Fluctuating component of wind speed
V	Basic wind speed
$V_{b,o}$	Basic wind velocity (10 minutes mean wind velocity at 10 m above ground level in open country terrain)
$\overline{V}_G$	Wind speed at gradient height
V_H	Flow velocity at roof height
V_R	Regional 3 seconds gust wind speed
z_o	Roughness length
Z	Edge/corner zone size
Z_G	Gradient height

Z_{ref}	Reference height above the wind tunnel floor
α_o	Roof slope
α	Power law exponent
λ_l	Length scale
λ_V	Velocity scale
λ_T	Time scale
λ_f	Frequency scale
μ	Dynamic viscosity
ν	Kinematic viscosity
ρ	Air density
σ	Standard deviation

CHAPTER 1

INTRODUCTION

1.1 General

Low-rise buildings form the larger percentage of buildings on the earth. They are in the lower region of atmospheric boundary layer, where both the speed gradients and the atmospheric turbulence are stronger. Therefore, wind loads on surfaces of low-rise buildings are highly fluctuating. Low-rise buildings widely vary in shape and geometry. For these reasons wind loads on the surfaces of low-rise buildings are difficult to determine. On the other hand, low-rise buildings have low natural frequencies causing negligent dynamic response (Cook, 1990).

1.2 Wind Damage

Wind is a part of our life! Wind is considered a very significant source of clean energy and is beneficial in a lot of respects. On the other hand, wind is a natural hazard to mankind. In case of accidents, damages to buildings and structures can be very costly. That is why civil and building engineers are concerned about the wind. It is also recognized that the kind of structures exposed to high wind risks are low-rise non-engineered residential buildings designed and constructed in traditional ways without resorting to qualified architects/engineers. Adequate treatment of wind effects in the design is essential to achieve safe and economic structures. Therefore, understanding the nature of wind-induced pressures on buildings will help the engineers design safer and more economical buildings.

The form of the structural failure and collapse due to wind loads is gradually progressing. Building cladding and components are the first phase on the wind load path. Wind pressure is applied to the external cladding of the buildings and then it is transferred to substrates, secondary components, main structural frames and foundations. Thus, the breaking down starts with local surface damage and finishes with reaching total collapse. Therefore, adequate cladding and component design is critical to minimize wind-induced damage. Small damages may evolve into larger scale, run to main frames and cause more severe damage. This "coherent phenomenon" in damage progress is a special feature of wind-induced building failure.

Depending on the approach flow properties such as the velocity profile, turbulence intensity and length scale; the variation in building size, roof geometry, etc., damage to roofs of buildings may occur either directly or indirectly. In most cases, roof damage is caused by local high suctions and large pressure fluctuations over the perimeter areas of the roof. Because of these local failures, the wind is allowed to enter under the roof cladding, and then the underneath pressure together with the roof surface suction may create significant lift forces. Therefore, local roof damage may lead to total roof destruction. Moreover, the broken parts of the destructed buildings that are less well-fixed may be carried away in strong wind events such as hurricanes, become windborne debris and strike downstream buildings causing additional building damage and destruction, causing a so-called "damage chain".

Assessment of wind-induced damage to structures revealed some consistent patterns (Minor and Mehta, 1979):

1. Structures failed, principally, because of wind-induced forces acting on critical building components;

2. Non-engineered and marginally engineered structures were susceptible to failures at relatively low wind speeds;

3. Small increase in the degree of engineering attention, using new wind engineering technology, could produce large dividends in increasing the wind resistance of structures; and

4. The geometry of a structure and its orientation were important determinants of wind resistance.

1.3 Thesis Motivation

There are many issues to be addressed by researchers and engineers in the wind engineering field to provide guidelines for secure and economic design. Over the past few decades, a lot of wind tunnel and full-scale experiments have been conducted to investigate the wind pressures of low-rise buildings. But until recently, most of them have been performed to model simple shapes of low-rise buildings with common, relatively small, dimensions.

Low-rise buildings have limitless possibilities of geometries that include different heights, roof slopes and horizontal plan dimensions. With the urban and industrial activity growth, low-rise buildings are also used for commercial and industrial purposes like malls and shopping centers with large roof sizes. Generally, roofs of large buildings are commonly flat or nearly flat. Figure 1.1 presents an example of an actual commercial building, the Mushroom warehouse, located in Southeastern Pennsylvania, United States. This barn is supported by a truss system of 1:12 pitch and has plan dimensions of 200 feet by 500 feet. The wall height is 16 feet at the eave and 20 feet at the aisle down the center of the building. Such structures may be indeed penalized by applying roof zone provisions currently in the international wind codes and standards. Indeed, specific guidelines for wind design of buildings with large roofs are not provided since wind code and standard provisions were produced by testing regular-shaped models with common, relatively small, dimensions. This lack of guidelines from an economic standpoint may lead to conservative design.

Figure 1.1: Large Low-rise buildings: The Mushroom warehouse, located in Southeastern Pennsylvania, U.S.A (http://www.constructionmagnet.com/rural-builder/post-frame-phenom-for-fungi).

Furthermore, a similar situation exists in retrofitting or refurbishing buildings. For example, extension of an existing building would modify the size of the roof zones (corner, edge and interior) even for the old portion of the building - see Figure 1.2. The question then arises whether the requirements of the wind codes and standards are really justified when building dimensions are increased.

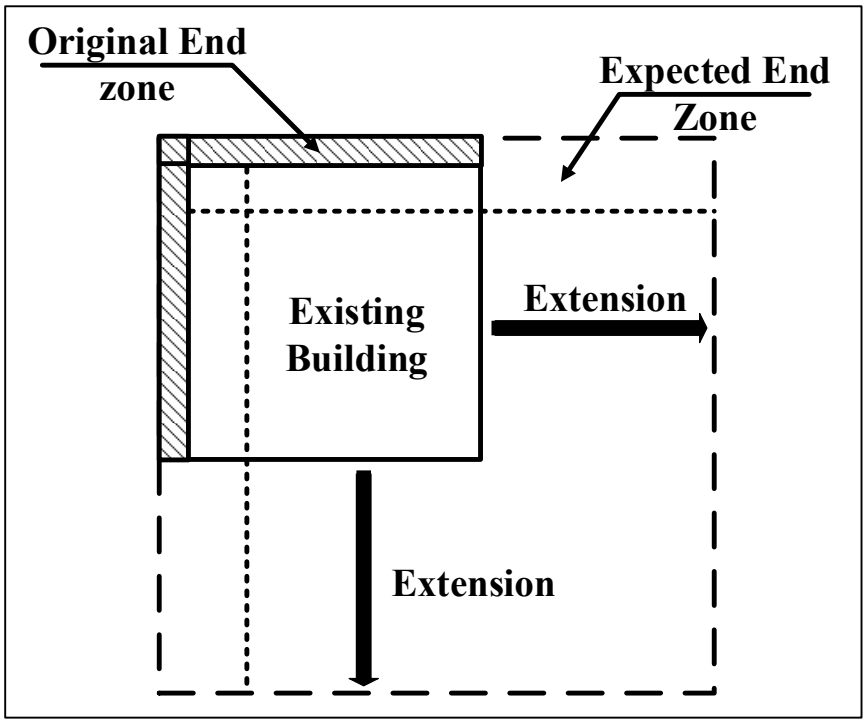

Figure 1.2: Depicting fanciful for an extension to an existing building.

1.4 Scope and Objectives

As previously mentioned, current wind provisions in the various national wind standards and codes of practice deal with regular-shaped buildings with common, relatively small, dimensions. Very long buildings have not been considered when these provisions were produced. As a result, there has been an urgent need to carry out a detailed research study

to describe the interaction between the wind and these kind of building geometries and to assess the efficiency of the current building code/standard provisions as to their applicability for very large buildings.

The general objective of this experimental research is to provide the necessary information about the characteristics of the fluctuating wind pressures generated on very large flat roofs compared with their heights. The scope of the present study is to compare the results with guidelines proposed by four international standards and codes of practice, namely: the American Society of Civil Engineers Standard (ASCE 7, 2010), the National Building Code of Canada (NBCC, 2010), the European Standard (EN 1991-1-4:2005) and Australian/New Zealand Standard (AS-NZS 1170-2, 2011) and provide possible improved provisions in this regard. Specific objectives of this study include the following:

1. To compare the design criteria recommended by four international codes and standards to show the differences between the current wind load provisions in terms of roof zones and design wind loads;

2. To investigate edge and corner zones of large flat roofs having horizontal plan dimensions greater than 10 times their building height;

3. To examine wind-induced suctions on edges and corners of low-rise buildings with large horizontal dimensions; including the effect of the building height and plan dimensions on the local and area-averaged pressure coefficients generated on flat roofs with large dimensions;

4. To assess the current building codes/standards provisions as to their applicability for very large buildings.

These objectives have been achieved through wind pressure measurements on roofs of tested buildings in the Boundary Layer Wind Tunnel Laboratory of Concordia University.

Nine flat roofs of large dimensions (60 m, 120 m and 180 m) have been tested for several wind directions (0°,15°, 30°, 45°, 60°, 75° and 90°). Particularly, the results of this study are expected to have a significant influence on construction cost of large roofs.

1.5 Thesis Outline

The following chapter provides a brief introduction to wind loads and building aerodynamics. It discusses the previous work in this area and presents the justification of the need for the present research.

Chapter 3 presents the description of the facilities, construction of the models, laboratory instruments and equipment. Detailed description of the model configurations, characteristics of the simulated upstream flow and data acquisition and processing are also provided. Comparisons with previous data are carried out for validation purposes.

In Chapter 4, the description of the provisions regarding flat roofs of low-rise buildings utilizing four international codes and standards is presented. Some historical issues related to the development of the North American codes and standards are discussed. In particular, the practical guidelines for creating roof zone sizes and the external design wind loads used for low-rise buildings with large roofs are reviewed. The resulted roof systems according to these codes/standards are compared and discussed.

Chapter 5 presents the findings of the current research in terms of dimensionless pressure coefficients at first. This includes distributions of local pressure coefficients on the roofs presented in terms of contours of pressure coefficients, variation with wind directions and with relative distance from the roof windward edge. The effects of building dimensions and the wind direction on the generated roof wind pressures are examined in this chapter. Also, area-averaged pressure coefficients measured are presented.

In Chapter 6, the suitability of the current wind codes/standards provisions for large roofs is examined. Detailed comparisons of the present results with the respective code design values of the current codes and standards considered in this study are conducted.

Chapter 7 argues that the current wind provisions of ASCE 7-10 and NBCC 2010 overestimate the size of the roof zones of flat low-rise buildings with large dimensions. Certain modifications seem to be necessary to improve the reliability of the current code guidelines to create the size of the roof zones with regards to large roofs. Consequently, suggestions to the current provisions are made and assessed from the efficiency point of view.

Finally, conclusions and suggestions for further research are provided in Chapter 8.

CHAPTER 2

LITERATURE REVIEW

There have been a lot of research studies conducted to measure the wind effects on a variety of low-rise buildings, either in wind tunnel or in full-scale. The review presented in this chapter covers information in the following topics:

Review of wind engineering basics, roof wind loads and previous work in area of roof wind loads of low-rise building.

2.1 Wind Engineering Basics

Wind, in climatology, is the movement of air on large-scale relative to the surface of the earth; it generates pressures on building surfaces. The main reason for air movement is the temperature gradient of the atmosphere due to solar radiation differences on the earth's surface. Consequently, the temperature differences produce density differences and then pressure gradient to drive the airflow on large-scale atmospheric circulations. Furthermore, seasonal effects, geographical effects and rotation of earth are factors contributing to additional variations to the atmospheric circulations. As wind travels around and over the building, it accelerates and produces outward-acting pressures on all surfaces except the windward surface.

Wind engineering is best described as the rational treatment of the interaction between wind in the atmospheric boundary layer and man and his works on the surface of earth (Cermak, 1975). The main sources for wind engineering knowledge are fluid mechanics, meteorology, structural mechanics and physiology. Whereas estimation of wind pressures

on building surfaces is obtained through the numerical and analytical method, full-scale experiments and extensively through wind tunnel experiments. The latest method is frequently done by boundary layer wind tunnels simulating atmospheric flows.

2.1.1 The Atmospheric Boundary Layer

It seems that the concept of boundary layer in fluid flows is ascribed to Froude. Through a series of laboratory towing experiments have been carried out by Froude to study the friction resistance of a thin flat plate when towed in still water in the early 1870s. The "boundary layer" as term was probably first introduced into the literature by Prandtl in his 1905 paper: "While dealing with a flow, the latter is divided into two parts interacting on each other; on one side we have the "free fluid", which is dealt with as if it was frictionless, according to the Helmholtz vortex theorems, and on the other side the transition layers near the solid walls. The motion of these layers is regulated by the free fluid, but they for their part give to the free motion its characteristic feature by the emission vortex sheets" (Prandtl, 1905).

The useful definition identifies the boundary layer as the layer of air directly above the earth's surface in which the effects of the surface (friction, heating and cooling) are felt directly on time scales less than a day, and in which significant fluxes of momentum, heat or matter are carried by turbulence motions on a scale of the order of the depth of boundary layer or less (Garratt, 1994). According to the preceding definition, the boundary layer is the airstream layer that influenced by the ground friction from terrain roughness, i.e. buildings, trees, etc., and the blockage effects from the topography on the surface of the earth. This will lead to a reduction in wind speed and increase in turbulence when the height becomes close to surface of the earth within the boundary layer.

Figure 2.1 represents a diagrammatic description of simplified atmospheric boundary layer. The structure of the boundary layer has an inner region (boundary layer wind) and an outer region (gradient wind). The wind speed at the ground surface, at which the height is zero,

is assumed to be zero. Within the inner region, wind speed increases with increasing height from the ground surface until a certain point where the speed reaches the maximum. Higher than this point, the movement of airstream is no longer affected by surface roughness. Thus, the wind speed within the outer region maintains a constant value called gradient wind speed, V_G. The height at this point is so-called gradient height, Z_G. Z_G is used to represent the thickness of the boundary layer (inner region).

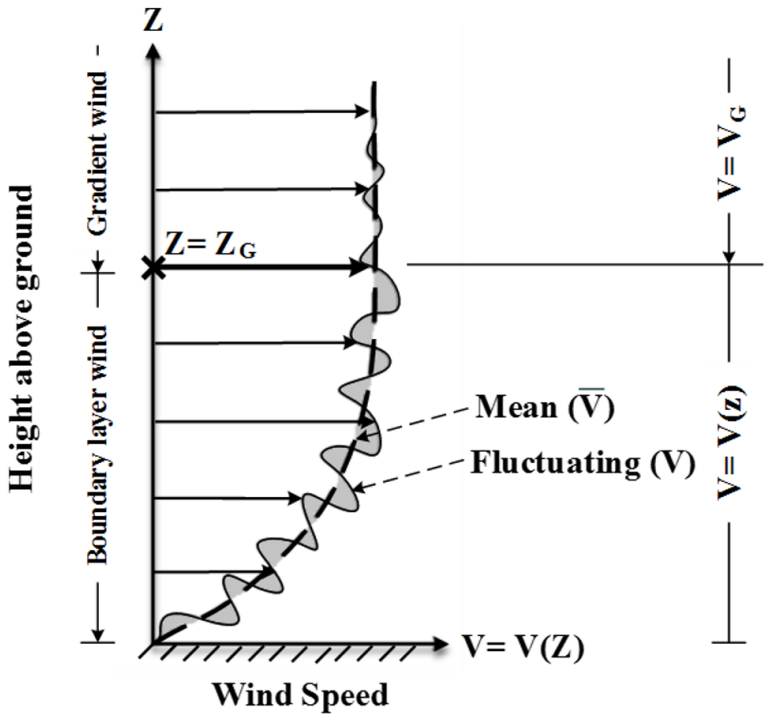

Figure 2.1: Instantaneous wind velocity profile in atmospheric boundary layer.

As shown in Figure 2.1, the wind speed (V) at certain height is equal to a mean speed ($\bar{V}$) plus a fluctuating component. The vertical distribution of horizontal mean wind speed of the boundary layer flow $\bar{V}(Z)$ can be approximated by a semi-empirical relationship called logarithm profile, while the wind speed of the boundary layer flow $V(Z)$ can be expressed

by the power law profile. The logarithmic profile and power profile are presented in the equations 2.1 and 2.2, respectively.

$$\overline{V}(Z) = \frac{1}{k} \times u^* \times \ln\left(\frac{Z}{Z_o}\right) \tag{2.1}$$

$$\frac{V(Z)}{V_G} = \left(\frac{Z}{Z_G}\right)^{\alpha} \tag{2.2}$$

Because of simplicity the power law is often used in the engineering applications and in some building codes/standards. The logarithmic law is based on the physics of the boundary layer and, therefore, the logarithmic law is used by both engineers and meteorologists.

The surface roughness is one of the most conspicuous factors that affect the variation of wind speed within atmospheric boundary layer with height. When the wind travels over different terrain categories it takes a long distance - called fetch length - to fully develop the speed profile of those terrain categories. The wind speed slows down at the surfaces of higher roughness and then the wind profile rises higher; thus, for rougher terrains the gradient heights are higher than those of smother surfaces. The gradient wind speed does not change and remains firm at all terrains. This kind of wind speed equilibrium can be illustrated using the power law (Equation 2.2). The equilibrium of the velocities at different terrains can be expressed as follows:

$$\frac{V_2(Z)}{V_1(Z)} = \left(\frac{Z_g}{Z}\right)^{\alpha_2 - \alpha_1} \tag{2.3}$$

In which Z_g and α are mainly functions of ground surface roughness. Suggested values for these characteristic parameters of the atmospheric boundary layer in codes and standards for different locations can be found in Table 2.1.

Table 2.1: Characteristic parameters in power law wind profile, power law exponent, terrain roughness and gradient height (Geurts and Bentum, 2007)

Exposure category and description	Power law exponent (α)	Roughness length (Z_o), m	Gradient height (Z_g), m
1: Open sea, ice, tundra, desert	0.11	0.001	250
2: Open country with low scrub or scattered trees	0.15	0.03	300
3: Suburban areas, small towns, well wooded areas	0.25	0.3	400
4: Numerous tall buildings, city centers, well developed industrial areas	0.36	3	500

Wind is characterized as randomly varying dynamic phenomenon. If the instantaneous velocity of the wind is recorded at a point versus time on a chart, the result will look like that in Figure 2.2. As is evident from the figure, the wind is also unsteady, thus the wind speed (V) at certain time is equal to a mean speed component ($\overline{V}$) plus a fluctuating component (V'), the latter is known as turbulence and responsible for creating gustiness. Structural engineers are predominantly concerned with the peak values of wind speed rather than the mean values.

Mean wind speed is the average of wind speed records over a certain period. In order to keep mean wind speed relatively stable over the record duration, an averaging period between 10 minutes and 1 hour is recommended. The influence of averaging time on mean wind speed is provided by a relation developed by Durst (1960). The Durst curve shows the comparison of wind speeds averaged over a time ($0\ \text{sec} \leq t \leq 3600\ \text{sec}$) and wind speeds averaged over 3600-seconds (one hour) of the same wind storm. According to that the relation between the length of the averaging interval and its corresponding maximum mean speed is inverse. The Durst Curve is presented in Appendix A.

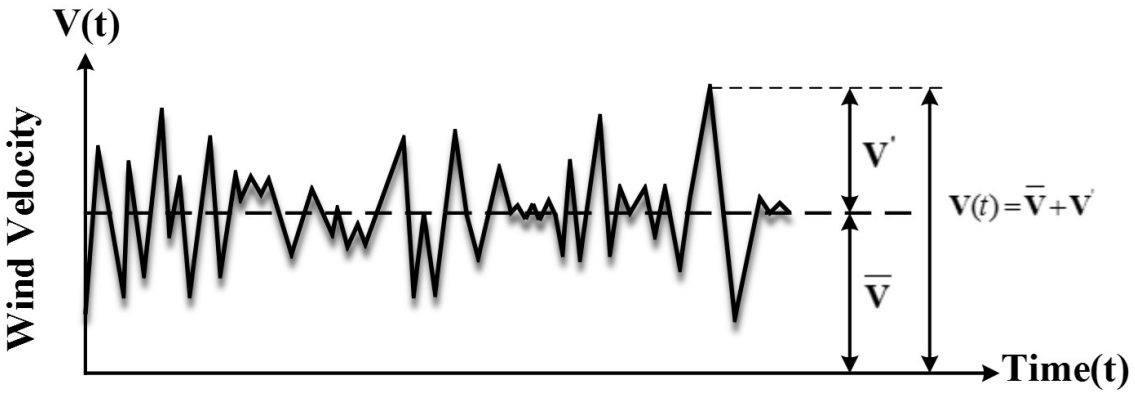

Figure 2.2: Variation of wind velocity with time for min period.

The characteristics of atmospheric turbulence may be described by different parameters; such as turbulence intensity, gust size (integral length scale) and wind-energy spectrum. These parameters become an important consideration for wind-sensitive flexible structures.

The longitudinal turbulence intensity (relative intensity of turbulence) at a point of elevation (Z) is defined as the ratio of root mean square (rms) of the longitudinal wind speed fluctuations to mean speed. Mathematically I_u is defined as follows:

$$I_u(Z) = \frac{\sqrt{\bar{u}^2(z,t)}}{\bar{V}(Z)} \tag{2.4}$$

Where:

$\sqrt{\bar{u}^2(z,t)}$ = Root mean square of the fluctuating velocity (σ).

$\bar{V}(Z)$ = Mean wind speed at elevation Z.

Turbulence intensity increases with roughness of the ground surface and decreases with height. It also varies with averaging time used in recording the mean velocity, thus larger values of relative intensity are yielded from longer durations of averaging time.

The integral length scale is used to measure the average longitudinal size of large eddies in the flow. The flow velocity at any instant can be decomposed into three components (longitudinal, lateral and vertical). Furthermore, each component can be decomposed into a mean and fluctuating component. Therefore, nine integral scales of turbulence are associated with the flow. The values of transverse and vertical integral length scales (L_u^y and L_u^z) are small compared to the dimensions of a panel normal to the mean wind. This may indicate that the effect of the longitudinal velocity fluctuations is the most relevant to the structural design. The longitudinal integral length scale is defined as follows:

$$L_u^x = \frac{1}{\sqrt{\bar{V}^2}} \int_0^\infty R_u(\tau) d\tau \tag{2.5}$$

Where $R_u(\tau)$ is the auto-covariance function of the fluctuation V(z,t).

The wind turbulence spectrum represents the total energy generated by eddies. The most common models of the longitudinal spectra of turbulence used for structural design are the following:

The Davenport spectrum model:

$$\frac{nS(z,n)}{V_*^2} = 4\frac{X^2}{(1+X^2)^{4/3}} \tag{2.6}$$

Where: $X = \frac{1200 \times n}{U_{10}}$

n = frequency in Hertz, and U_{10}= mean wind speed in meters per second.

The Von Karman spectrum model:

$$\frac{nS(n)}{V_*^2} = 4\frac{\beta\frac{nL_u^x}{U}}{\left(1+70.8\left(\frac{nL_u^x}{V}\right)^2\right)^{5/6}} \tag{2.7}$$

The Harris spectrum model:

$$\frac{nS(z,n)}{V_*^2} = 4\frac{X}{(2+X^2)^{5/6}} \tag{2.8}$$

Where: $X = \frac{1800\times n}{U_{10}}$

These spectrum models do not reflect the variation of the spectrum with height.

2.1.2 Boundary Layer Wind Tunnel

Experimental approaches, by physical simulation, are the mainstay of the wind engineering development. However, persistent efforts have been made on the development and refinement of theoretical approaches. The early wind tunnel tests were carried out in aeronautical tunnels, in which the flow was uniform. Significant changes occurred when Jensen (1958) carried out experiments on building models and observed that, "the current model test for phenomena in the wind must be carried out in a turbulent boundary layer and the model law requires the boundary layer to be scaled as regards the velocity profile." Since that time the development of the boundary layer wind tunnels began its upward trajectory.

The current wind tunnels are considered as an effective tool to aid in structural design against wind by means of physical model tests in simulated atmospheric boundary layer.

The purpose of the current wind tunnel tests is to provide the designers with accurate information and data on wind patterns, wind loads and wind induced structural vibration.

At present, wind tunnels are available in two main types, open-circuit and close-circuit. In the first type, the air is expelled, whereas in the second type the air is re-circulated. The wind-tunnel simulations for atmospheric boundary layer of natural flow must concentrate on the following basic characteristics: the velocity profile, turbulence intensity and power spectra of turbulence. Thus, the wind tunnel must be sufficiently long to generate a thick vertical boundary layer. Also, it must have a proper working section with sufficient height to provide convenient vertical space, far from the ceiling of the tunnel, to the generated boundary layer. Wind tunnel must be constructed with a proper width to be able to house topographic features and the neighboring structures.

In order to maintain aerodynamic pressure coefficients on cladding of sharp-edged buildings by boundary layer wind tunnel experiments consistent with the pressure coefficients on surface of full-scale structure: length, time and velocity scales of the wind tunnel must be consistent with respective atmospheric conditions. The scaling relationships for wind tunnel experiments are defined as follows:

$$\lambda_l = \frac{L_{FS}}{L_{WT}} \tag{2.9}$$

$$\lambda_V = \frac{V_{FS}}{V_{WT}} \tag{2.10}$$

$$\lambda_T = \frac{T_{FS}}{T_{WT}} = \frac{\lambda_V}{\lambda_l} \tag{2.11}$$

Where λ_l= length scale; λ_V= velocity scale and λ_T = time scale (whose reciprocal is the frequency scale, λ_f). The subscripts FS and WT refer respectively to full scale building and wind tunnel model. To simulate the natural wind successfully, the above ratios must be constant from full-scale to model scale as follows:

$$\left(\frac{\lambda_l}{\lambda_V \lambda_T}\right)_{WT} = \left(\frac{\lambda_l}{\lambda_V \lambda_T}\right)_{FS} \quad (2.12)$$

Furthermore, another issue related to wind tunnel simulation requirements is similarity of Reynolds number (ratio of inertial forces to viscous forces, $Re_b = \frac{V_h L_b}{\nu}$, where V_h is the mean flow velocity, L_b characteristic length of the building and ν is the kinematic viscosity). The scale reduction commonly used result in model Reynolds numbers three to four orders of magnitude smaller than found in the atmosphere (Snyder, 1981). Accomplishment of flow field in wind tunnels similar to that in full-scale is rather difficult and impractical. For example, to satisfy Reynolds number similarity requirement for a model installed in wind tunnel at length scale of $\lambda_l = 1{:}100$, a velocity scale on order of 1:100 is required, thus the mean wind speed in the wind tunnel must be 100 times the full-scale velocity, which is very high and hard to implement.

Similarity of Reynolds number is necessary for a body of curved surface. This is due to the fact the location of flow separation depends first and foremost on Reynolds number. For a cylindrical model of circular section the separation happens when the inertial forces induced on the surface of the model become sufficient to decelerate the fluid particles of the flow until reaching point where the flow becomes reversed.

However, in case of sharp-edged structures immersed in boundary layer flow, the flow separation occurs mainly as a result of flow-edge interaction. Therefore, the similarity of Reynolds number is less significant here. “Sharp corners tend to cause immediate flow separation, independently of the Reynolds number of the flow. For this reason it is generally assumed that if the flow is adequately simulated, pressures on rectangular and other sharp-cornered structures are adequately reproduced in the wind tunnel” (Simiu and Scanlan, 1996). Consequently, the similarity of model and full-scale Reynolds number is not a serious constraint and can be relaxed; this applies well to bodies with sharp edges in turbulent flow.

Some researchers have identified key issues for Reynolds number similarity or Reynolds number independence as guarantee for neglecting Reynolds number effects. Snyder (1981) suggested an index to realize Reynolds number independence called roughness Reynolds number ($R_{e,r} = \frac{U_* Z_o}{\nu}$, where U_* is the friction velocity and z_o is the roughness length), such that a flow is considered aerodynamically rough for $R_{e,r}$ larger than 2.5;–flow over aerodynamically rough surface can be characterized as having Reynolds number independence. Neff and Meroney (1982) recommended that laboratory wind speed should be high enough, such that obstacle Reynolds numbers exceed 11,000 for sharp-edged objects or 100,000 for round objects.

So far, wind tunnel testing for buildings and other structures (ASCE-7, 2010 and ASCE-49, 2012) sets criteria to accurately simulate the wind tunnel experimental studies. These standards provide minimum requirement for Reynolds number of the model simulation in wind tunnel to neglect the variation in pressure distributions on account of the expected distortion in the flow; accordingly, model Reynolds number shall be more than 11,000 ($Re_b = \frac{V_h L_b}{\nu} \geq 11{,}000$). Also, European standard (EN 1991-1-4:2005) defines the Reynolds number of the model based on the width of the structure and the mean wind velocity at building height (Geurts and Bentum, 2007).

It is well known that the characteristic length for cylindrical model immersed in wind flow is the cross section diameter (D). Rectangular models can be characterized at least by three dimensions. Thus, the overall representative dimension of the model could be length, width or height of the building. In case of rectangular model immersed in atmospheric boundary layer the choice is still indefinite.

In addition to the similarity parameters mentioned above, blockage ratio (ratio of the cross-sectional area of the model(s) over the wind tunnel test section area) approximately less than 5% should be considered during wind tunnel experiments.

2.1.3 Wind Pressure Coefficients

External wind loads exerted on building cladding depend upon the flow pattern around and over the building that developed through the wind flow-building interaction. This interaction in a complex manner depends on geometry of the building, building height, roof shape and dimensions (breadth and depth) and the approaching wind characteristics. The civil engineering structures are space bodies with limitless shapes and geometries creating very complex flow patterns, and therefore, a variety of wind loads. In particular, the assessment of wind-induced loads to low-rise buildings is difficult due to many factors (Holmes, 2001):

1. They are usually immersed within the layer of aerodynamic roughness on the earth's surface, where the turbulence intensities are high, and interference and shelter effects are important, but difficult to quantify;

2. Roof loadings, with all the variations due to changes in geometry, are of critical importance for low-rise buildings. The highest wind loadings on the surface of a low-rise structure are generally the suctions on the roof, and many structural failures are initiated there;

3. Low-rise buildings often have a single internal space, and internal pressures can be very significant, especially when a dominant opening occurs in a windward wall. The magnitude of internal pressure peaks, and their correlation with peaks in external pressure, must be assessed.

It is useful and easier to study the wind-building interactions in term of a dimensionless number normalized by velocity. Surface pressure will offer greater flexibility than velocity information such as expressing the measurement results as resultant forces and moments. Moreover, the surface pressure can be expressed in the form of a non-dimensional pressure coefficient.

The relation between the pressure, p, and velocity, V, in atmospheric and wind tunnel flows is widely governed by Bernoulli's equation. However, the form of Bernoulli's equation presented in (2.13) is valid for non-viscous ($\mu = 0$), steady and irrotational flow and the flow around buildings is turbulent.

$$P + \frac{1}{2}\rho V^2 = \text{constant} \tag{2.13}$$

in which this expression remains constant along the same stream line. V represents the velocity on the streamline outside the boundary layer that formed on the body surface where the Bernoulli's equation is only valid. In order to calculate the local pressure, the atmospheric pressure (P_o) will be used as a reference pressure.

$P + \frac{1}{2}\rho V^2 = P_o + \frac{1}{2}\rho {V_G}^2$, where V_G is the free stream flow velocity, hence:

$$P - P_o = \frac{1}{2}\rho\left({V_G}^2 - V^2\right) \tag{2.14}$$

Therefore, the pressure coefficient is generally expressed as:

$$C_p = \frac{P - P_o}{\frac{1}{2}\rho {V_G}^2} \tag{2.15}$$

Also it can be expressed as:

$$C_p = \frac{\frac{1}{2}\rho_a\left({V_G}^2 - V^2\right)}{\frac{1}{2}\rho {V_G}^2} = 1 - \left(\frac{V}{V_G}\right)^2 \tag{2.16}$$

where:

$\frac{1}{2}\rho {V_G}^2$ = dynamic pressure.

ρ= air density.

In wind tunnel tests, the velocity (V_G) is measured usually by a Pitot tube. This velocity is zero at stagnation point. According to equation 2.16, the mean pressure coefficient will be the maximum at the stagnation point and equal to +1. At the region around the point of the interaction wind will be accelerated $V > V_G$ and therefore C_p values will be negative with no limit.

Peak, mean and RMS pressure coefficients are defined as:

$$C_p(\text{peak pressure coefficient}) = GC_p = \frac{P_{peak} - P_o}{\frac{1}{2}\rho {V_G}^2} \quad (2.17)$$

$$C_p(\text{mean pressure coefficient}) = \frac{P_{mean} - P_o}{\frac{1}{2}\rho {V_G}^2} \quad (2.18)$$

$$C_p(\text{root mean square, rms}) = \frac{P_{rms} - P_o}{\frac{1}{2}\rho {V_G}^2} \quad (2.19)$$

2.2 Wind Loads on Roofs of Low-Rise Buildings

In wind engineering, buildings design against wind loading requires precise evaluation of local and overall wind effects. Overall wind-loading effects govern wind forces on relatively large portions of a structure, for example portion of a roof supported by a single truss. Local wind loading effects govern wind forces acting on small areas like components and cladding (i.e. fasteners or individual windows). This thesis will concentrate on wind loading on flat roofs of low-rise building.

2.2.1. Wind Flow Patterns on Roofs of Low-Rise Buildings

Large magnitude of fluctuating negative pressures on the roof, which are working like suction forces to lift the roof cladding, are generated when wind passes over the roof. As the wind moves around the sharp edge of the obstruction, it will be separated into two distinct regions, named as outer region and wake region, separated by a layer of intense shear, called shear layer. Shear layer is developed in the vicinity of the separation point where the flow velocity and the turbulence are very high.

The wind flow discussed here is idealized but it is very complex in reality. The wind flow over and around an object depends upon the characteristics of wind speed profile (i.e. wind speed and turbulence) and the shape of the building. Based on that, interaction of the wind with buildings will vary. Therefore, the generated wind load distribution on the building roofs will change. The impact of building configuration i.e. roof slope and building dimensions on the flow patterns has been summarized in Figure 2.3, which presents the wind flow patterns over roofs of different geometries (modified from Evans, 1957):

1. Roof pitch is very important and critical consideration should be given in roofing systems. In general, as the roof pitch increases, the wind flow will be pushed up even further and consequently the length and height of low-pressure zone will be extended. Therefore, as the slope is reduced further and further, higher local sections could be developed near the edges.

2. Almost similar wind patterns above the building occur in case of increasing the building height, while the length of the wake region is directly proportional to the building's height. See diagrams in the right set of Figure 2.3.

3. Increasing building width shows similar wind patterns over narrow and wide roofs - see the two diagrams in the upper set - while the length of the wake region increases with increasing width. Also, when the roof is long, the probability of the flow to be sucked back down and re-attach on roof surface increases.

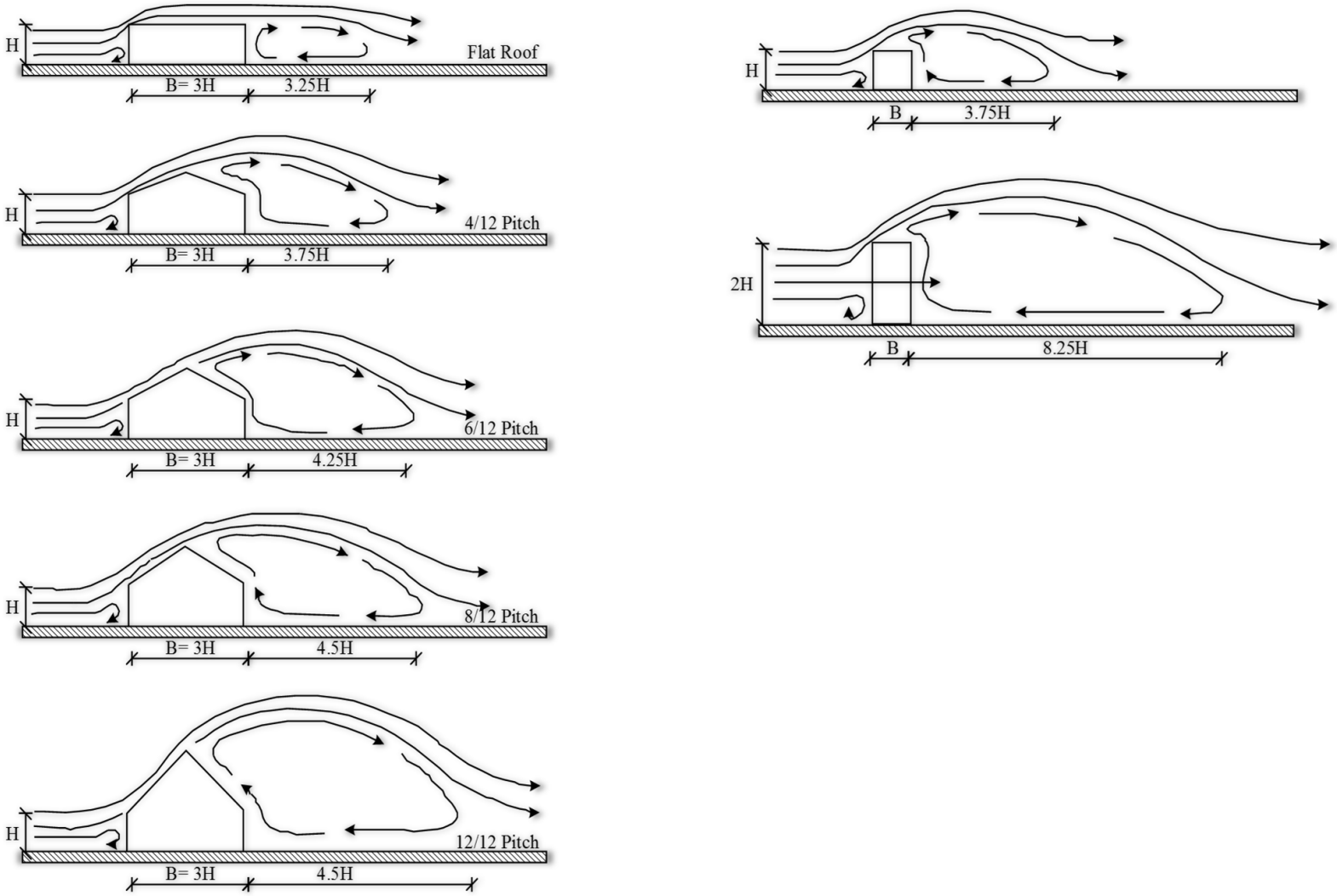

Figure 2.3: Wind flow patterns created over different building configurations (modified from Evans, 1957).

2.2.2. External Pressure Distribution on the Roofs

As discussed previously, the magnitudes of the pressures are proportional to the square of the wind speed (according to Bernoulli's equation), and for most sharp-edged buildings the distribution of pressures does not change with wind speed. Since the pressure distributions are normalized by the stagnation pressure $\left(\frac{1}{2}\rho {V_G}^2\right)$ in order to express them independent of wind speed, to obtain the actual wind pressure distribution, the stagnation pressure is multiplied by dimensionless pressure coefficients derived from full-scale or wind tunnel tests.

Uplift roof pressures are considered one of the most destructive forces generated on building cladding by wind. High suction pressures occur on the perimeter areas of the roofs along the leading edges with extremes in certain sections. Positive wind pressure, i.e. downward pressure may also occur on roofs of buildings but this is relatively small, unless it is combined with snow loads. The distributions of the wind pressures on the building surfaces are affected by the turbulence intensity of the oncoming flow.

2.3 Description of Previous Work

Over the past few decades a quantum leap on wind pressures of low-rise buildings has been realized through a series of comprehensive studies. This started by pioneering comprehensive research in the mid-seventies (Davenport et al 1977, 1978) and continued for several years. This research investigated various geometries of low-rise buildings throughout wind tunnel tests, where the importance of the boundary layer flow and the effect of turbulence were included. Also, the study introduced several techniques to measure and codify the results of the wind-tunnel tests such as the pneumatic-averaging method (Surry and Stathopoulos, 1978) to estimate instantaneous area-averaged pressure coefficients. The results of this pioneering research have formed the backbone of the NBCC and ASCE 7 wind provisions (wind loads for components and cladding and MWFRS-envelope method). Detailed information concerning the development of main

wind load resisting system (MWFRS) and components and cladding loads of ASCE 7-10 and NBCC 2010 is provided by Shoemaker (2014).

A number of wind-engineering investigators have also presented wind measurement results in the form of wind loads and reviews for low-rise buildings. Probably the most quoted examples for reviews of wind load on low-rise buildings during the last four decades are Stathopoulos (1984-B); Holmes (1993); Krishna (1995); Kasperski (1996); Stathopoulos et al (1996); Uematsu and Isyumov (1999); Ho et al (2005); and St. Pierre et al (2005).

Stathopoulos (1979) carried out a series of experimental studies on low-rise buildings with different dimensions, heights, roof slopes and upstream exposures. Four roof slopes, of (0^o), 1:12 (4.8^o), 4:12 (18.4^o) and 12:12 (45^o), were considered for tests. So various wind tunnel models were taken into account to evaluate the influence of different parameters. The work of Stathopoulos (1979) has provided a sufficient description for the wind loads on low-rise buildings. Subsequent codification work, to extend the experimental results of Stathopoulos (1979), was made by Stathopoulos et al (1985). The current NBCC and ASCE-7 wind provisions were primarily built to reflect the results of this study in a simplified format.

Stathopoulos et al (1996) measured experimentally the local and area-averaged wind pressures on mono-sloped roofs in a simulated atmospheric boundary layer for a variety of models and wind directions. They discussed the effects of the height (3.6 - 12.2 m), width (12.2 - 24.4 m), roof slope (1:12 - 4:12), model scaling and the width and the roof pitch on the generated wind pressures. They found that both the mean and the instantaneous peak pressures were higher than those for buildings with gabled roofs, especially on roof corners and narrow buildings of smaller plan width.

Krishna (1995), in his review to wind loads on low-rise buildings, compared mean pressure coefficients from various codes of practice on a gabled roof building with a roof pitch of 30^o, height to width ratio less than 0.5 and length to width ratio in the range of 1.5 to 4. It

was observed that the results differ from one code to another. This variation is attributed to differences in the method of data acquisition, technological capabilities and the accuracy of the experiments.

Holmes (1986) investigated the wind pressures on walls and roofs of gable-roofed of tropical houses experimentally in wind tunnels. The effects of the elevation of the models above the ground, the roof pitch and wind directions on the external pressure coefficients were considered in this study. Results showed that for the same roof pitch, the high set (elevated) houses performed worse than the low sets ones. On the windward side of the roof, 15^o pitch recorded all negative pressure coefficients while 20^o had near zero and 30^o almost zero. In addition, the magnitude of the pressure coefficients on downwind half of the roof was more significant for 15^o and almost the same for 20^o and 30^o. The reason for this was that the flow did not reattach after the second separation at the ridge. Also, results showed that the effect of elevation is to increase the external wind pressures significantly. The roof pitch has large effects on the roof pressures when there is a significant wind component normal to the ridge.

Over the past years wind load on the interior areas of flat roofs of low-rise buildings has been intensely investigated by wind tunnel and full-scale experiments. Gerhardt et al (1992) studied the influence of relative building height (eave height/width, H/B) on the pressure distribution over flat roofs. Wind tunnel models of constant height and varying height to width ratios (0.04 to 0.4) have been investigated in smooth wind tunnel flow and in three different simulated atmospheric boundary layer flows. Accordingly, Gerhardt and Kramer (1992) noted: "The relative building height for buildings with $H/B \geq 0.1$ influences the roof pressure distribution strongly". Also, the results show that the measured maximum values of time-averaged suctions depend on the pressure tap density and, in particular, on the proximity of the pressure taps to the roof edges. The most critical pressure distribution of largest wind loads on the corner and edge regions were obtained for smooth wind tunnel flow exposure (open country exposure).

Milford et al (1992) presented a comparison between full-scale and wind tunnel results obtained at the Division of Building Technology for the Jan Smuts Airport hangar. Comparisons of mean and root-mean-square pressure coefficients were generally satisfactory. However, a noticeable divergence between the full-scale and wind-tunnel mean pressure coefficients was observed for certain datasets. Moreover, the comparison between the peak pressure coefficients was less satisfactory.

Lin et al (1995) studied roof pressures of low-rise buildings for a series of models of varying height and plan size in two different flows in the Boundary Layer Wind Tunnel Laboratory (BLWTL) at the University of Western Ontario (UWO). The study investigated the roof pressure distribution under the corner vortices and its variation with wind angle, building dimensions and approaching flow characteristics. Lin et al (1995) suggested that near corners of flat roofs the collapse patterns of pressure coefficients, $C_p(x/H, y/H)$ or $C_p(b, s/H)$, are analogous if the location of the measured pressure relative to the corner is defined non-dimensionally as function of the building height (H) and the oncoming flow characteristics. Where x and y are rectilinear coordinates measured from the leading edges, or alternatively, s is the distance along a ray from the leading corner, making an angle b with the leading edge.

Based on the results obtained from all investigated models, Lin et al (1995) concluded that no limitation can be defined yet for the extreme suction towards the corner; however, the highest values of mean and peak pressure coefficients have been found near the corner for the highest model investigated, at a wind angle of about 30^o or 60^o. The area-averaged suctions significantly decrease with increasing averaging area embracing the corner. The pressure coefficients of the same locations will change with the building height (H), but are not very dependent on plan dimensions within the range of H/W from 0.1 to 0.45 as investigated. Empirical formula for estimating design wind pressure coefficients on flat roofs along a line extending from the roof corner at a certain angle with the edge was created in the form of $C_{pi} = C_i(S/H)^{-0.5}$, where the factor C_i is a function of the line angle (b), the wind angle and the incident flow characteristics. Finally, this study provided suggestions to improve wind tunnel measurements techniques.

Lin and Surry (1998) examined the effect of spatial averaging of roof pressures on peak loads over various tributary areas near the corner of flat-top low-rise buildings. Worst area-averaged pressure coefficients distribution, C_pC_g, for 0.375 m x 0.375 m tributary areas for the three largest buildings with different heights measured by Lin and Surry (1998) are shown in the Figure 2.4. The results indicated clearly that the magnitudes of C_pC_g are increased with increasing the building height.

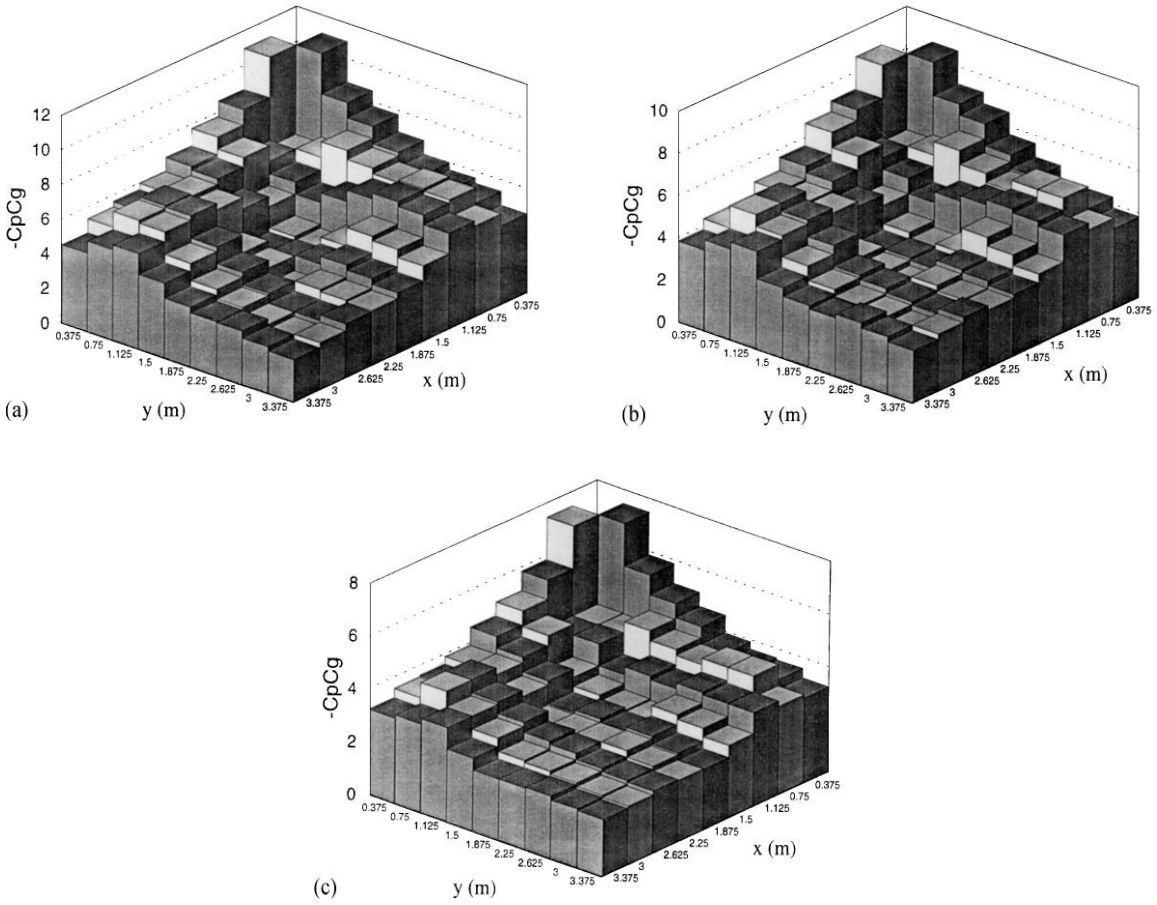

Figure 2.4: Variation of area-averaged pressure coefficients with locations within the corner region for square tributary areas of 0.375 mx0.375 m: a) H= 12 m x 40 m x 40 m; b) H= 8 m x 40 m x 40 m; c) H= 4 m x 40 m x 40 m, (Lin and Surry, 1998).

The effects of building attachments on the generated roof wind loads have been studied, e.g., Leutheusser (1964) investigated the effect of wall parapets on roof pressure

coefficient. Kind (1988); Baskaran and Stathopoulos (1988) and Stathopoulos et al (1999) also investigated the effects of parapet on wind loads of flat roofs.

Ultimately, Blackmore (1988) conducted a study to investigate the effects of chamfered roof edges on the generated wind pressures on flat roofs experimentally in the BRE Boundary Layer Wind Tunnel. The largest reduction was observed at the corners regions, thus, a 30^o chamfered edge reduced the area-averaged loads on the corners by 70 % and gave an overall load reduction of 30 %. Steep chamfers increased the local peak suctions along the windward roof edge while shallow chamfers give a slight reduction. The significant load reduction on the corner panel was due to narrower separation bubble and as a result a much narrower highly loaded edge region, resulting from the suppression of vortices generated at the windward corner.

2.4 Justification of the Present Study

Controversy over the large flat roofs of low-rise buildings has arisen in recent studies against the provisions of the current international wind codes and standards, e.g., Morrison and Kopp (2007) and Geurts et al (2013). The latest study has shown the lack of knowledge and significant differences among the current wind load provisions in evaluating the wind loading zones for the design of flat roofs. It was found that for relatively small-sized buildings, the sizes of the roof zones are in the same order of magnitude. However, when the footprint of the roof becomes relatively large compared to the height, differences in sizes for edge and roof zones of a factor 2 occur when comparing some of the major wind loading standards. In fact, detailed comparisons should also address the peak pressure coefficients and the methodology of roof zones size prediction.

Morrison and Kopp (2007) have extended the work done by Ho et at (2005) and have compared mean and RMS pressure coefficients normalized by roof height for different building heights and plan dimensions. The study found that the definition of the edge zone in ASCE 7 requiring that the edge zone be a minimum of 4% of the smallest building plan dimension affects buildings with very large plan dimensions when compared to the roof

height. However, the study has also found that there is very little change in the wind loading on the roofs of buildings based on plan dimensions and seems to scale primarily with the roof height. Consequently, the requirement that the edge zone be at least 4% of the smallest building plan dimension may artificially increase the size of the edge zone, although no increase in wind loading on the roof really exists.

Therefore, the present study will address and clarify various issues related to the historical development of this theme - wind provisions of the North American codes and standards - which have been developed over the past decades.

In summary, the literature review shows that previous experiments have been performed to model simple shapes of low-rise buildings with common, relatively small, dimensions. As a result, the design criterion of ASCE 7-10 (USA) and NBCC 2010 (Canada) in regards with the 4% of the least horizontal dimension (0.04Ds) could become extremely uneconomic for flat roofs of large low-rise buildings. Hence, the present study is really warranted. Therefore, the aim of this research is to investigate wind pressures on edges and corners of roofs of low-rise buildings with very large dimensions compared with their heights found through a wind tunnel experimental study; also, to examine the wind provisions given by international wind codes and standards with emphasis on North American codes and standards in order to assess their applicability to very large buildings.

CHAPTER 3

EXPERIMENTAL METHODOLOGY

Wind tunnels are now considered as a very useful engineering tool for application of wind testing. This chapter includes a description of the facilities, construction of the models, boundary layer simulation in the wind tunnels, the instruments and the equipment (velocity measurement system and DSM 3400 pressure measurement system) used in this study. In addition, this chapter presents the model configurations, wind tunnel testing requirements and the implementation of the measured pressures. Finally, the present results are compared with similar repeated tests and with data obtained from another study for validation purposes; the results of these comparisons are presented in this chapter.

3.1 Building Aerodynamic Laboratory at Concordia University

All experiments for the present study have been carried out in the Boundary Layer Wind Tunnel (BLWT) at the Building Aerodynamics Laboratory, Concordia University. The blow-down tunnel is of the open-circuit design with working section of 1.80 m in width, 12.2 m in length and has adjustable roof height in the range of 1.40 m to 1.80 m to provide the necessary height for different exposures. Top, side and front views retrieved from the original construction plans are shown in Figure 3.1.

The flow is generated by a MARK HOT double inlet centrifugal blower with a flow rate capability of 40 m^3/s. The wind speed at the test section ranges between 3 m/s and 14 m/s. The wind speed in the wind tunnel is controlled by manually adjusting the outlet control.

The tunnel floor is covered with a polypropylene carpet and the ceiling consists of wooden panels of adjustable height. Different terrain exposures may be simulated by adding floor panels with specific roughness elements and by adjusting the ceiling to achieve a zero longitudinal pressure gradient. The tunnel is provided with a turntable of 1.60 m diameter at tunnel test section, which allows testing models for different wind directions. An acrylic glass window has been placed at the wind tunnel wall to facilitate flow visualization experimentation without having the equipment interfere with the flow. Detailed information about the wind tunnel including construction details and its simulations are provided by Stathopoulos (1984-A).

3.2 Atmospheric Boundary Layer Simulation and Terrain Exposure

The boundary layer wind flow was simulated using triangular boards, a steel plate and carpet roughness. Four boards of the same triangular shape (spires) were erected side by side on the screen of the tunnel entrance and bound to the screen. The base and the height of each of these spires are 19 cm and 120 cm, respectively. The distance between the centers of the two end boards to the tunnel wall is 35 cm and the distance between the boards themselves, center to center, is 36.5 cm. The steel plate of 15 cm height was placed on the floor at a distance of 75 cm parallel to the screen.

For this study, all experiments have been conducted for an open-country exposure. It must be noted that the thick carpet is used along the floor to generate the required velocity and turbulence profiles of open-country exposure, as shown in Figure 3.2. Velocity and length scales were determined at first. The length scale depends on the ratio of the thickness of the simulated boundary layer to that in reality. The gradient height of 60 cm developed over the wind tunnel floor is approximately equivalent to 240 m boundary layer thickness in full-scale at the selected length scale of 1:400. The free-stream wind speed (gradient velocity) in the wind tunnel was set at 11.0 m/s at velocity scale of 1:3, to simulate the full-scale gradient velocity of 33.0 m/s at the atmospheric boundary layer height. Corresponding to the length scale of 1:400 and the velocity scale of 1:3, the time scale was determined as 1:133.

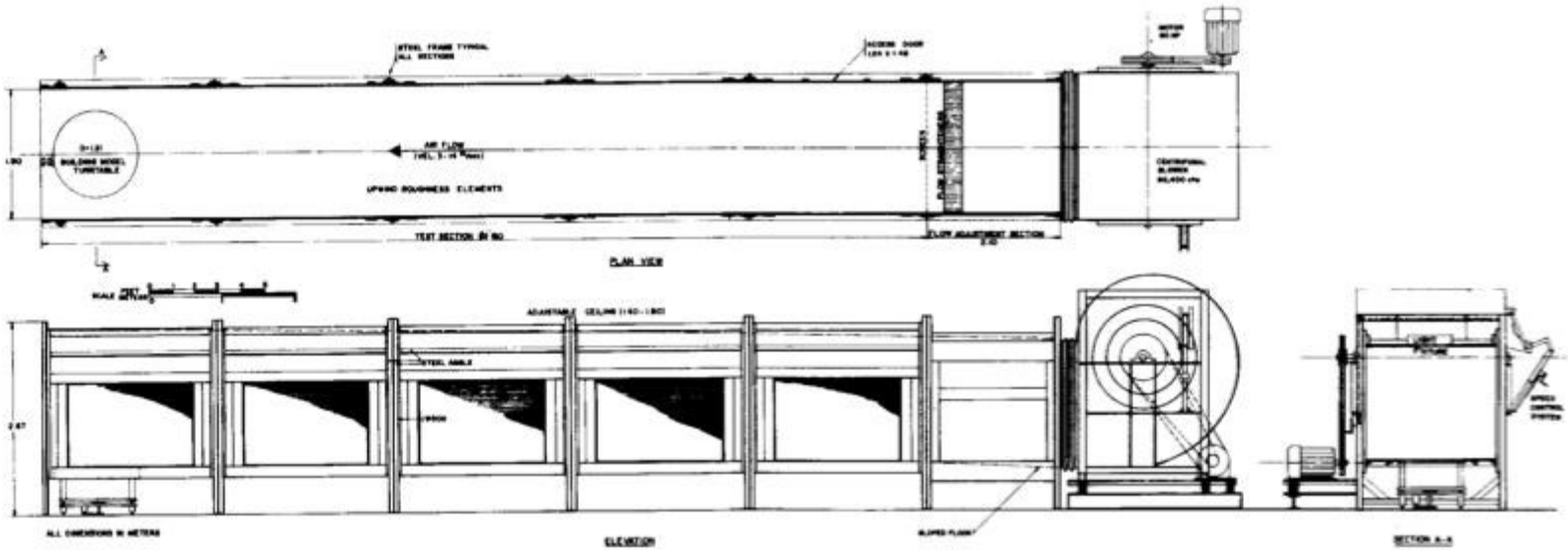

Figure 3.1: Construction Plans of the Boundary Layer Wind Tunnel at Concordia University/ Building Aerodynamic Laboratory, Stathopoulos (1984-A).

Figure 3.2: Boundary layer wind tunnel at Concordia University (Front view)

Figure 3.3 shows the approaching flow profile of longitudinal mean wind velocity ($\overline{V}_Z/\overline{V}_G$) and turbulence intensity ($I_U\%$) at the test section measured using a 4-hole Cobra probe (TFI). In this figure, Z is the height above the tunnel floor and Z_G is the gradient height over the floor; $\overline{V}_Z$ is used to denote the mean wind speed while $\overline{V}_G$ is used to denote the tunnel wind speed at the gradient height. As recommended, high wind speeds are desirable in wind tunnels for effective response and for more accurate readings of the measuring instruments. The gradient mean wind speed was set at 11.0 m/s. The wind characteristics at the test section is described by power-law model and according to that the variation of mean wind speed with height was generated with power law index (α) of 0.15.

Figure 3.4 shows the experimental and theoretical longitudinal power spectral densities of the approaching flow measured by Stathopoulos (1984-A) at height of one-sixth of the boundary layer depth. The scattered points, shown in this figure, represent the experimental power spectral density for the simulated open terrain exposure and the solid curves represents the spectra obtained by the Von Karman's equation and Davenport's empirical expression. The longitudinal integral scale L_u^x =112 m in full-scale for a given length scale 1:400 was estimated based on Von Karman's equation; see equation 2.7.

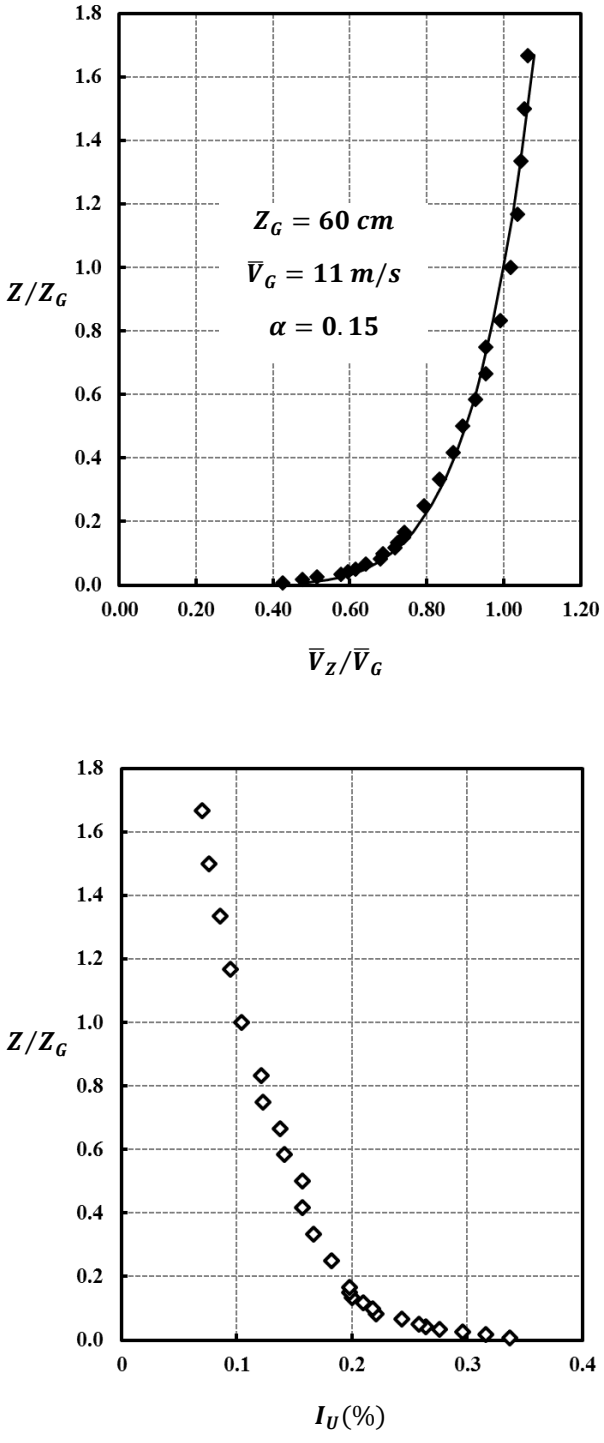

Figure 3.3: Vertical distribution of mean wind speed and longitudinal turbulence intensity for open country exposure ($\overline{V}/V_G = (Z/Z_G)^{0.15}$).

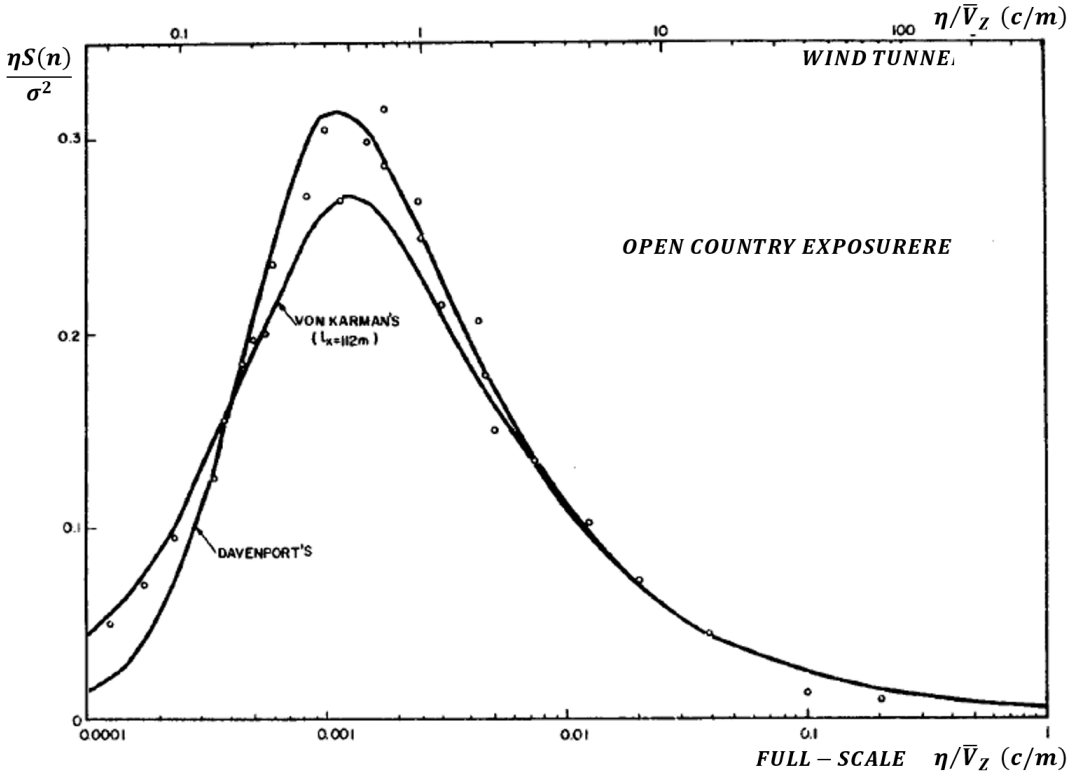

Figure 3.4: Spectra of the longitudinal turbulence component at $Z/Z_G = 1/6$ (Stathopoulos 1984-A).

3.3 Model Configurations

Wind tunnel tests have been conducted for nine low building models with flat square roof with full-scale equivalent dimensions ranging from 60 m to 180 m. The basic model of the tested buildings has full-scale equivalent plan dimension of 60 m; it is made of Plexi-glass and is equipped with 127 roof pressure taps. Figure 3.5 shows the perspective view of the pressure taps layout on the roof of the basic model. As shown there, the highest density of pressure taps is located at the windward corner of the roof. Also, the taps were placed as close as possible to the roof edges. The distance from the first line of pressure taps to the adjacent roof edge is 0.01 of the building width (B) of 60 m model (0.6 m in full-scale). The wind directions considered in this study are also indicated in this figure, such that the wind direction at 0^o when the wind was normal to the windward edge of the model plan and increased in counter-clockwise direction to complete a quarter cycle ($0^o$to 90^o) at increments of 15^o.

The basic model has been used in simulation of the other buildings of large roofs that were taken into account in this study i.e. buildings of plan dimensions of 120 m and 180 m. This has been done by combining the basic model (equipped with pressure taps) with a matrix of similar geometry wooden blocks, as shown in Figure 3.6. The measurement results of large roofs (width = 120 m and 180 m) have been collected independently by placing the basic model at different locations, for which the pressure coefficients on the entire roof of the building have been scanned for a particular wind direction, whereas the roof pressure coefficients of the basic model (width = 60 m) have been measured simultaneously.

All buildings were tested at equivalent full-scale heights of 5.0, 7.5 and 10.0 m, by sliding the models downwards within a precise tightly fit slot in the turntable. Figure 3.7 illustrates all configurations of low-rise buildings tested in this study.

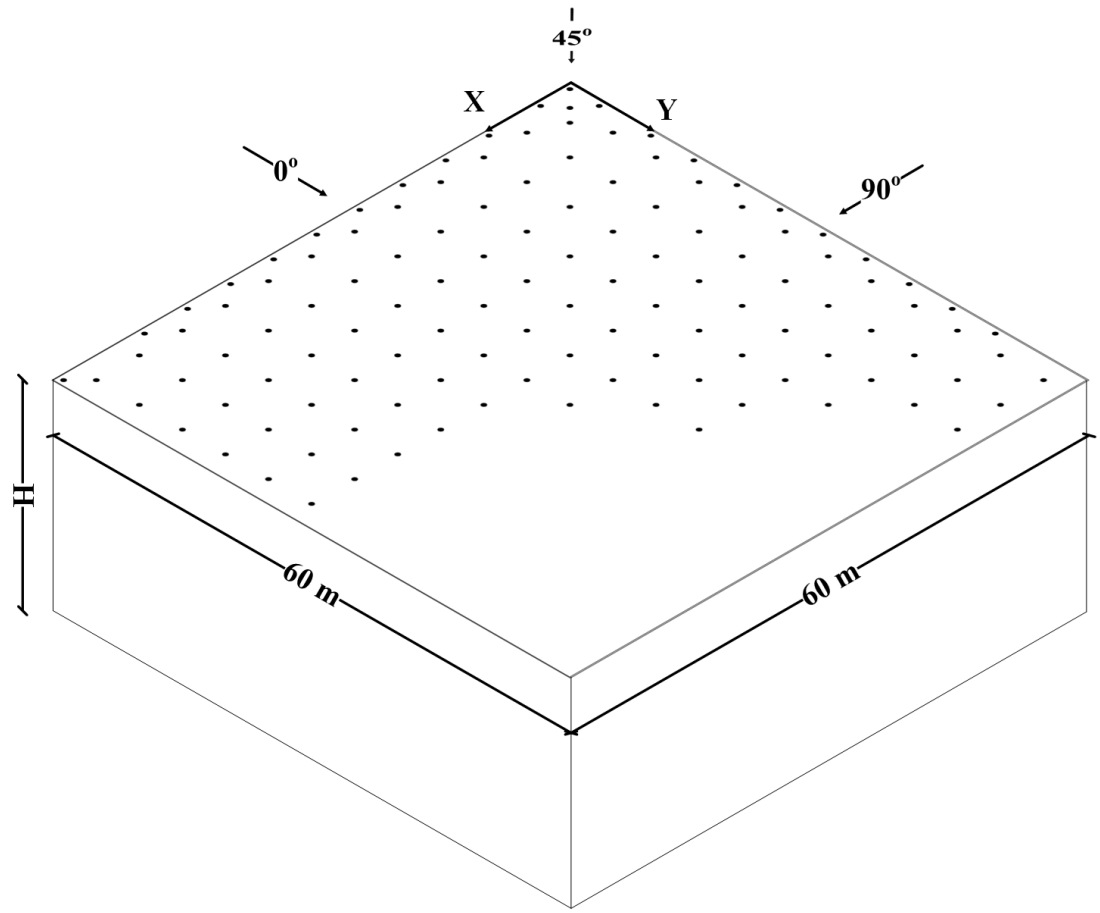

Figure 3.5: Perspective of the 60m x 60m building model with pressure taps layout on the roof; the pressure taps are indicated by the symbol, ●.

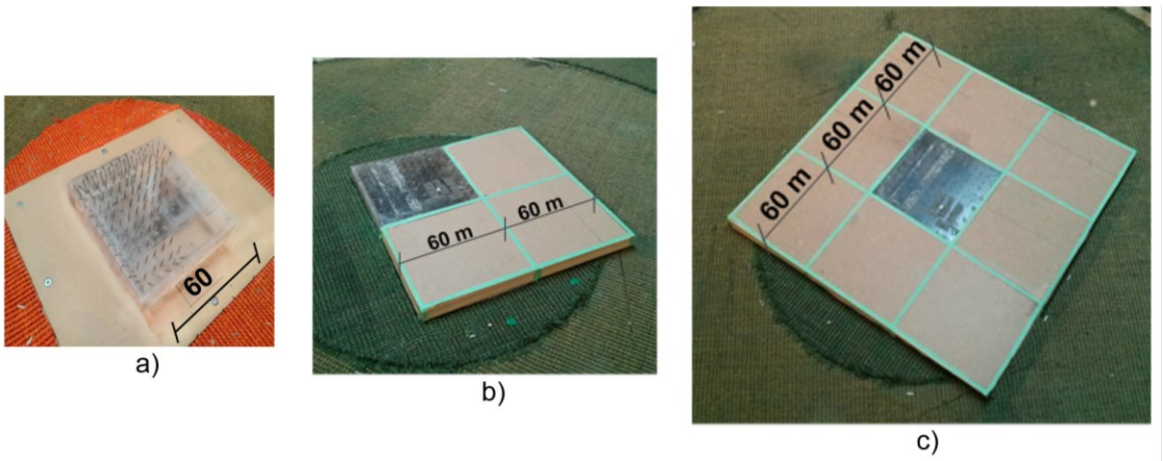

Figure 3.6: Close-up photographs for the typical building models with equivalent full-scale square plan dimensions tested in the wind tunnel: a) 60 m, b) 120 m and c) 180 m.

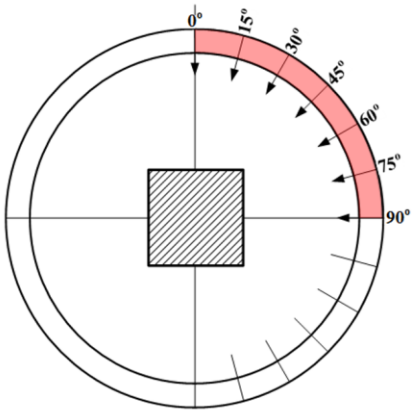

Model	Dimensions					
	Full scale (m)			Model Scale (mm)		
	H	L	W	H	L	W
B1		60	60		150	150
B2	10	120	120	25	300	300
B3		180	180		450	450
B4		60	60		150	150
B5	7.5	120	120	18.8	300	300
B6		180	180		450	450
B7		60	60		150	150
B8	5.0	120	120	12.5	300	300
B9		180	180		450	450

Figure 3.7: Schematic illustration of the building models (dimensions in full scale and model scale).

Reynolds numbers of the tested building configurations were estimated and presented in Table 3.1. Reynolds numbers were estimated based on the mean flow velocity at roof height with model dimensions (either width or height) taken as characteristic lengths. It must be noted that the linear dimension (L_b) derived from the ratio of model volume to quarter-model side area is equal to cross section diameter in case of cylinder ($L_b = D$) or the quarter of the building width in case of rectangular model ($L_b = B$).

Table 3.1: Estimated model Reynolds number characterized by different linear dimensions.

Building Dimensions (m)	$\bar{V}_H$ (m/s)	Re×10^4 Based on H	Re×10^4 Based on B
B1: 60X60X10	6.8	1.1	6.8
B2: 120X120X10	6.8	1.1	13.7
B3: 180X180X10	6.8	1.1	20.5
B4: 60X60X7.5	6.5	0.8	6.5
B5: 120X120X7.5	6.5	0.8	13.1
B6: 180X180X7.5	6.5	0.8	19.6
B7: 60X60X5	6.2	0.5	6.2
B8: 120X120X5	6.2	0.5	12.3
B9: 180X180X5	6.2	0.5	18.5

$v = 1.5 \times 10^{-5}$ (m²/s) is the typical value of kinematic viscosity for air 20°C and standard atmospheric pressure. (Simiu and Scanlan, 1996).

Table 3.1 shows that minimum Reynolds number criteria are thus satisfied in case of models Reynolds number characterized by the model plan width.

3.4 Data Acquisition and Processing

Mainly two groups of equipment have been used to carry out the wind tunnel experiments of the current study. The first group was used to measure the wind velocity to derive the wind profile. The second group was used to measure the wind pressures. Detailed description of each group instruments is presented in the following sections.

3.4.1. Data Acquisition System and Measurement Settings

The wind velocities were measured using Turbulent Flow Instrumentation (TFI) by 4-hole Cobra probe, which is capable to measure the three components of the wind velocity corresponding to X, Y and Z directions. This instrument is considered very efficient in measuring the turbulent flow at high accuracy. The Cobra probe has a length of 160 mm and its location inside the wind tunnel is remotely controlled by a three-dimensional traversing system. Thus, the Cobra probe is fitted onto the arm of the traversing system and can be moved in three dimensions. The Cobra probe is connected to a computer with windows operating system to collect the measurement results during the testing process.

The wind profile of this study was measured by positioning the Cobra probe close to the middle of the turntable nearby the model. The location of the Cobra probe was changed only with height by entering the Cartesian coordinates of the desirable height. The software has stored the data in files exported to spreadsheets. Finally, with some simple calculations on the collected data the simulated profile of turbulent boundary layer flow for open exposure was created – see Figure 3.3.

The wind pressures are measured using a system of sensitive pressure scanners. The system consists of Digital Service Module (DSM 3400) fabricated by Scanvalve and two Electronic Pressure Scanners (ZOC33/64 Px). DSM 3400 can be connected up to eight Electronic Pressure Scanners of 64 channels each. DSM 3400 features an impeded computer, RAM memory and a hard disk drive and works with windows embedded XP as an operating system. The DSM 3400 module is designed to let the Electronic Pressure Scanners to be utilized in an Ethernet system. For insulation purposes, the ZOC scanner is placed inside a thermal unit to keep the temperature of the scanner constant during the scanning process.

Each roof pressure tap consists of 15 mm length brass tubes of 0.8 mm internal diameter. These taps were implanted on the model roof from inside. The pressure measurements on roof of the models were accomplished by connecting the roof pressure taps to a system of miniature pressure scanners made up of Scanvalve pneumatically modules (ZOC33/64Px), each capable of handling 64 channels (pressure taps) and the digital service module (DSM

3400). A PC-computer with windows interface is utilized to host the DSM 3400 system through Ethernet network via Ethernet port and to control the data acquisition by ScanTel program. It supports communication in BINARY formats.

A flexible plastic tube of 550 mm length with interior and exterior diameter of 2.18 and 1.37 mm respectively were used to connect each roof pressure tap with the pressure transducer. Traditional custom-made brass restrictors were placed within the tubes at a specific location (at distance of 300 mm measured from the pressure tap) to add damping to minimize the Gain and Phase shifts of pressure signals due to Helmholtz's resonance effects. Cross-section diagram of the wind tunnel and wind tunnel facilities set up are schematically presented in Figure 3.8.

The 127 tubes connected to the basic model were divided into 2 groups: the first one includes 63 tubes while the second one includes 64 tubes. Thus, the 63 pressure taps of the first group were connected to the first 63 pressure channels on the pressure scanner (ZOC33/64Px), while the remained pressure channel was allocated to the Pitot tube in order to measure the reference free-stream velocity pressure.

3.4.2. Data Processing System

The pressure scanners are calibrated to scan the pressure signals at frequency of 300 Hz (300 samples per second) for a total period of 27 seconds on wind-tunnel scale or 3600 seconds in full-scale.

The instantaneous surface pressures over the entire roof have been measured in the test section of the wind tunnel for all wind directions in terms of time history wind load. The measured pressures have been normalized by the mean dynamic pressure measured at reference height to express them as non-dimensional pressure coefficients.

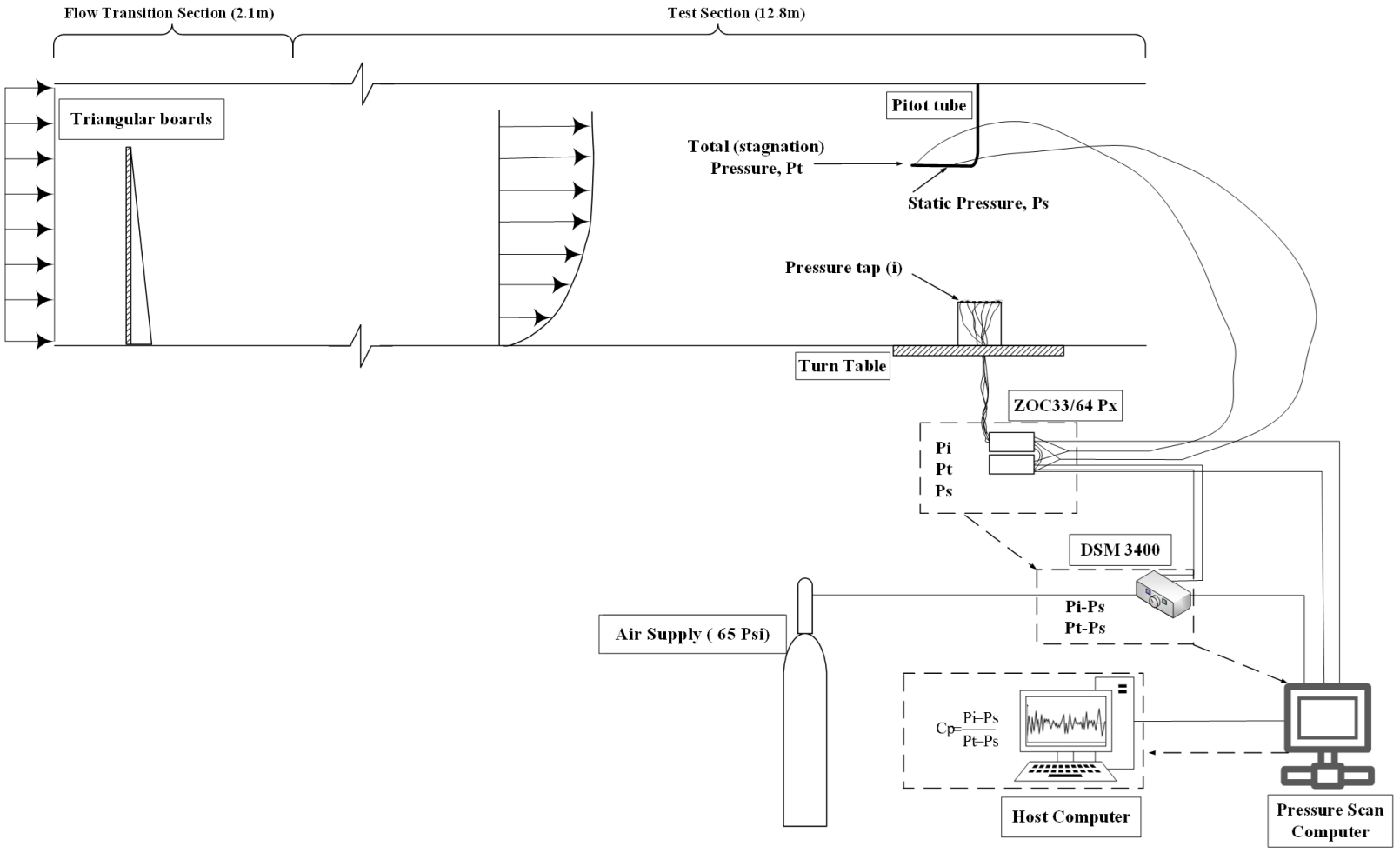

Figure 3.8: Schematic illustration of the wind tunnel instrumentation and measurement technique.

The external wind pressure coefficients at measurement pressure tap (i) is defined as

$$\text{Pressure coefficient: } C_{Pi}(t) = \frac{P_i(t) - P_s}{\bar{q}_z}, \qquad \bar{q}_z = \frac{1}{2}\rho \bar{V}_H^2 \tag{3.1}$$

in which C_{Pi} is the instantaneous wind pressure coefficient at pressure tap (i), P_i is the wind pressure at tap (i), P_s is the static pressure at reference location, $\bar{q}_z$ is mean value of the dynamic pressure at reference height Z_{ref}, ρ is the density of the air and $\bar{V}_H$ is mean value of the wind velocity at roof height. In the present study, the reference height was taken at the position of the Pitot tube in the free stream (Z=650 mm).

The $P_i(t) - P_s$, which represents the wind pressure acting at particular pressure tap (i), was derived directly by the laboratory transducer (ZOC33/64Px) as the differential pressure between the instantaneous pressure at measurement pressure tap (i) and the static pressure from Pitot tube during the measurement process. As simply as schematically possible, wind pressure processing at particular pressure tap is presented in Figure 3.8

Peak pressure coefficients in the time history records are determined based on analysis methods used in many previous studies, e.g. Elsharawy et al (2014). According to this method, the overall peak of 1-h full-scale equivalent time history record is defined as the average of the maximum 10 values. This method provides reliable extreme peak for the recorded peaks. The mean pressure coefficients are taken as the averaged values of the samples in the time history. Finally, the sign of the wind pressure coefficient indicates the direction of wind pressure on the surface of building model; positive value indicates wind pressure acting towards the surface and negative value indicates wind pressure acting away from the surface (suction pressure).

3.4.3. Area-Averaged Pressure Coefficients

The design wind load of components and cladding includes both the local peak pressure coefficients (e.g. wind loads on small areas like fasteners with small tributary areas) and the area-averaged wind pressure coefficients for wind design loads on large areas (e.g. wind loads on windows). Therefore, the scope of this study is not limited to only the measured local pressures, but it includes both the local and area-averaged pressure coefficients.

Two methods are used to estimate the area averaged wind load; pneumatic integration method (several pressure taps physically connected through a pressure manifold to a single pressure tube) and the numerical integration of individual pressure coefficients method. The latter provides considerable flexibility for selecting the tributary area shapes and sizes.

The instantaneous area-averaged wind pressures over the effective area are calculated for each wind direction by integrating the instantaneous local wind pressures after being factored by the contributing area to each pressure tap being considered in the effective area. The area-averaged pressure coefficient time history for each tributary area is generated using the following equation:

$$\text{Area-averaged pressure coefficient: } C_{P,A}(t) = \frac{1}{\sum_{i=1}^{n} A_i} \sum_{i=1}^{N} C_{Pi}(t) A_i \qquad (3.2)$$

in which $C_{P,A}(t)$ is the area-averaged wind pressure coefficients at instant (t), A_i is the contributing area to the i^{th} pressure tap and N is the number of pressure taps in the specified area A. The potential errors during integration are minimized by using a high pressure tap density to the models tested in the wind tunnel. The negative peak area-averaged pressure coefficient is taken as the average of the smallest 10 values within the average pressure time history of the tributary area, as described for the single pressure tap.

3.5 Repeatability of Measurement Results

The uncertainty and variability of the measurements are examined in order to check the reliability of the results. This was carried out by a comparative process, which consists of

two parts: The first part compares wind tunnels peak and mean pressure coefficients for central line of pressure taps for 0^o wind direction from the original tests and similar repeated tests. Figure 3.9 shows the pressure coefficients of this study and of the repeated tests for building configurations B4 and B7. As shown in Figure 3.9, a good agreement is achieved between the original measurements and the repeatability results for both mean and peak pressure coefficients.

The second part compares the measurements of this study with another set of wind tunnel data obtained by Stathopoulos and Dumitrescu-Brulotte (1989). Figure 3.10 shows the mean and peak pressure coefficients along the center of the roof for wind direction perpendicular to the windward edge from Stathopoulos and Dumitrescu-Brulotte (1989) for building dimensions (61X61X12 m), and those from this study for building model B1 (60X60X10 m). Both studies were carried out on wind tunnel open country exposure with same power law exponent values. The values of the pressure coefficients shown in this figure are in very good agreement.

Therefore, the good agreement of the original test results with the repeated test data and the results of another wind tunnel study is quite encouraging for further application of these wind tunnel results.

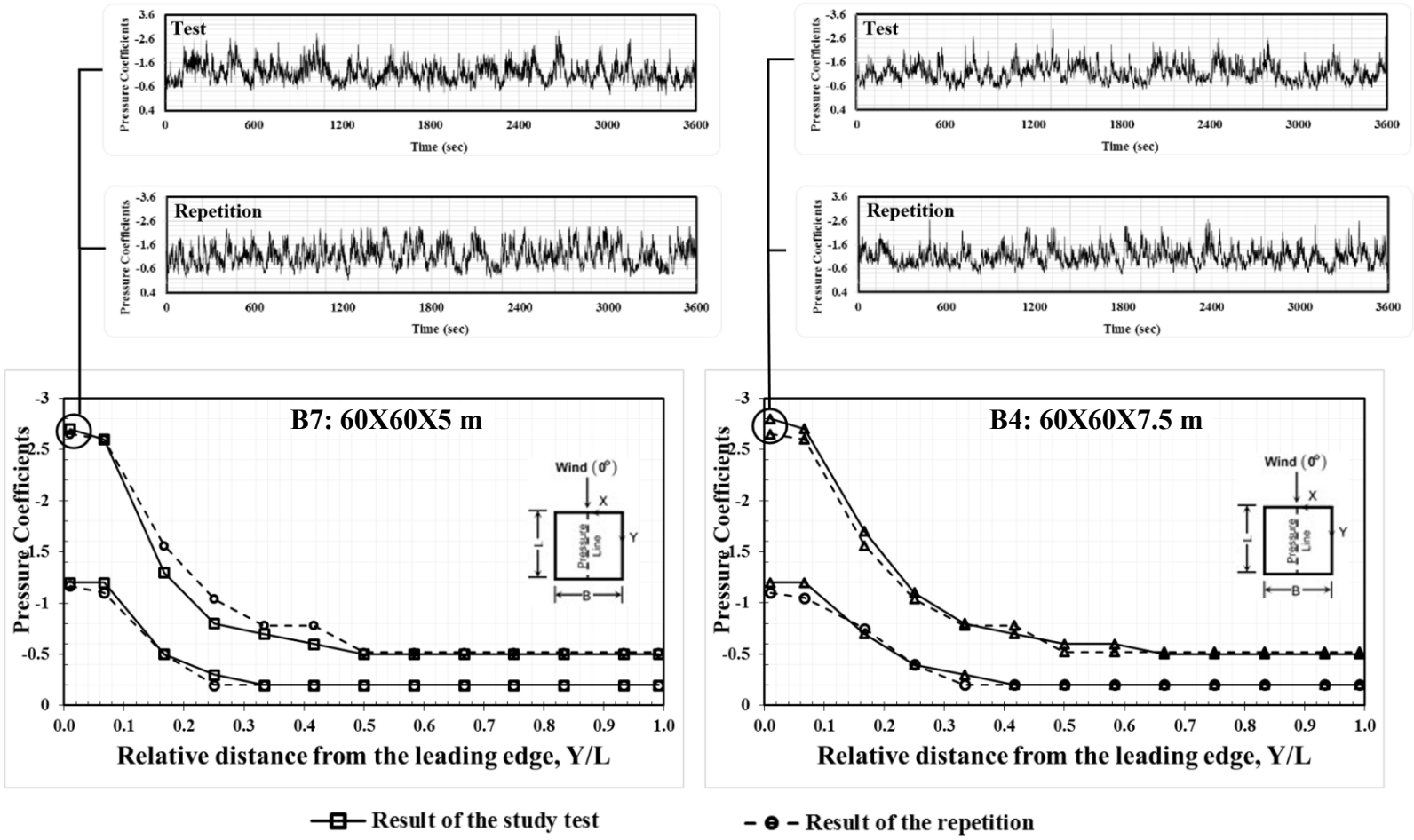

Figure 3.9: Pressure coefficient distributions for buildings B7 and B4 and pressure coefficients measured in two tests at same flow characteristics.

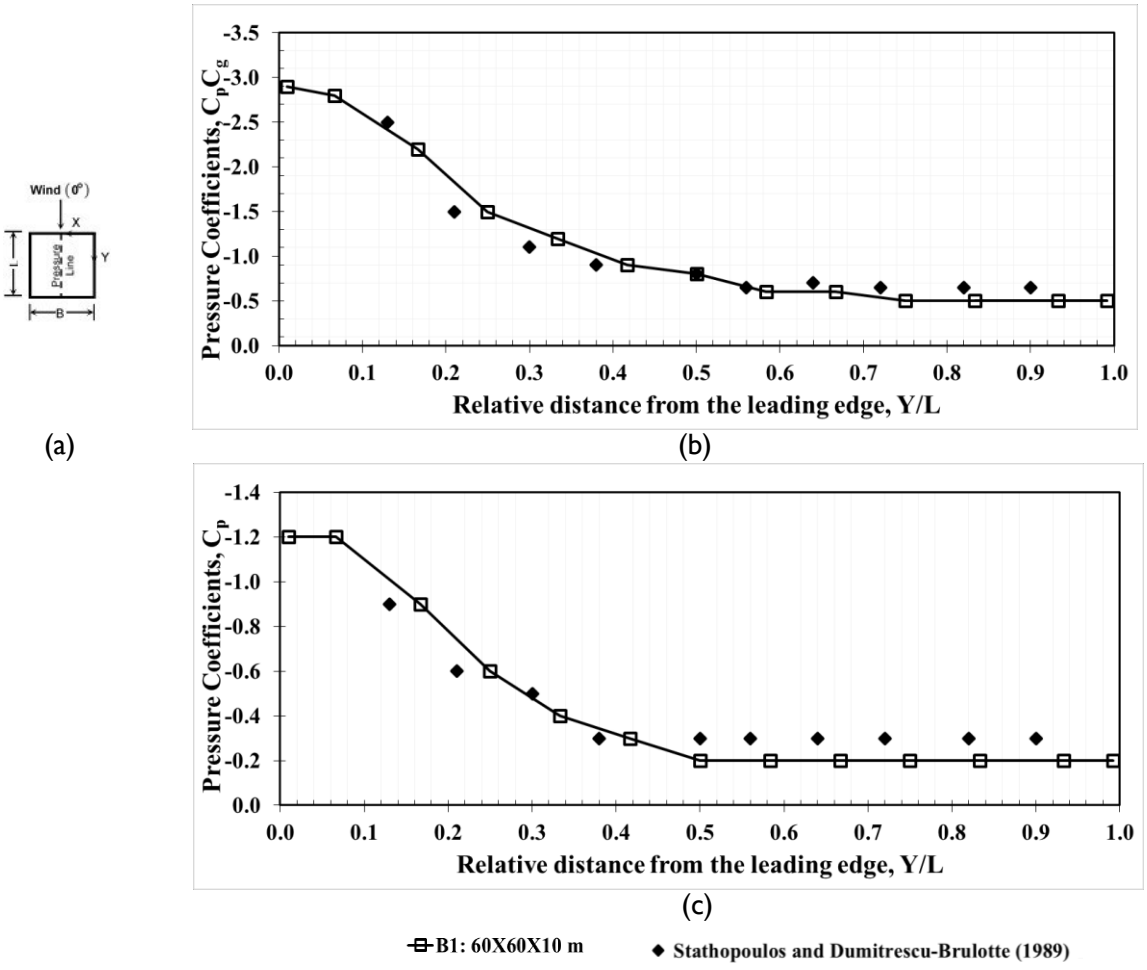

Figure 3.10: Pressure coefficient distributions for building B1 in comparison with data of Stathopoulos and Dumitrescu-Brulotte (1989) measured with similar flow conditions: (a) Location of pressure taps, (b) Peak pressure coefficients, C_pC_g and (c) Mean pressure coefficients, C_p.

CHAPTER 4

WIND STANDARDS AND CODES OF PRACTICE

This chapter presents a description of the methodologies used by current wind standards and codes of practice for flat roofs of low-rise buildings. The description includes the recommended design wind pressures and the roof zones given by four national wind codes and standards, namely: ASCE 7-10, NBCC 2010, EN 1991-1-4:2005 and AS-NZS 1170-2, 2011, with some emphasis on the historical development of the current North American wind standard/code (ASCE 7-10 and NBCC 2010).

4.1 Introduction

In the scope of the current wind codes and standards, wind load is classified into horizontal wind load for structural frames, roof wind load for structural frames and wind load for components/cladding. The wind load for structural frames is calculated from the product of velocity pressure, gust effect factor, force coefficient and loading area. The wind load for components/cladding is calculated from the product of velocity pressure, peak wind force coefficient and loading area.

In general, wind standards and codes specify wind loads in terms of pressures or forces. Generally, two approaches are proposed to determine the wind-loading effects on structures. The first is a relatively simple procedure appropriate for the majority of wind loading applications, including the structural design of low and medium rise buildings. These are situations concerning quasi-rigid structures and can be dealt with equivalent static loads. Wind standards and codes often specify non-dimensional pressure coefficients for different structural elements for limited variations of buildings and force coefficients for other structures. These coefficients are used in conjunction with site-specific wind data

and terrain characteristics to determine the design wind loads. In most cases, the pressure coefficients are established from wind tunnel tests conducted in simulated atmospheric boundary layers.

The other approach is applicable when the buildings and other structures are likely to be susceptible to wind-induced vibrations. For these buildings and structures, customized wind-tunnel tests or other experimental methods, or a detailed procedure is to be followed to determine wind loads. Wind-tunnel tests are more appropriate when more exact definition of dynamic response is needed and for determining exterior pressure coefficients of buildings with complicated geometry. It is to be noted that this study is concerned with flat roofs of low-rise buildings and, therefore, the simple procedure approach is implemented in this study.

4.2 Wind Loads on Roof Cladding of Low-Rise Buildings

The definition of low-rise buildings and the roof angle (α_o) ranges are somewhat different in various national wind standards and codes of practice. The definitions of flat-roofed low-rise buildings provided in the American Society of Civil Engineers Standard (ASCE 7, 2010), the National Building Code of Canada (NBCC, 2010), the European Standard (EN 1991-1-4:2005) and the Australian/New Zealand standard (AS-NZS 1170-2, 2011) are presented in Figure 4.1. For the range of these heights and roof angles wind codes/standards provide the design wind pressures for the components and cladding of roofs, walls and frames of low-rise buildings regardless the building plan dimensions.

NBCC 2010:

h < 10 m, or h < 20 m and h < B.

$0^o \leq \alpha_o \leq 7^o$.

ASCE 7-10:

h < 18 m and h < B.

$0^o \leq \alpha_o \leq 7^o$

EN 1991-1-4:2005:

h < 15 m.

$-5^o \leq \alpha_o \leq 5^o$

AS/NZS 2011:

h < 25 m.

$0^o \leq \alpha_o \leq 10^o$

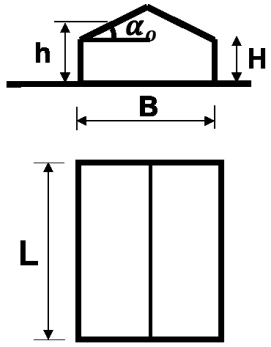

Figure 4.1: Flat-roofed low-rise building definitions in different wind standards and codes of practice.

The methodologies used by the four codes/standards mentioned above, for calculation of building pressures are summarized in Table 4.1. Clearly the approaches in the various codes and standards are different. Even though the basic wind speed (V) in all of the wind codes/standards is defined at 10 m above ground surface in open country exposure, the averaging time and wind velocity profiles are different. For instance, the basic wind speed used in NBCC-2010 has a longer averaging time (1-hr) compared with the 3-sec averaging time used in ASCE 7-10 and the wind velocity profiles are fitted by either the power law or logarithmic law, as indicated. Therefore, since the gust factors for computing pressure coefficients used in ASCE 7-10 will be lower than those in NBCC-2010, the current values of the gust pressure coefficients used in the ASCE7-10 will be lower than those in NBCC-2010 in order to yield comparable design wind pressures.

Table 4.1: Wind code and standard approaches for calculating design wind pressure.

	ASCE 7-10	NBCC 2010	EN 1991-1-4 2005	AS-NZS 1170-2 2011
Basic wind speed	V	V	$V = V_{b,o}C_{dir}C_{seas}$	$V = V_R M_d M_{z,cat} M_s M_t$
Velocity pressure, q	$0.5\rho V^2 K_z K_{zt} K_d I$	$0.5\rho V^2 I$	$0.5\rho V^2$	$0.5\rho V^2$
Design building pressure	$q(GC_p)$	$qC_e(C_g C_p)$	$qC_e C_{p,e}$	$qK_a K_{c,e} K_l K_p (C_{p,e})$
Terrain factor	K_z	C_e	C_r	$M_{z,cat}$
Topographic factor	K_{zt}	C_e^*	C_o	M_t
Directionality factor	K_d	-	C_{dir}	M_d
Basic wind speed averaging time	3 s	1 h	10 min	3 s
Wind velocity profile	Logarithmic law Power law	Power law	Logarithmic law	Logarithmic law

When the topographic factor is used in NBCC, C_e^* is placed instead of C_e.

C_e: Exposure factor defined as follows: $C_e = [1 + 7I_V]C_r^2 C_o^2$, in which I_V is the turbulence intensity.

C_p and $C_{p,e}$: External pressure coefficient. C_{seas}: Seasonal factor.

G and C_g: Gust effect factor.

I : Turbulence intensity.

K_a: Area reduction factor. $K_{c,e}$: Combination factor for external pressures.

K_l : Local pressure factor.

K_p: Porous cladding reduction factor. M_s: Shielding multiplier.

$V_{b,o}$: Fundamental value of the basic wind velocity (10 minutes mean wind velocity at 10 m above ground level in open country terrain). V_R: Regional 3-second gust wind speed.

The design external wind pressure is determined by multiplying the external building pressure by the loading area. The design wind velocity pressure is calculated based on the basic wind speed, V, and factors that account for the terrain conditions, topographic conditions, surface permeability, and for other conditions such as building importance, shielding and season.

4.3 Zonal Systems for Flat Roofs in Current Wind Codes and Standards

Wind experiments conducted on different roof configurations have expressed the wind loading on the roof typically (but not always) within boundaries of three zones. Pressure coefficients range from the lowest values on interior areas of the roof, to higher values around the perimeter of the roof, to the highest values on the roof corners.

Wind standards and codes of practice divide the entire flat roof of the building into at least three loading zones, namely: corner, edge and interior. The loading zones of the current wind codes and standards are defined as a function of different parameters such as building plan dimensions and building height. The parameters that demonstrate the zone sizes are defined differently. The detailed definitions for the zonal system recommended by the wind codes/standards considered in this study are presented in the following sections.

4.3.1 North American Provisions (ASCE7-10 and NBCC 2010)

Wind pressures values obtained by Davenport et al (1977, 1978) at the University of Western Ontario; Best and Holmes (1978) at the James Cook University of North Queensland; and Stathopoulos (1981), Stathopoulos and Zhu (1988), Stathopoulos and Luchian (1990, 1992), and Stathopoulos and Saathoff (1991) at Concordia University were refined to reflect results of full-scale tests obtained by Marshall (1977) at the National Bureau of Standards; and Eaton and Mayne (1975) at the Building Research Station, England. Then, these values were used to generate current wind pressures of chapter 30 in ASCE7-10 (components and cladding) for enclosed or partially enclosed low-rise buildings with flat roof, hip roof and gable roof.

ASCE 7-10 and NBCC 2010 give the external peak pressure coefficients on building cladding directly as GC_p and C_pC_g, respectively. Thus, the gust factor on the pressure coefficients and the mean pressure coefficients are given directly together for the loading zones (edge, corner and interior zones) in simple graphs versus the tributary area. Figure 4.2 presents ASCE 7-10 and NBCC 2010 roof zones and the external peak pressure coefficients, CpCg, on edge, corner and interior zones of flat roof buildings. As reference

for a purpose of comparison, mean hourly velocity pressure at mean roof height is used for the pressure coefficients in this figure.

Figure 4.2 shows that there is numerical variation between the ASCE 7-10 and NBCC 2010 values, such that the values recommended by ASCE 7-10 are somewhat higher than those recommended by NBCC 2010 for each zone. This disparity is due to the directionality factor $K_d = 0.85$ which applies to ASCE 7-10 but not to NBCC 2010, the latter has already incorporated this effect in the CpCg values. Therefore, to make the code pressure coefficients comparable, the values of ASCE 7-10 in Figure 4.2 have been multiplied by 0.85. ASCE 7-10 and NBCC 2010 provide also positive pressure coefficients for all zones as functions of tributary area.

The current definition of roof zones of ASCE7-10 and NBCC 2010 depends on the distribution of the local peak and area-averaged peak pressure coefficients. The entire roof is grouped into a set of zones; square corner, edge and interior zones; such that the width of the corner zones and edge zones are equal. The zone sizes are uniquely defined as a function of the building height and the least horizontal dimension of the building with ratios built up to provide the suitable size for various low-rise building geometries. These ratios are 0.1Ds, 0.4H and 0.04Ds with a lower limit of 1.0 m. The current ASCE 7-10 and NBCC 2010 define the edge zone width (Z) as follows:

"*End- zone width z is the lesser of 10% of the least horizontal dimension and 40% of the height, h, but not less than 4% of the least horizontal dimension or 1m*". (NBCC 2010).

These conditions are shown graphically at the lower part of Figure 4.2 with buildings with three different H/D ranges denoted by Ⅰ, Ⅱ and Ⅲ. The size of the edge zone may be small or large depending on the building configuration. So the reference should be made to situations where each parameter of ASCE 7-10 and NBCC 2010 (0.1Ds, 0.4H or 0.04Ds) could dominate the edge zone width. For example, roofs of buildings of very large

horizontal dimensions compared with their heights may be designed according to the design criterion (0.04Ds) - see lower part of Figure 4.2.

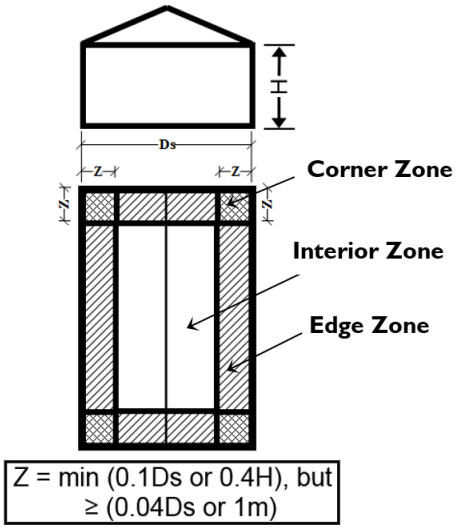

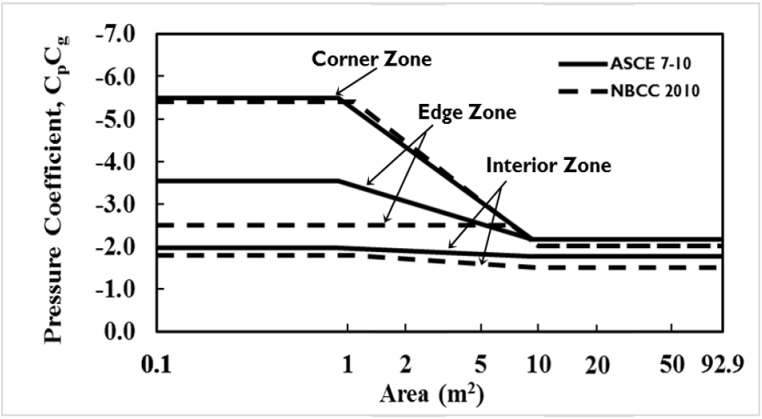

Ds: Minimum horizontal dimension
H: Eave height

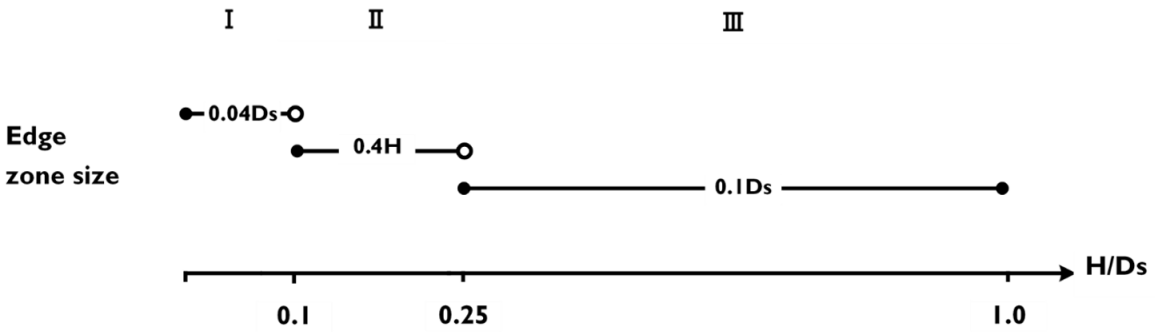

Figure 4.2: Roof zones and external peak pressure coefficients, CpCg, on edge, corner, and interior zones of building roofs with a slope of 7° or less in ASCE 7-10 and NBCC 2010.

The current roof patterns and the guidelines to create the roof zones adopted by ASCE 7-10 and NBCC 2010 are largely based on works conducted in the late 1970s by Stathopoulos (1979). This comprehensive study was aimed directly at the codification and zone description suitable for design pressure coefficients to be used for wind loading. Roof zones were generated by examining roof pressures from several studies with different building heights, plan dimensions, wind simulation conditions and scales. Table 4.2 summarizes all examined experimental studies along with their sources. Generally, the investigation included every combination of different near-flat roofs with angles between 0 and 7 degrees; and different plan dimensions. Also, experiments carried out at different scales (full scale and wind tunnel scale) with different terrain exposures were considered. Wind tunnel experiments were from different boundary layer wind tunnel laboratories, so a fair amount of variability of the results was expected.

For normal wind direction two patterns of pressure distribution have been observed depending on the building plan size; see Figure 4.3. Figure 4.3(a) represents the general simplified trace of pressure distribution over relatively small roofs - for this group of buildings the pressure distribution collapses slowly; moreover, the reattachment (if any) occurs further away from the leading edge. Figure 4.3(b) represents the general simplified trace of pressure distribution over relatively large roofs. For this case, the pressure distribution collapses rapidly until the point of first reattachment and thereafter the flow is retreated close to the surface and runs away smoothly.

Based on the observed pressure distribution patterns, a methodology of two forms was derived to define the sizes of the roof zones: first, the edge zone size was defined as the distance required for the maximum negative peak or mean pressure coefficient at the leading edge to reach to 70% of its value - see Figure 4.3(a). Second, the edge zone size was defined as the distance from the leading edge to the point where the flow is being reattached - see Figure 4.3(b).

The edge/corner zone sizes created according to this methodology are denoted by “Z” and shown in Table 4.2 for all different cases. The ratios of edge zone size to building height

(Z/H) and edge zone size to minimum horizontal plan dimension (Z/B) have been provided. These ratios (Z/H and Z/B) were developed and transformed to be the design parameters of the roof zoning guidelines as minimum of 0.4H and 0.1Ds. In addition, a minimum size of 0.04Ds or 1m was introduced to accommodate all cases. Indeed, the parameter 0.04Ds was found to be the least among all Z/B ratios examined. Also, the least edge zone size among all examined buildings was found equal to 1m, so this was considered the lowest possible edge zone size.

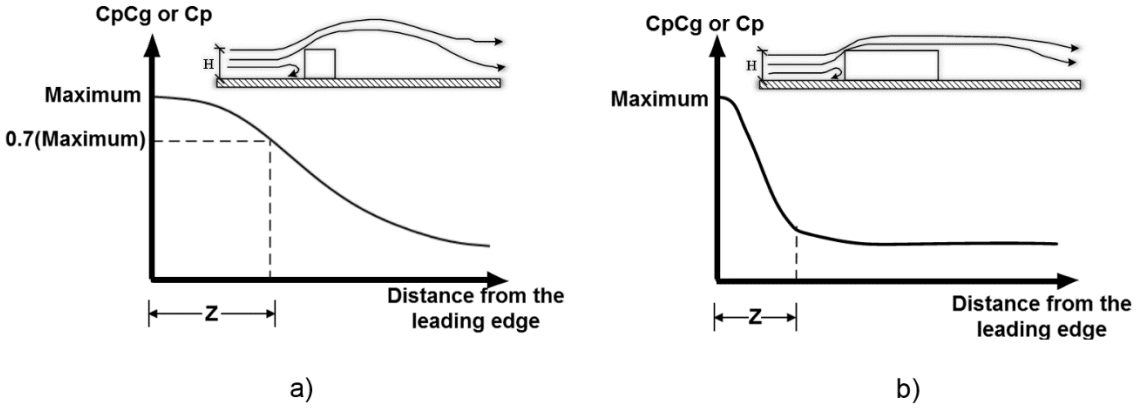

Figure 4.3: Mean and negative peak pressure distribution curves over building roofs:

a) Common roofs, b) Large roofs.

Table 4.2: Literature sources of experimental studies investigated by Stathopoulos (1979).

Building #	Reference	Scale	Building dimensions, m (ft)		H/B	Zone width, Z, m (ft)	Z/H	Z/B
			Height	Width				
1	Barnaud and Gandemer, 1974	1:75	5 (16)	7 (23)	0.70	1 (3.2)	0.20	0.14
2	Davenport and Surry, 1974	1:500	15 (50)	76 (250)	0.20	5 (18)	0.36	0.07
3	Davenport and Surry, 1974	1:500	15(50)	137 (450)	0.11	5 (18)	0.36	0.04
4	Davenport and Surry, 1974	1:500	15 (50)	152 (500)	0.10	7 (24)	0.48	0.05
5	Hellers and Lundgren, 1974	1:250	5 (18)	12 (40)	0.45	1 (4)	0.22	0.10
6	Hellers and Lundgren, 1974	1:250	11 (35)	12 (40)	0.88	2 (6)	0.17	0.15
7	Hellers and Lundgren, 1974	1:250	22 (72)	12 (40)	1.80	3 (10)	0.14	0.25
8	Hillier, 1973	1:250	19 (62)	44 (145)	0.43	6 (20)	0.32	0.14
9	Holmes and Best, 1978	1:50	5 (16)	7 (23)	0.70	1 (2.5)	0.16	0.11
10	Jensen and Frank 1965	Full Scale	2 (5.3)	2 (5)	1.06	0.4 (1.3)	0.25	0.26
11	Kramer and Gerhardt, 1975	1:250	VARIABLE				0.12 to 0.50	0.12
12	Marshall, 1974	Full Scale	2 (8)	4 (12)	0.67	1 (2.5)	0.31	0.21
13	Marshall, 1974	Full Scale	5 (16)	7 (23)	0.70	1 (3)	0.19	0.13
14	Stathopoulos, 1975	1:500	15 (50)	76 (250)	0.20	3 (10)	0.20	0.04
15	Stathopoulos, 1975	1:500	69 (225)	76 (250)	0.90	3 (10)	0.04	0.04
16	Stathopoulos, 1979	1:250/1:500	5 (16)	24 (80)	0.20	2 (6)	0.37	0.07
17	Stathopoulos, 1979	1:250/1:500	7 (24)	24 (80)	0.30	2 (6)	0.25	0.07
18	Stathopoulos, 1979	1:250/1:500	10 (32)	24 (80)	0.40	2 (6)	0.19	0.07
19	Surry et al., unpublished	1:500	23 (74)	50 (164)	0.45	8 (25)	0.34	0.15
20	Surry et al., unpublished	1:500	23 (74)	378 (1240)	0.06	20 (67)	0.91	0.05
21	Surry et al., unpublished	1:500	32 (105)	132 (433)	0.24	13 (42)	0.40	0.10
22	Vickery, 1976	1:300	8 (25)	30 (100)	0.25	4 (12.5)	0.50	0.13
23	Vickery, 1976	1:300	15 (50)	30 (100)	0.50	8 (25)	0.50	0.25
24	Vickery, 1976	1:300	20 (66)	98 (320)	0.21	10 (33)	0.50	0.10
25	Wiren, 1971	1:1500	29 (95)	61 (200)	0.48	9 (28.5)	0.30	0.14
26	Wiren, 1971	1:1500	29 (95)	122 (400)	0.24	9 (28.5)	0.30	0.07

4.3.2 European Standard (EN 1991-1-4:2005)

The European standard (EN 1991-1-4:2005) divides the roof into three loading zones, namely corner, edge and two zones in the middle area of the roof. The European standard recommends L-Shape corner zone. The size of the roof zones depends on building height and crosswind dimension of the building plan, as depicted in the plan view given in Figure 4.4. The length of the corner zone is defined as the minimum of the 25% of the crosswind plan dimension (D) or 50% of the building's eave height (H), while the width of the corner and edge zones is the minimum of the 10% of the crosswind plan dimension or 20% of the eave height of the building.

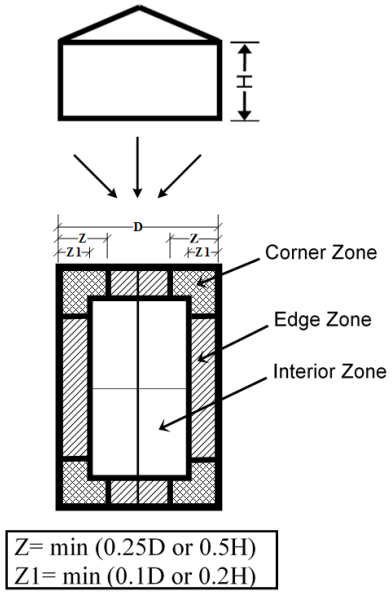

Figure 4.4: Roof zones of building roofs with a slope of $-5^o \leq \alpha \leq 5^o$ recommended by European Standard (EN 1991-1-4:2005).

In EN 1991-1-4:2005, the terrain and topographic effects on the design wind pressures are taken into account together with the effect of exposure. The following equation expresses this relation:

$$C_e(z) = [1 + 7 \times I_V(z)] \times C_r^2 C_o^2 C_{dir}^2 C_{season}^2 \quad (4.1)$$

where $C_e(z)$ is the exposure coefficient, $C_r(z)$ is the roughness factor representing variability of the mean wind velocity at the site of the structure on account of the height above ground surface and ground roughness of the terrain in the wind direction considered; $C_o(z)$ is the orography factor, like hills and cliffs, representing increase in wind speed. However, for cases when the average slope of the upwind terrain is less than 3^o (i.e. flat terrain), $C_o(z)$ is taken as 1.0. Finally, $I_V(z)$ is the turbulence intensity at height z above the ground, and the term $[1 + 7 \times I_V(z)]$ is considered as a gust factor on the pressure.

EN 1991-1-4:2005 specifies two values for external mean pressure coefficients on building cladding. The first is assigned for loaded area of $1m^2$ or smaller and presented by $C_{pe,1}$ as a local coefficient. The second is for loaded areas of $10m^2$ or larger and represented by $C_{pe,10}$ for overall coefficient. Logarithmic interpolation is recommended for intermediate values - see Appendix A4. The EN 1991-1-4:2005 is the only wind code/standard that considers the variation of the wind load with height for low-rise buildings; indeed, the exposure factor is given in a figure as a function of height above terrain and as function of terrain category. EN 1991-1-4:2005 provides only positive pressure coefficients on the leeward half of the roof.

4.3.3 Australian/New Zealand Standard (AS-NZS 1170-2, 2011)

Australia / New Zealand divides the roof of low-rise buildings into square corner zones, edge zones and interior zones (with maximum possible of 3 zones). Uniquely, the zones are also divided into sub-zones on the basis of recommended tributary area that intended for the roof external pressure coefficients $(C_{P,e})$ through the values 0.5h, h, 2h and 3h, where h is the mean roof height and the local pressure factor (K_l) through the dimensions of the building (the minimum of mean roof height, 20% of the cross wind dimension and 20% of the windward dimension). Figure 4.5 shows the zonal system specified by

Australian/New Zealand Standard for flat roofs of low-rise buildings. Figure 4.5 shows the zonal system specified by Australian/New Zealand Standard for flat roofs of low-rise buildings.

AS-NZS 1170-2 (2011) recommends the use of rectangular corner zone (or square in case of buildings with square plan) - see Figure 4.5.

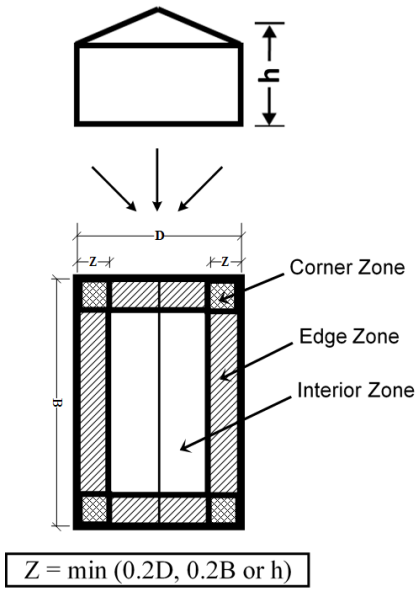

Figure 4.5: Roof zones of building roofs with a slope of 10^{o} or less recommended by Australian/New Zealand Standard.

According to the AS-NZS 1170-2 (2011), the external design pressures on building envelope depend on the aerodynamic shape factors (C_{fig}), which are determined from section five of AS-NZS 1170-2 (2011) by using the following equation:

$$C_{fig} = C_{p,e} K_a K_{c,e} K_l K_P \tag{4.2}$$

The area reduction factor (K_a) for roofs depends on the tributary area (A). The area reduction factor has a maximum value of 1.0 for $A \leq 10\ m^2$, 0.9 for $A = 25\ m^2$ and 0.8 for $A \geq 100\ m^2$. For intermediate areas, linear interpolation can be used to find K_a. The

combination factor $(K_{c,e})$ does not apply for roof cladding, thus it has a value of 1.0 in case of roof pressures acting alone. The local pressure factor (K_l) accounts for high wind pressures on small areas near the corners and edges of the building. Values of (K_l) are provided in Appendix A5 of this thesis.

For flat roofs or roofs with slope less than 10^o local pressure factors, based on the area and location of the area under consideration, are taken 3.0, 1.5 and 2.0 for the designed areas RC1, RA1, and RA2, respectively. The definition of the locations RC1, RA1, and RA2 are provided in Appendix A6. For the area extending beyond the zone Z, as defined in Figure 4.5, K_l =1. Permeable cladding reduction factor (K_P) is given in AS-NZS 1170-2 to consider the effect of surface permeability on the negative pressure.

Values of external pressure coefficients for flat roofs of enclosed rectangular buildings $(C_{p,e})$ of AS-NZS 1170-2 are presented in table form in Appendix A7. Based on the specified $(C_{p,e})$ values, it can be observed that AS-NZS 1170-2 is the only wind code/standard that provides two values for the pressure coefficients on the roofs. Thus, the roof surfaces are subjected to two zonal wind loads; these two values are negative on the windward zones but positive and negative on the leeward zones.

4.4 Comparison of Zonal System Developed by Current Standards/Codes for Large Roofs

As discussed previously, the provisions of the current wind codes and standards were established mainly based on wind tunnel experiments of common model configurations; models with relatively small dimensions. Therefore, it would be of interest to apply the provisions of these codes/standards on flat roofs of low-rise buildings with large dimensions. Such a comparison between the roof zone patterns and sizes of ASCE7-10, NBCC 2010, EN 1991-1-4:2005 and AS-NZS 1170-2 (2011) were conducted for the nine building geometries considered in this study. Figures 4.6, 4.7 and 4.8 show the roof zone patterns introduced by ASCE 7-10 (NBCC 2010), EN 1991-1-4:2005 and AS-NZS 1170-

2 (2011), respectively. Sizes of the roof zones are provided with tables attached to these figures.

Clearly, the differences in the layout of the zonal systems of the roofs are significant between the four international codes/standards considered in this study. As well as significant differences are found in the zone sizes for large roofs. For instance, in ASCE 7-10 (NBCC 2010) roof zone sizes are created by the design criterion of 40% of the least horizontal dimension (0.4Ds) for most geometries. According to EN 1991-1-4:2005, the width of edge/corner zones for all geometries are created by the design criterion of 20% of the eave height (0.2H) and the length of the corner zones are defined by 50% of the eave height (0.5H). Whereas, the width of edge and corner zones of AS-NZS 1170-2 (2011) are determined by the mean roof height (h); the sub-zones within the edge zones are governed by (0.5h), while the interior sub-zones by (h) for all geometries considered in this study.

EN 1991-1-4:2005 underestimates the width of the edge zone for all buildings compared to ASCE 7-10 (NBCC 2010) with factors in the range of 2 to 7 and with a factor of 5 compared to the size of the edge zone of AS-NZS 1170-2 (2011). On the other hand, the results of the comparison show that the edge zone width for building geometries of relatively large roofs estimated by ASCE 7-10 (NBCC 2010) are roughly comparable to those estimated by AS-NZS 1170-2. For example, for building geometries B6, B8, B9 the edge zone widths of ASCE 7-10 (NBCC 2010) are 7.2, 4.8 and 7.2 m, respectively; while those estimated by AS-NZS 1170-2 (2011) are 7.5, 5.0 and 5.0 m, respectively.

However, ASCE 7-10 (NBCC 2010) and AS-NZS 1170-2 recommend square corner zones and the sizes are different. In detail, the corner zones sizes of ASCE 7-10 (NBCC 2010) are in range of 2 to 3 lower than those of AS-NZS 1170-2 (2011) for buildings of large sizes. For instance, ASCE 7-10 (NBCC 2010) and AS-NZS 1170-2 (2011) assigned 0.64% and 1.2% of the roof area for corner zones on the roof of the building B3, respectively. For building B9 of larger roof dimensions and lower height, ASCE 7-10 (NBCC 2010) and AS-NZS 1170-2 (2011) assigned respectively 0.64% and 0.31% of the roof area for corner zones area. Clearly, the smaller corner zones are recommended by EN 1991-1-4:2005;

0.08% to 0.20% of the roof area specified for corner zones of buildings with the largest roofs (width = 180 m).

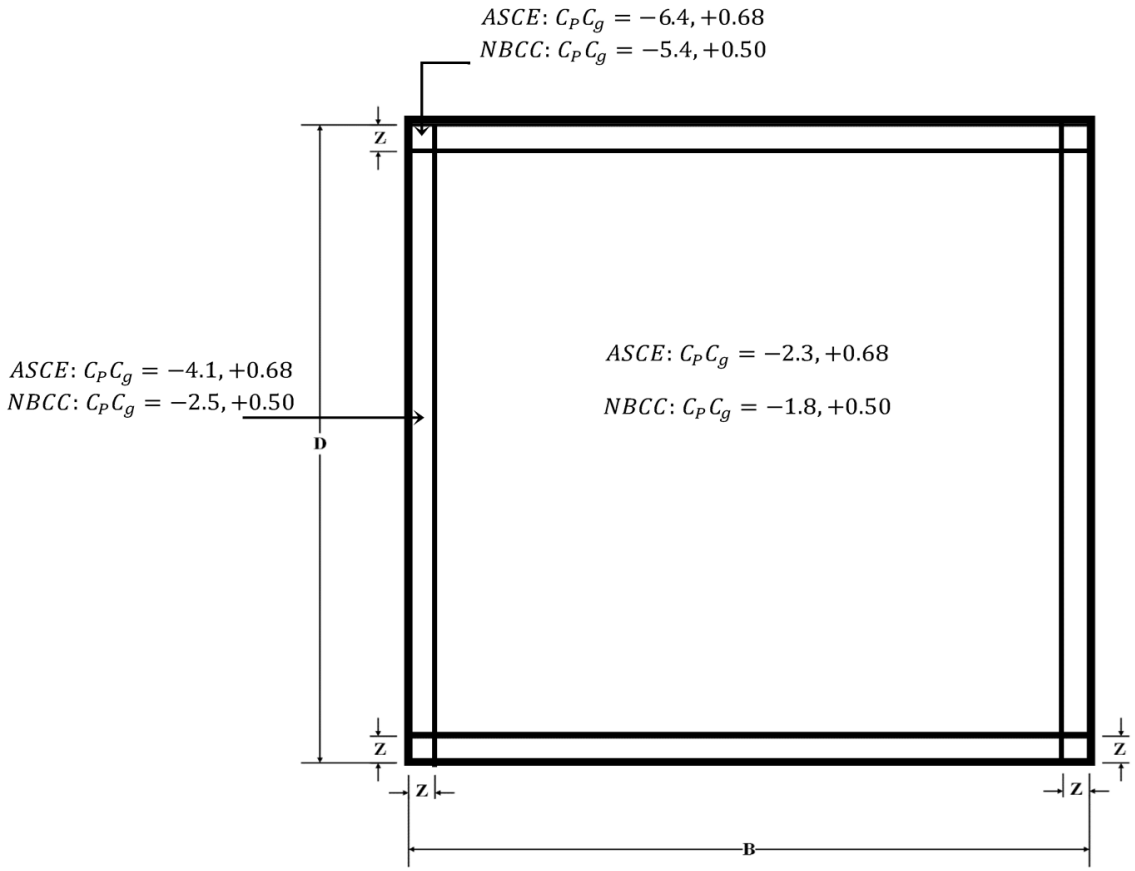

Building dimensions (m)	Z (m)
B1: 60X60X10	4.0
B2: 120X120X10	4.8
B3: 180X180X10	7.2
B4: 60X60X7.5	3.0
B5: 120X120X7.5	4.8
B6: 180X180X7.5	7.2
B7: 60X60X5	2.4
B8: 120X120X5	4.8
B9: 180X180X5	7.2

Figure 4.6: Local pressure coefficients and roof zone sizes provided by ASCE 7-10 and NBCC 2010 for flat roofs of large sizes. (For all wind directions, $C_P C_g$ are based on 1-hr mean wind speed).

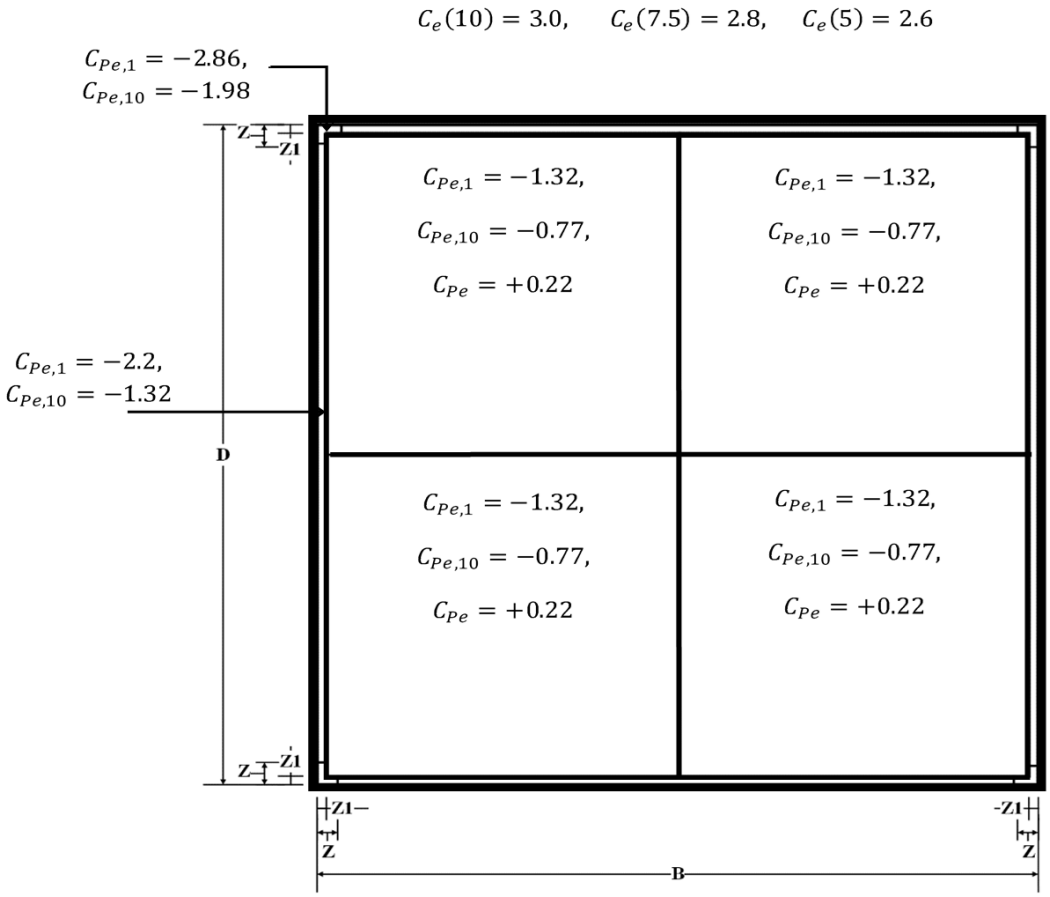

Building dimensions (m)	Z1 (m)	Z (m)
B1: 60X60X10	2.0	5.0
B2: 120X120X10	2.0	5.0
B3: 180X180X10	2.0	5.0
B4: 60X60X7.5	1.5	3.8
B5: 120X120X7.5	1.5	3.8
B6: 180X180X7.5	1.5	3.8
B7: 60X60X5	1.0	2.5
B8: 120X120X5	1.0	2.5
B9: 180X180X5	1.0	2.5

Figure 4.7: Pressure coefficients and roof zone sizes developed by EN 1991-1-4:2005 for flat roofs of large sizes. (For all wind directions, Terrain Category (0), $C_{P,e}$ are based on 1-hr mean wind speed).

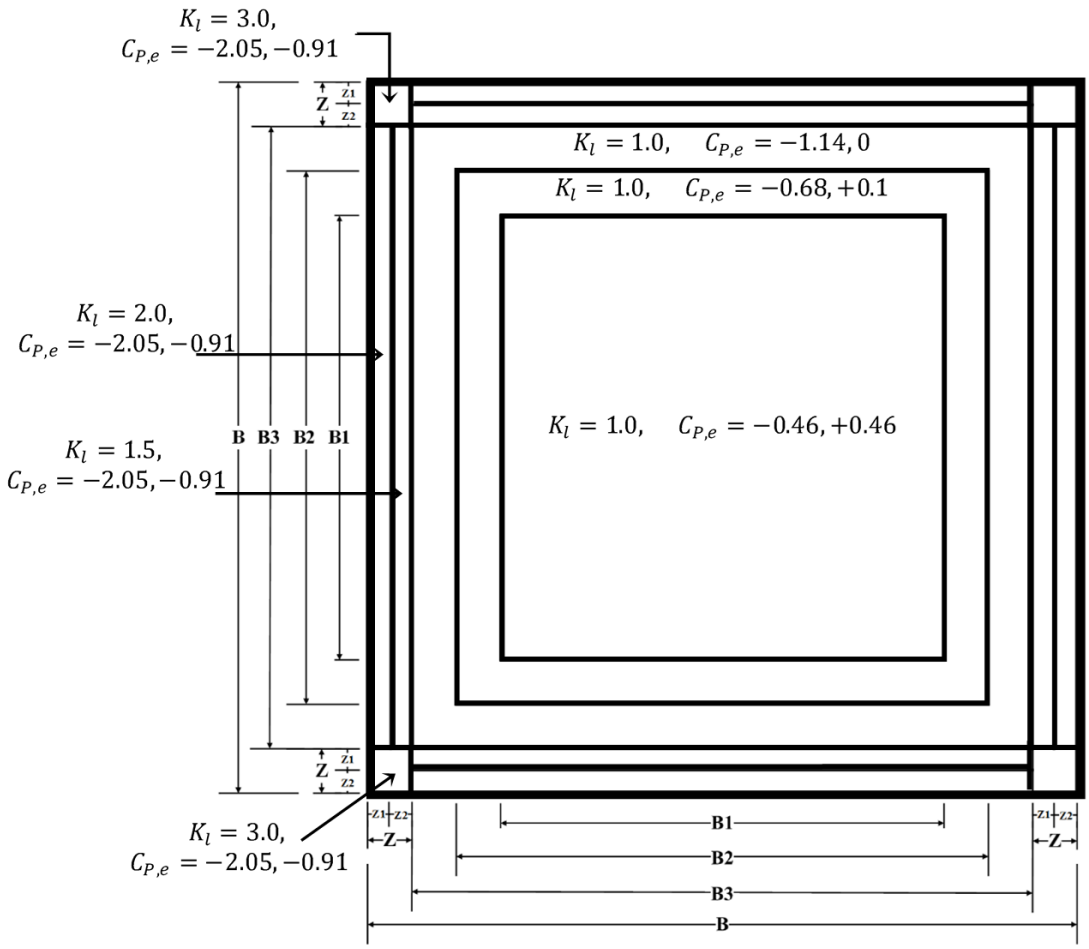

Building dimensions (m)	B1 (m)	B2 (m)	B3 (m)	Z1 (m)	Z2 (m)	Z (m)
B1: 60X60X10	0	20	40	5	5	10
B2: 120X120X10	60	80	100	5	5	10
B3: 180X180X10	120	140	160	5	5	10
B4: 60X60X7.5	20	30	45	3.8	3.8	7.5
B5: 120X120X7.5	75	90	105	3.8	3.8	7.5
B6: 180X180X7.5	135	150	165	3.8	3.8	7.5
B7: 60X60X5	30	40	50	2.5	2.5	5.0
B8: 120X120X5	90	100	110	2.5	2.5	5.0
B9: 180X180X5	150	160	170	2.5	2.5	5.0

Figure 4.8: Pressure coefficients and roof zones developed by AS-NZS 1170-2 for flat roofs of large sizes. (For all wind directions, $C_{P,e}$ are based on 1-hr mean wind speed).

The design wind loads recommended by the current codes/standards, which are considered in this study, were applied on building geometries of this study. The developed local loads (wind loads on small areas; $A \leq 1m^2$) over the roof zones given by ASCE 7-10 (NBCC 2010), EN 1991-1-4:2005 and AS-NZS 1170-2 (2011) are also shown in Figures 4.6, 4.7 and 4.8, respectively. It must be noted that directionality effects are not considered in these figures.

All codes and standards specify the maximum negative pressure coefficients for corner zones – see Figures 4.6, 4.7 and 4.8. The peak local cladding loads at corner zones of ASCE 7-10, NBCC 2010 and AS-NZS 1170-2 (2011) are roughly equal (–6.4, -5.4, and -6.2, respectively). For peak local loads on the edge zone, the values provided by the ASCE 7-10 and NBCC 2010 are -4.1, -2.5, respectively. The edge zone of the AS-NZS 1170-2 (2011) is divided into two loading sections with peak local loads -4.1 and -3.1.

The values provided by EN 1991-1-4:200 for the corner zones are -8.6, -8.0 and -7.4 and the values for the edge zones are -6.6, -6.2 and -5.7 for building heights 10, 7.5 and 5.0 m, respectively. Clearly, the values provided by EN 1991-1-4:200 for the corner and edge zones are higher than those provided by the other codes and standards by 25% and 50%, approximately.

For the interior zone, ASCE 7-10 and NBCC 2010 provide -2.3 and -1.8, respectively. AS-NZS 1170-2 (2011) divides the interior roof zones into three sections of lower design loads of -1.14, -0.68 and -0.46. Finally, the highest local pressure coefficient is provided by EN 1991-1-4:200: -4.0, -3.7, and -3.4 for building heights 10.0, 7.5 and 5.0 m respectively.

Similar differences have been found for area-averaged pressure coefficients as they apply to tributary areas of various sizes.

It might be concluded from Figures 4.6, 4.7 and 4.8 that for building geometries of relatively low height and very large roof dimensions, the estimated edge and corner zones

are significantly different. These inconsistencies in roof layouts and design wind loads are due to the incoherence among specifications of current national wind code/standard provisions.

CHAPTER 5

RESULTS AND DISCUSSION

Wind pressures over nine large flat roofs of isolated low-rise building models have been investigated experimentally in the wind tunnel of Concordia University. For simplicity and convenience, the results are provided in terms of non-dimensional pressure coefficients. The distribution of the most critical (envelope) pressure coefficients on roofs is important to define appropriate design wind loads. Local pressure coefficients, followed by most critical coefficients of the local pressure and roof zone sizes of the large roofs examined in the present research will be presented in this chapter.

5.1 External Local Pressure Coefficients

The scope of this research is to investigate the characteristics of the fluctuating wind pressure generated over large flat roofs. Figure 5.1 represents the instantaneous wind pressures over the center of a large flat roof for wind direction normal to the leading edge for a total period of 27 seconds (3600 seconds in full-scale). This figure was obtained by superposition of the measured pressure-time history records at different locations on the mid-span roof of building (B7) - see Figure 3.7. As depicted in the figure, the wind pressure fluctuations on the windward area are much higher than the fluctuations on the leeward area (in the range of four to five). Indeed, as evidenced by the time history records attached to the figure, at the windward edge and middle of the roof. Consequently, the statistical correlation between pressures separated by large distances will be very small. Generally, local positive wind pressure (instantaneous values) ranging between 0 and +0.6 on the large roofs tested in this study has been noticed.

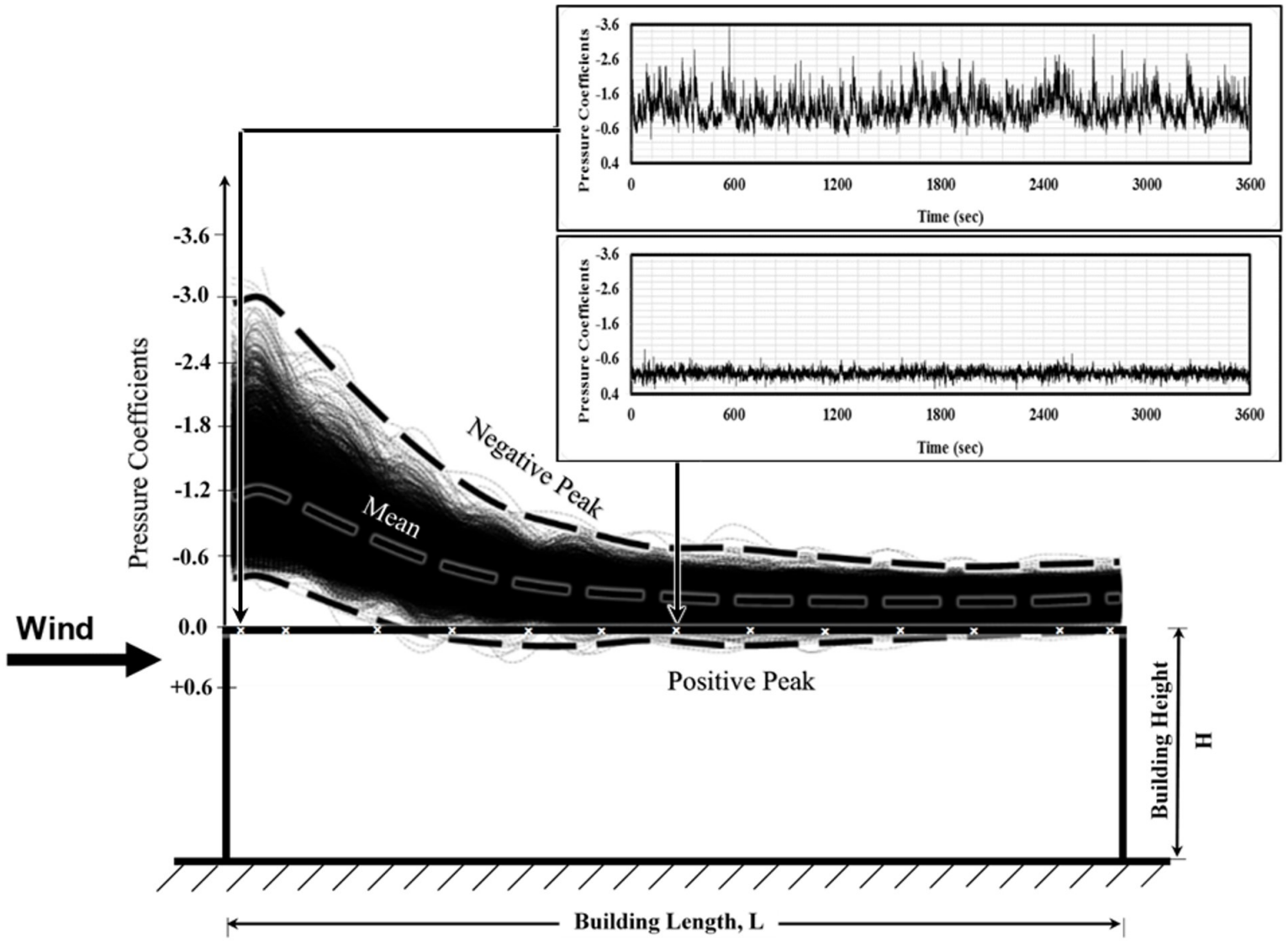

Figure 5.1: Instantaneous pressure distributions and negative peak, mean, and positive peak coefficient values on large flat roofs; the pressure taps are indicated by the symbol, ×.

The negative peak and mean wind pressure coefficients have been determined for all wind directions during the investigation of the wind pressure distributions on building roofs. The distributions of the most critical local pressure coefficients measured from all pressure taps and envelope for all wind directions considered in this study are presented in form of pressure coefficients contours in Figures 5.2 through 5.10. It must be noted that all the contours shown in this thesis were drawn by Surfer (version 11.0.642, 64-bit). Data were fitted using method of triangulation with linear interpolation with 200 nodes in the horizontal and vertical directions and 0.5 contour interval. Moreover, for more accurate drawing, blank grid outside convex hull of the data was not permitted. The distributions of the local pressure coefficients at normal and diagonal wind directions are presented in Appendix B. Since the roof models are square, these pressure contours are shown only on a quarter of the roof but reflect the pressure distribution on the entire roof considering symmetry.

The most critical local pressure coefficients on most parts of the roof regions near windward edge are very high, particularly at windward corners. On the other hand, most critical local pressure coefficients on the rest of the roof regions are relatively low. This is due to the separation of flow occurring at the leading edges. For normal wind direction, high negative peak pressure coefficients appear near the windward edge. However, they decrease towards the leeward edge, so low values of negative peak pressure coefficients appear there. Most critical negative peak pressure coefficients on the windward regions of the roofs are produced by normal or nearly normal wind directions. For example, for (0^o) wind direction, higher negative peak pressure coefficients than for diagonal wind direction have appeared on the edge and corner regions.

Wind-induced pressures on the roofs of isolated buildings depend on roof geometry and dimensions, building height and the characteristics of the approaching wind. Roof dimensions affect the external flow patterns over the roofs, such as flow reattachments on roofs with large dimensions. This implies lower pressure on most part of the roof in comparison with smaller roofs.

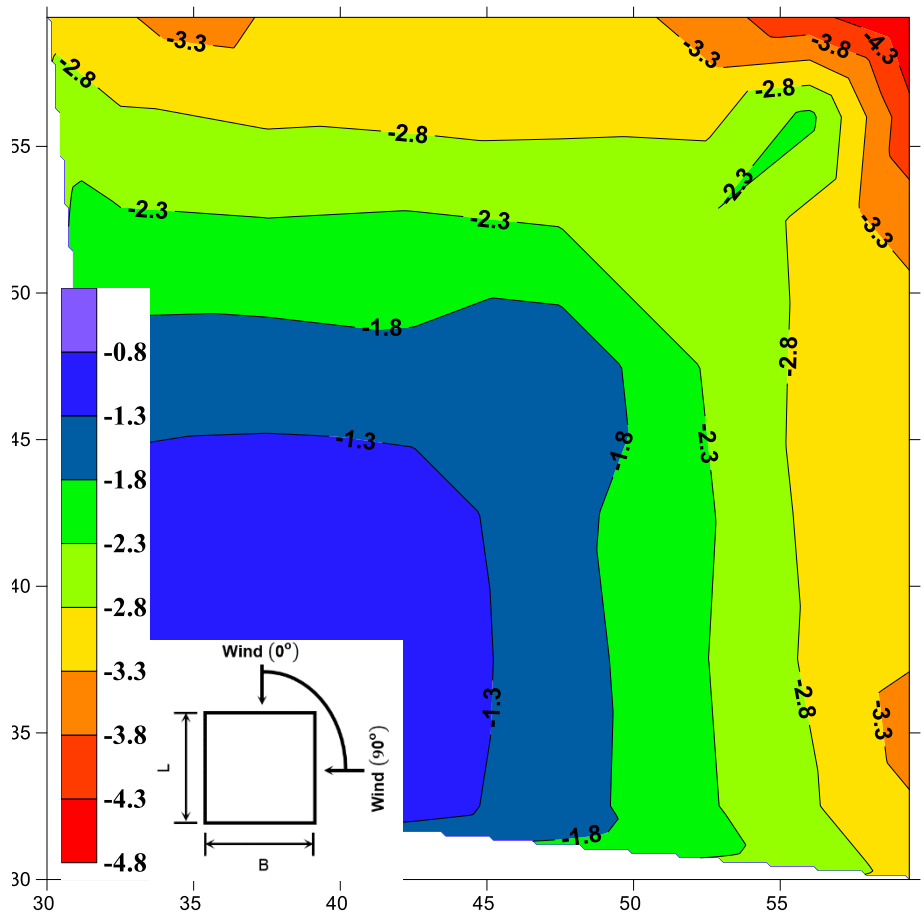

Figure 5.2: Contours of most critical negative peak pressure coefficients (envelope for all wind directions) for building B1:60X60X10 m.

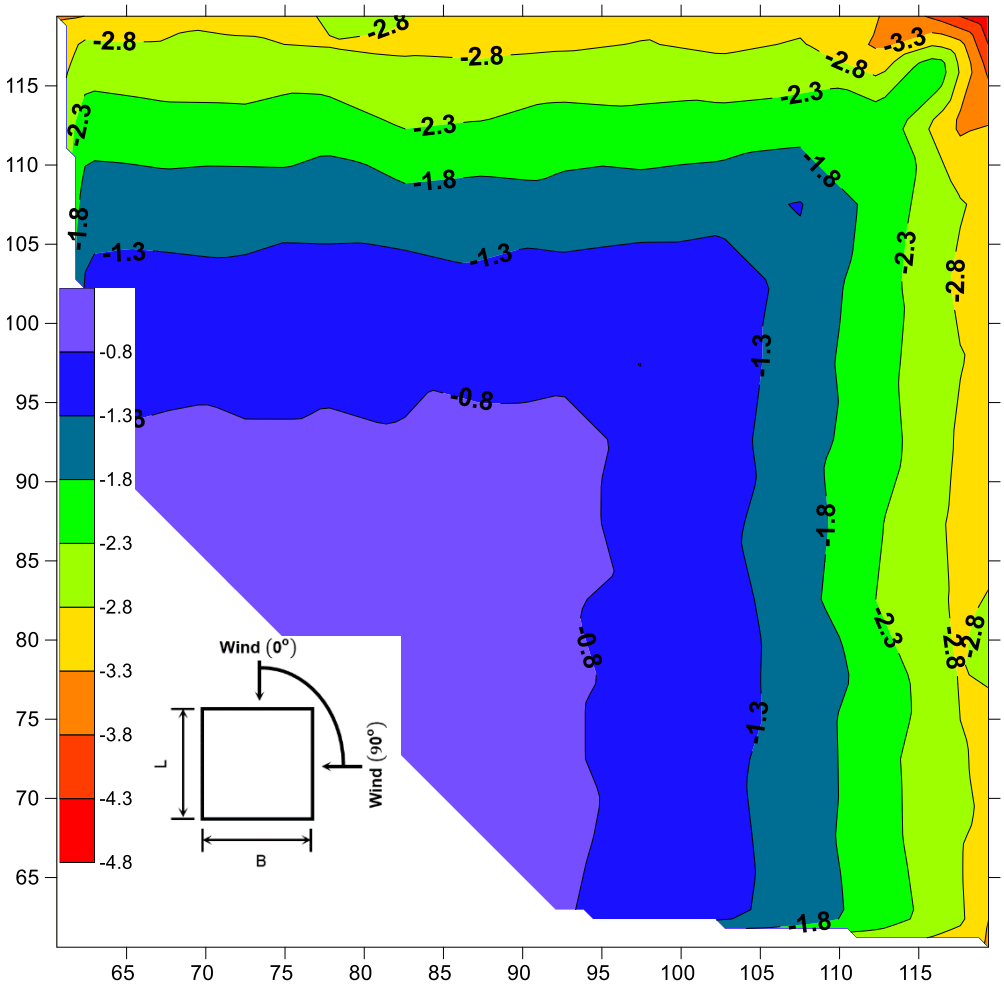

Figure 5.3: Contours of most critical negative peak pressure coefficients (envelope for all wind directions) for building B2:120X120X10 m.

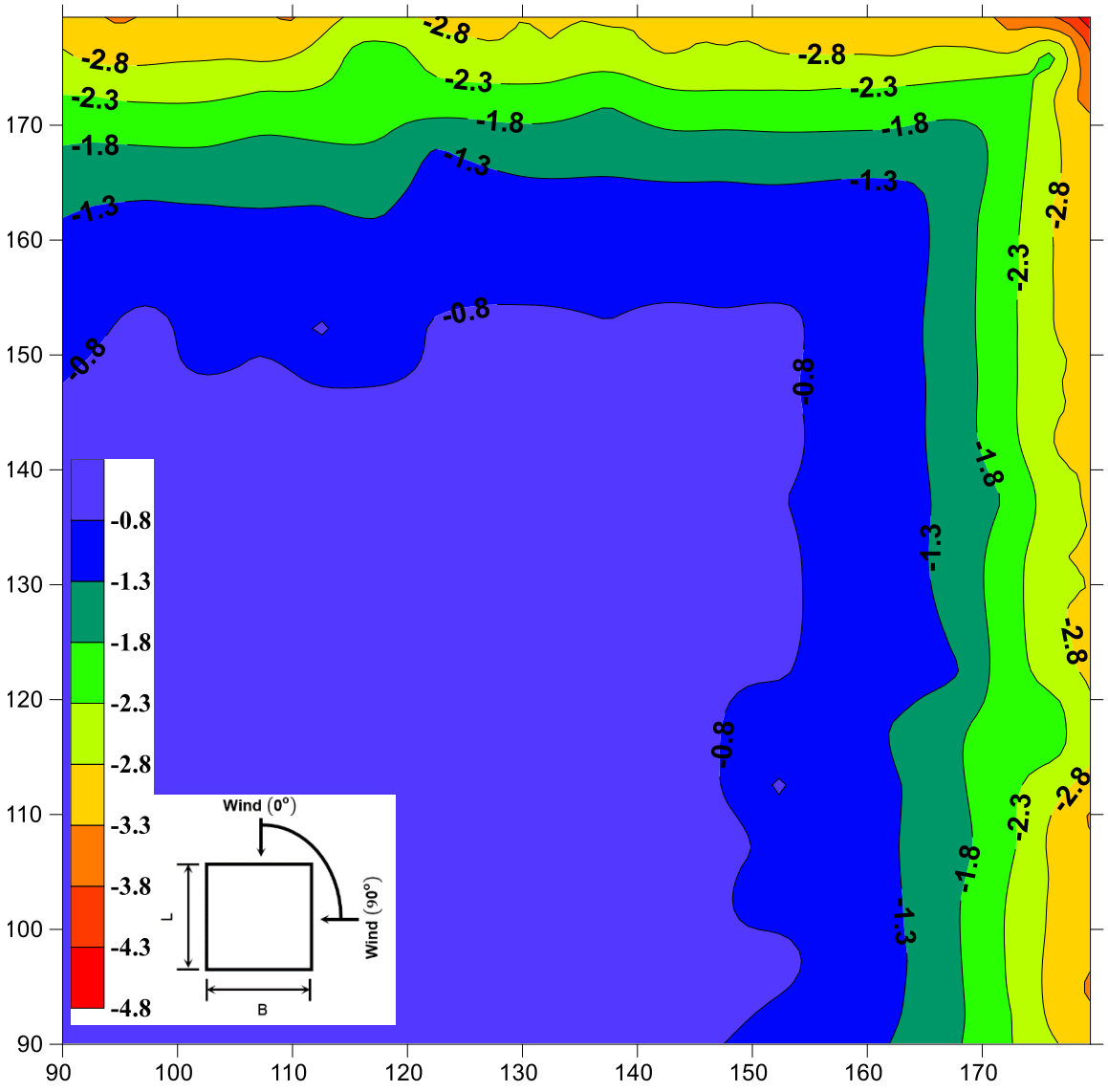

Figure 5.4: Contours of most critical negative peak pressure coefficients (envelope for all wind directions) for building B3:180X180X10 m.

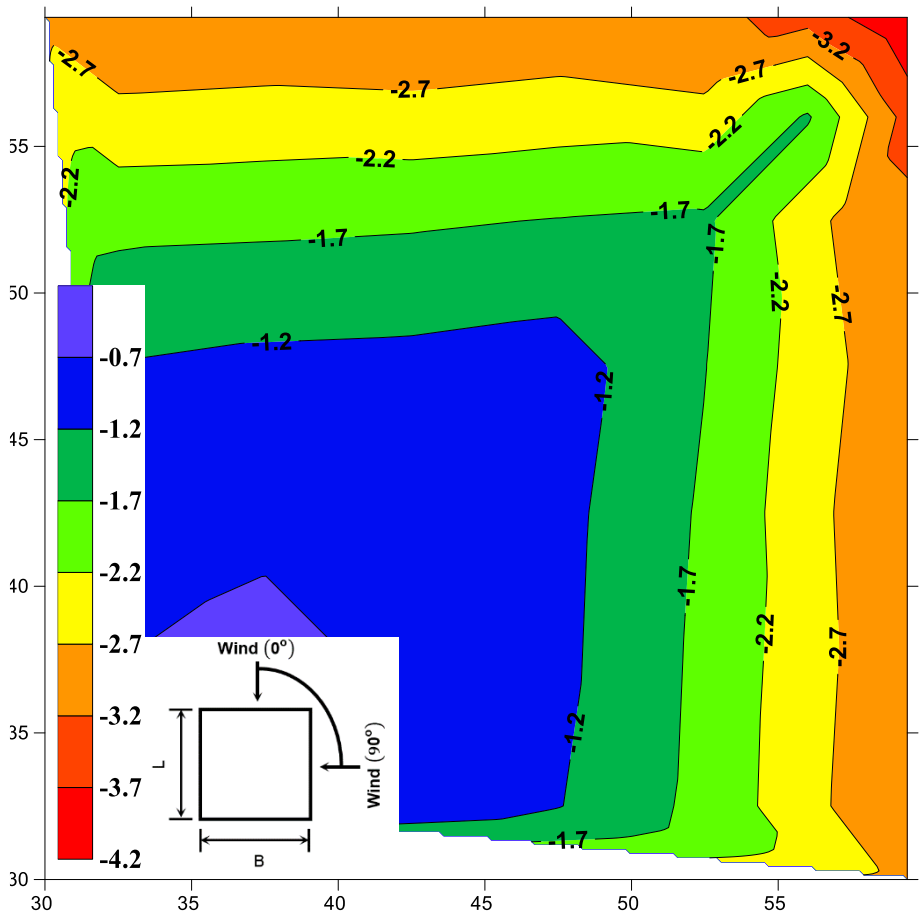

Figure 5.5: Contours of most critical negative peak pressure coefficients (envelope for all wind directions) for building B4:60X60X7.5 m.

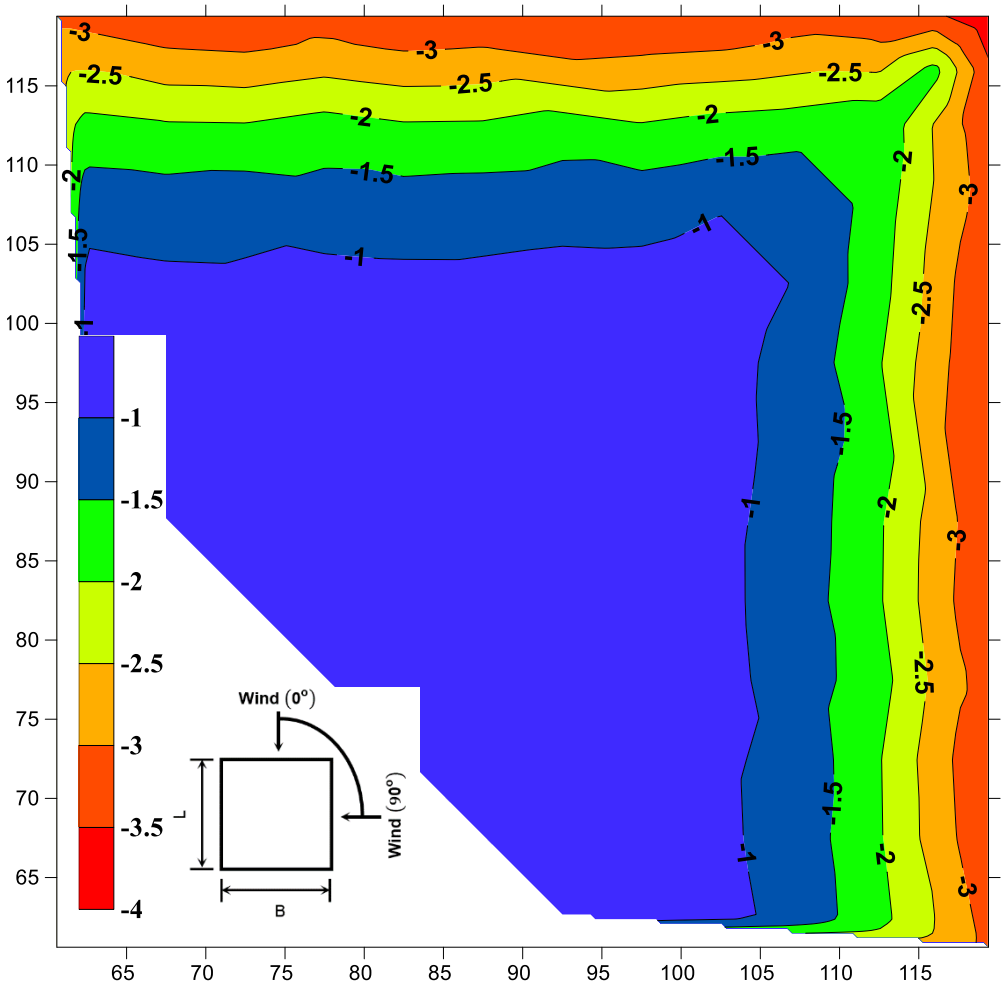

Figure 5.6: Contours of most critical negative peak pressure coefficients (envelope for all wind directions) for building B5:120X120X7.5 m.

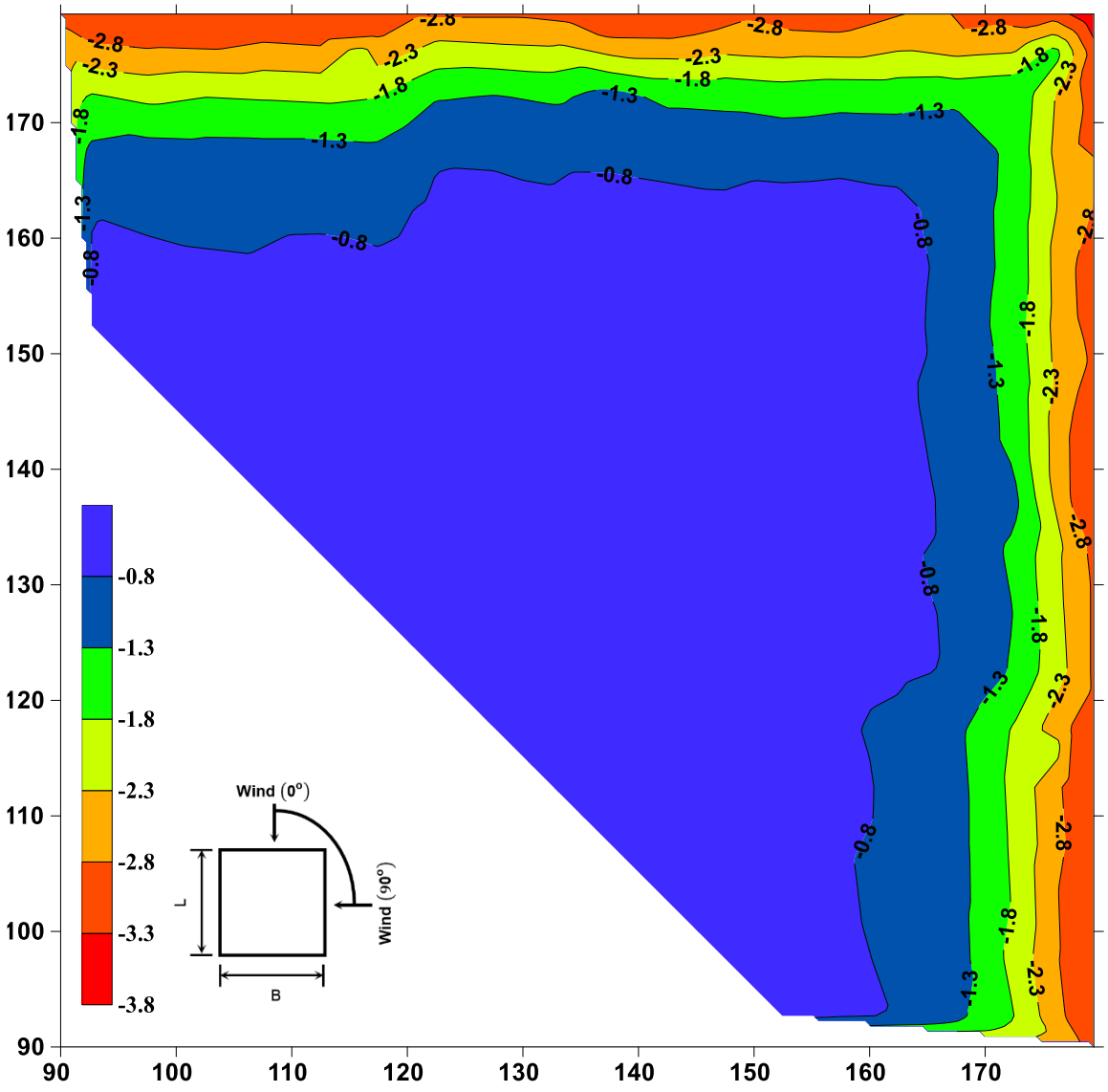

Figure 5.7: Contours of most critical negative peak pressure coefficients (envelope for all wind directions) for building B6:180X180X7.5 m.

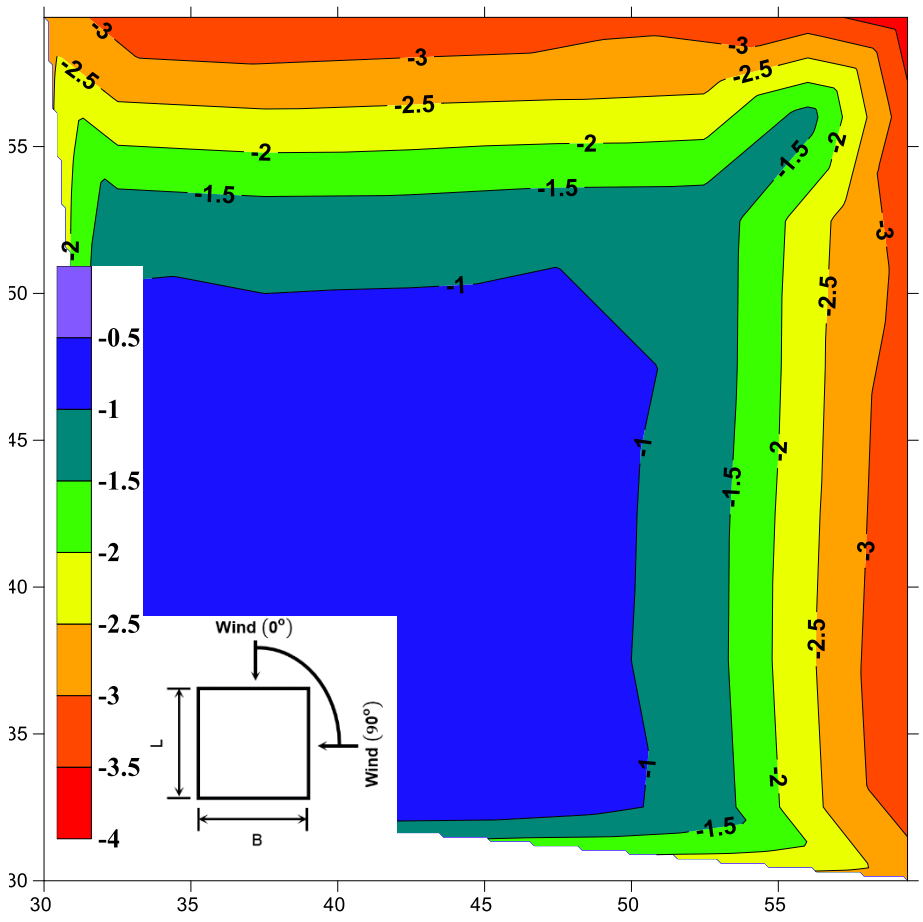

Figure 5.8: Contours of most critical negative peak pressure coefficients (envelope for all wind directions) for building B7:60X60X5 m.

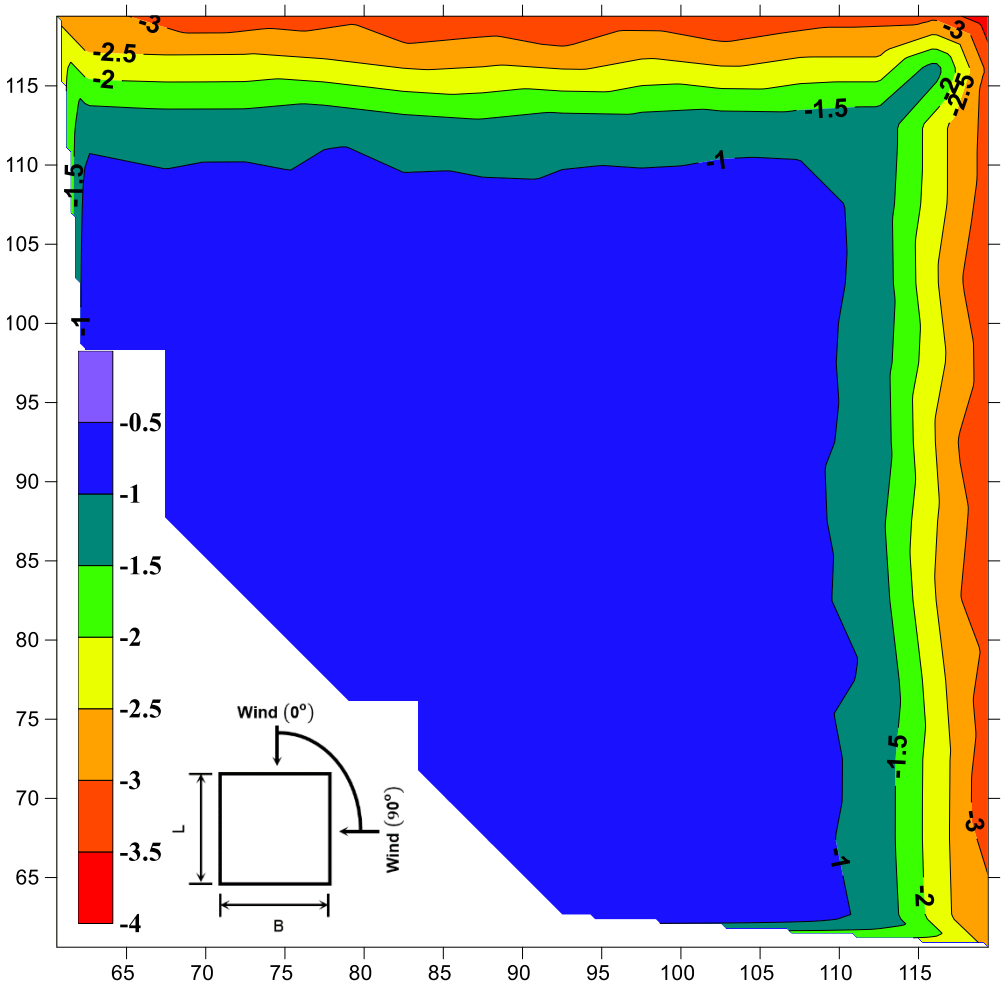

Figure 5.9: Contours of most critical negative peak pressure coefficients (envelope for all wind directions) for building B8:120X120X5 m.

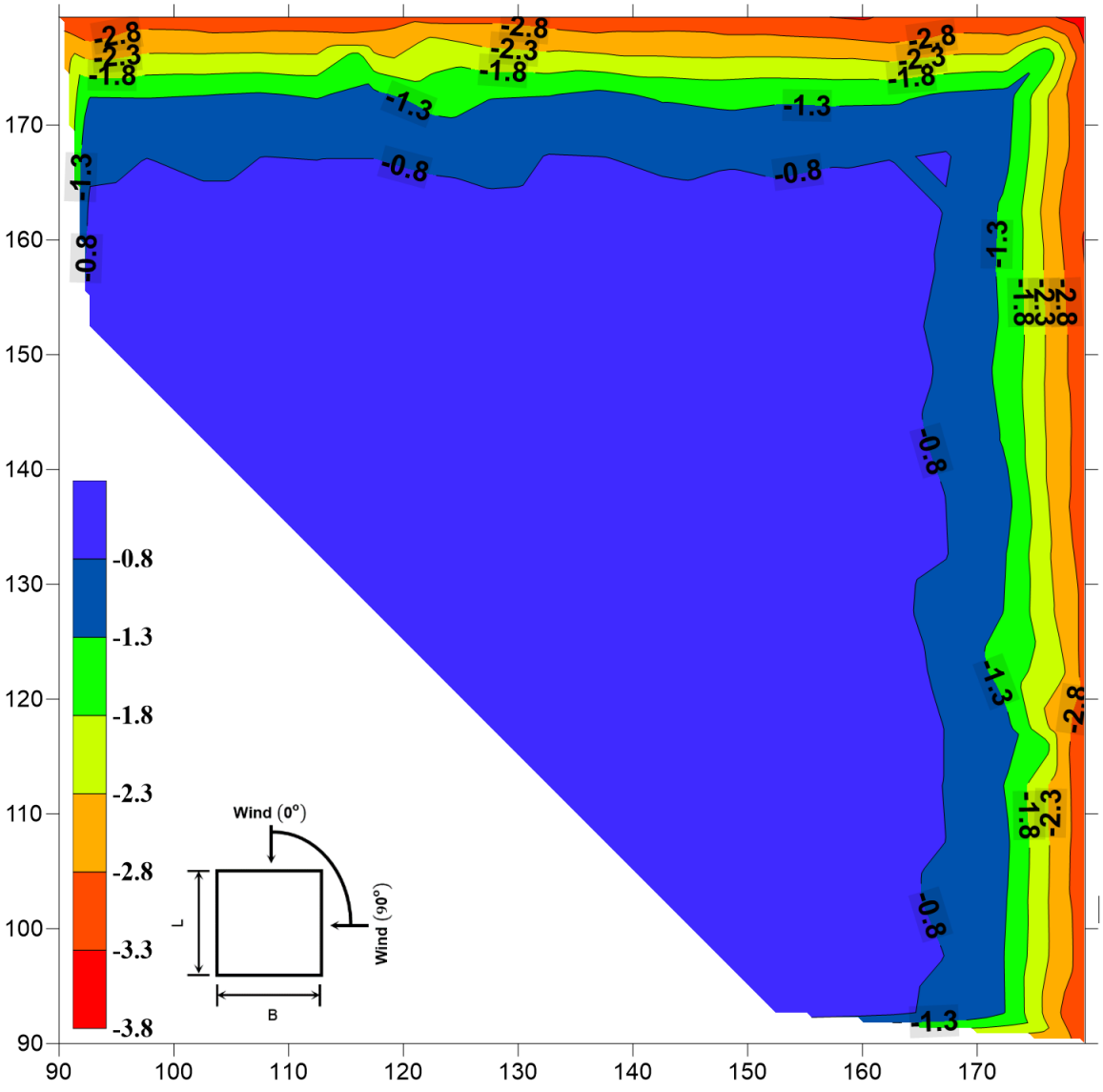

Figure 5.10: Contours of most critical negative peak pressure coefficients (envelope for all wind directions) for building B9:180X180X5 m.

The effect of building height on wind loads acting on large building roofs has been examined. This was by comparing the measured wind pressure coefficients on the roof of tested buildings. The comparison was performed using three different building heights (5.0, 7.5 and 10 m) for 0^o wind direction. Different line groups of pressure taps were used having similar plan dimensions and different roof heights in order to maintain similar ratios of Y/L for comparison, such that the location of the pressure taps relative to leading edge (Y) is normalized by the horizontal plan dimension (L). Figure 5.11 shows the negative peak and mean pressure coefficients along the mid-span.

The results show that the pressure coefficients are relatively high near the leading edge, then they collapse rapidly within the separated flow region for all buildings - see Figure 5.11. The values of negative peak pressure coefficients throughout the separation regions increase with increasing the building height. However, the mean pressure coefficient values beside the leading edge are well close for all buildings of same plan dimension, but their values throughout the separation region are different and increase with the increasing in the building height.

The results show that the lower buildings show the steeper pressure lines throughout the separation zones. Moreover, the distance until the flow gets to reattach to the roof is little affected by the height of the building. For instance, the roof pressure gradients of buildings of width B = 60 m occur to Y/L < 0.5 for the buildings of heights 5, 7.5 and 10 m; see Figure 5.11(a).

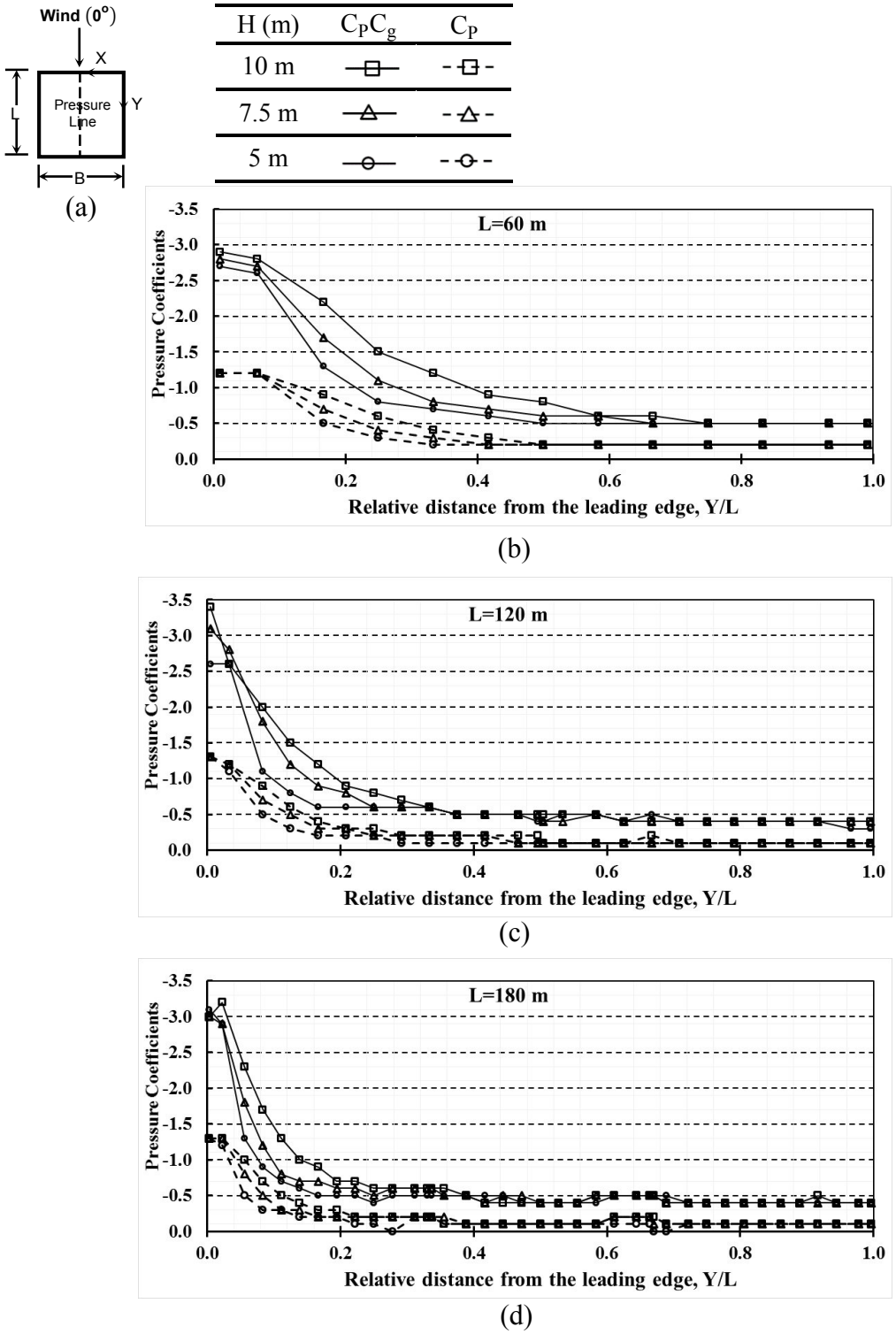

Figure 5.11: Variation of negative peak and mean pressure coefficients along the center line of the tested roofs for 0° wind direction: (a) Model plan view and pressure tap line, (b) H=10 m, (c) H=7.5 m and (d) H=5 m.

For a certain roof height, three buildings of different plan dimensions are chosen for comparison to investigate the effect of the building plan size on the generated wind pressures. The buildings selected are B3, B2 and B1. Figures 5.12 and 5.13 show the negative peak and mean pressure coefficients trace along pressure tap lines selected at mid-span for 0^o wind direction and near the concurrent roof edge for 45^o wind direction.

As can be seen in Figure 5.12, the highest suction near the windward edge decreases with increasing distance from the windward edge. Additionally, Figure 5.12 shows that for normal wind direction the value of the reattachment length increases by a factor of 1.5 for buildings of very large roofs (i.e. B3) as compared to that for other buildings. In terms of relative distances, the position of the reattachment point for buildings of smaller dimensions (B=60 m) is at around Y/L=0.6, whereas for buildings of larger dimensions (B=120 m and B=180 m) reattachment points are at around Y/L=0.3. This shows that the pressure coefficients of relatively low values exist throughout most of the large roof area. On the other hand, for buildings with smaller plan dimensions, most of the roof area is engulfed under the separated flow, and therefore, pressures of relatively high values exist over most of the roof area.

The results for 45^o wind direction are presented in Figure 5.13. The lines were selected near the concurrent roof edges in order to cross the path of the conical vortices in these zones. The location of pressure lines is also shown in Figure 5.13. The traces of the mean and negative peak pressure coefficients shown are clearly affected by the two Delta wing vortices developed along each concurrent roof edge. Note that the buildings of width B=180 m show a somewhat different behavior, particularly at Y/L near 0.4. This is to say that in general, the wind flow reattachment pattern is somewhat different for very large buildings.

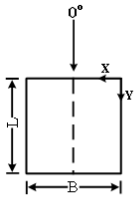

a)

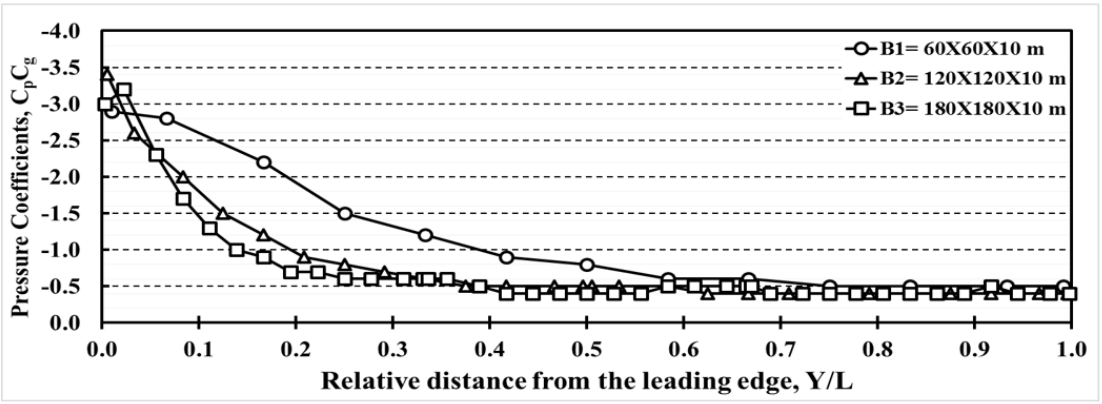

b)

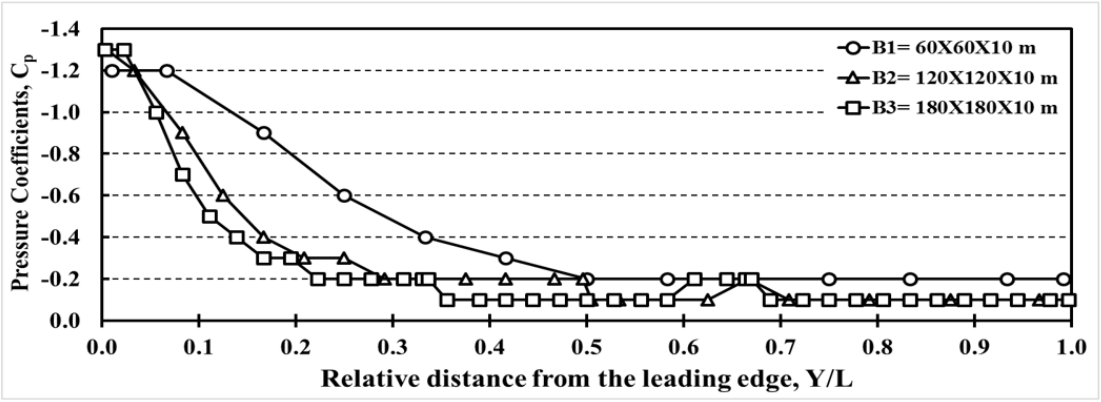

c)

Figure 5.12: Variation of negative pressure coefficients along the roof centerline for the tested buildings of 10 m height for 0°: (a) Model plan view and pressure tap line location, (b) Peak pressure coefficients, C_pC_g and (c) Mean pressure coefficients, C_p.

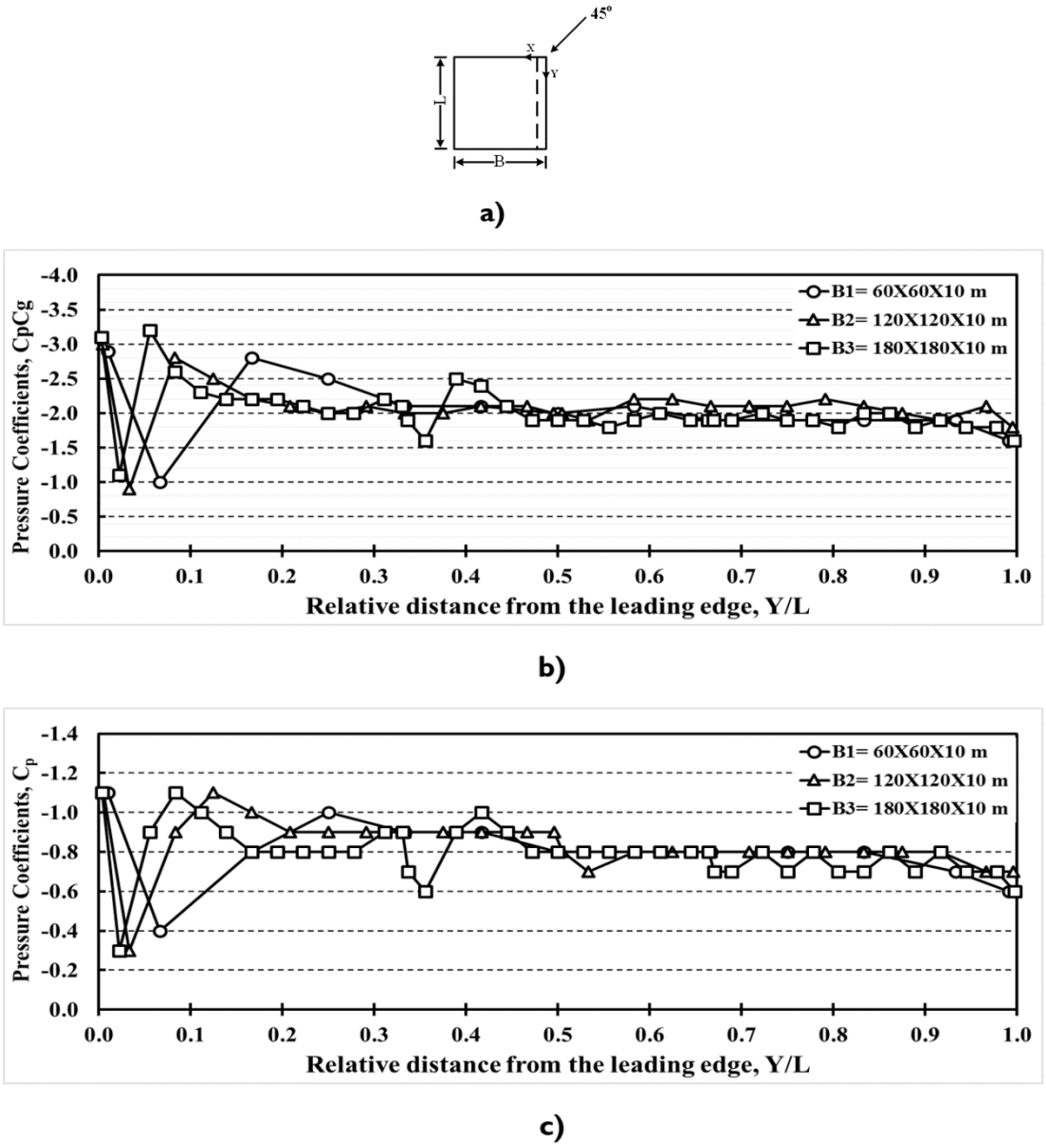

Figure 5.13: Variation of negative pressure coefficients along the line at the concurrent edge for the tested buildings of 10 m height for 45°: (a) Model plan view and pressure tap line location, (b) Peak pressure coefficients, C_pC_g and (c) Mean pressure coefficients, C_p.

The variations of extreme negative peak and mean pressure coefficients on windward corner and edge of the roofs were determined as a function of the wind direction and compared among all tested models. Figure 5.14 presents the extreme negative peak and mean pressure coefficients over the corner zone, whereas Figure 5.15 presents the extreme negative peak and mean coefficients over the edge versus the wind direction. The comparisons were carried out for wind directions between 0^o and 90^o with 15^o increments. The pressure variations in the figures have taken the advantages of the symmetries of the roofs, therefore values for wind directions between 0^o and 45^o are only presented.

As shown in Figure 5.14, the values of negative peak and mean pressure coefficients vary with wind direction. The highest values are observed at normal wind direction (0^o and 15^o), then the variation turns down to the lowest values at oblique direction (45^o). The magnitude of extreme pressure coefficients over the corner zones is mainly affected by the building height; the highest building has the worst pressure coefficient on the corner.

Figure 5.15 shows the variation of extreme negative peak and mean pressure coefficients on windward edge versus the wind direction. The magnitude of extreme negative peak and mean pressure coefficients decreases as the wind orientation changes from normal to oblique wind azimuth (from 0° to 45°). The patterns show that, extreme pressure coefficients over the edges are particularly less vulnerable to the impact of building height than those in corner regions.

5.2 Area-Averaged Pressure Coefficients

In addition to local pressure coefficients, area-averaged negative peak pressure coefficients are very important. The wind loads acting on roof members and cladding are generally reduced due to area-averaging of wind pressures. Also, since the design wind loads of most current wind codes and standards are specified as a function of the loading area (tributary area), the most critical area-averaged pressure coefficients are important in order to examine the suitability of the current wind load provisions for very large low buildings.

In this section, variations of the negative peak area-averaged pressure coefficients obtained in the present study with loading areas will be discussed. Therefore, the most critical negative peak area-averaged pressure coefficients are provided as functions of tributary area, consistently with the current North American standards and codes. For purpose of calculating the area-averaged wind pressure coefficients, eight square tributary areas of different sizes ranging from 2.4 m^2 to 827 m^2 were selected at the windward corner of the building roof for one pressure tap and 48 pressure taps, respectively. Figure 5.16 shows the tributary areas and the pressure taps used in the evaluation of area-averaged wind pressure coefficients.

The negative area-averaged peak pressure coefficients of the corner zones of all tested models and for each wind direction considered in this study are determined simultaneously and presented in Appendix C. Clearly, the most critical values occur when the wind direction is normal or nearly normal to the edge of the roof (between 0^o and 15^o).

Figure 5.17 presents the most critical negative peak area-averaged pressure coefficients for the corner zones recorded over all wind directions for each tested model. As expected, the area-averaged pressure coefficients decrease in value over the tributary area with significant reduction from the local peak negative pressure coefficient. Greater reductions are observed at larger tributary areas.

For tributary areas larger than 2.5 m^2 and smaller than 100 m^2, the area-averaged pressure coefficients decrease more rapidly with the tributary area. Moreover, Figure 5.17 indicates that the values of the most critical negative peak pressure coefficients (local and area-averaged coefficients) measured over the leading corners of the roofs seem to be a little affected by the building plan dimensions for the three heights considered in this study. Generally, the area-averaged pressure coefficient values do increase with height.

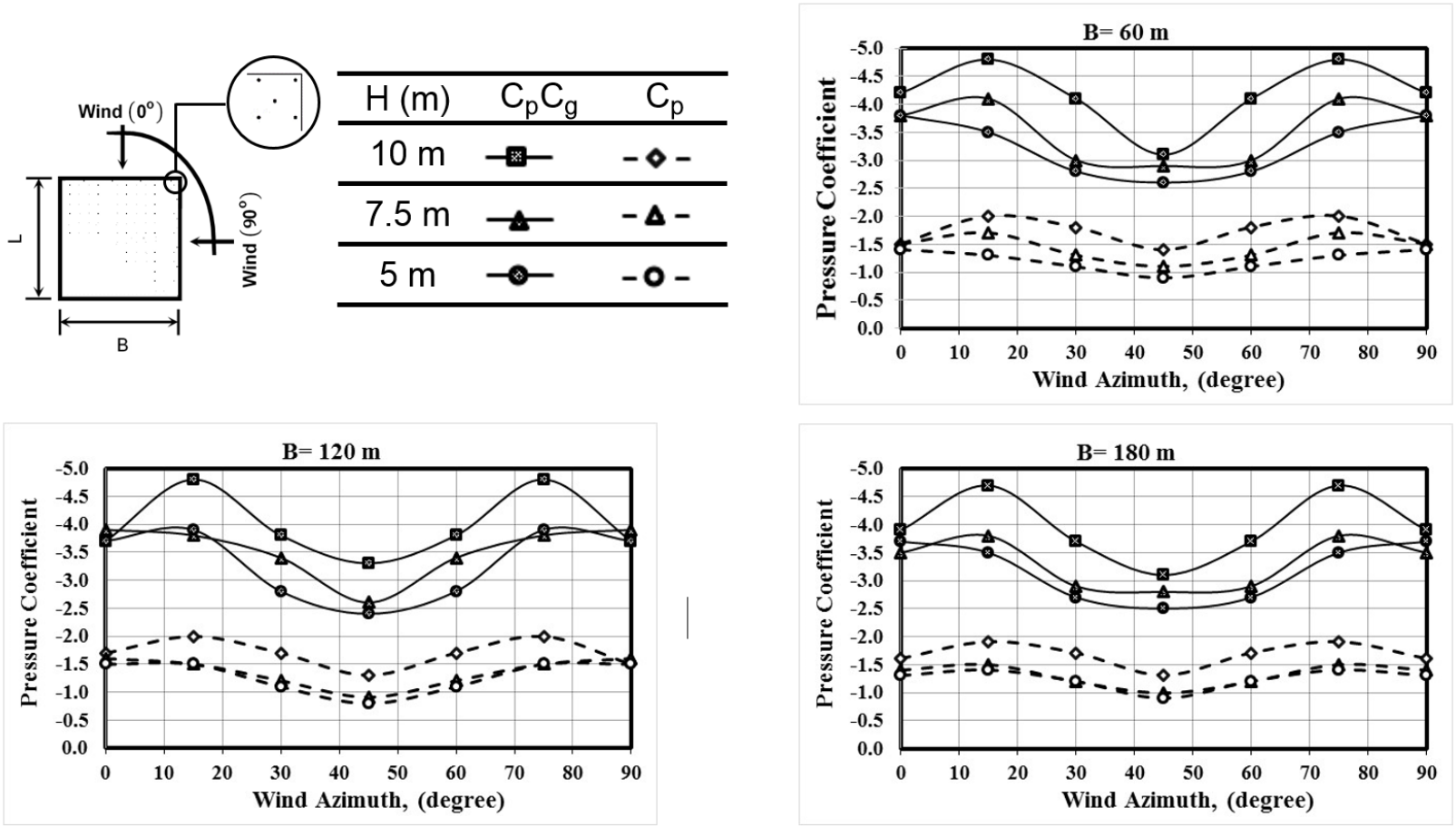

Figure 5.14: Extreme negative peak and mean pressure coefficients on windward corner of the building versus wind direction.

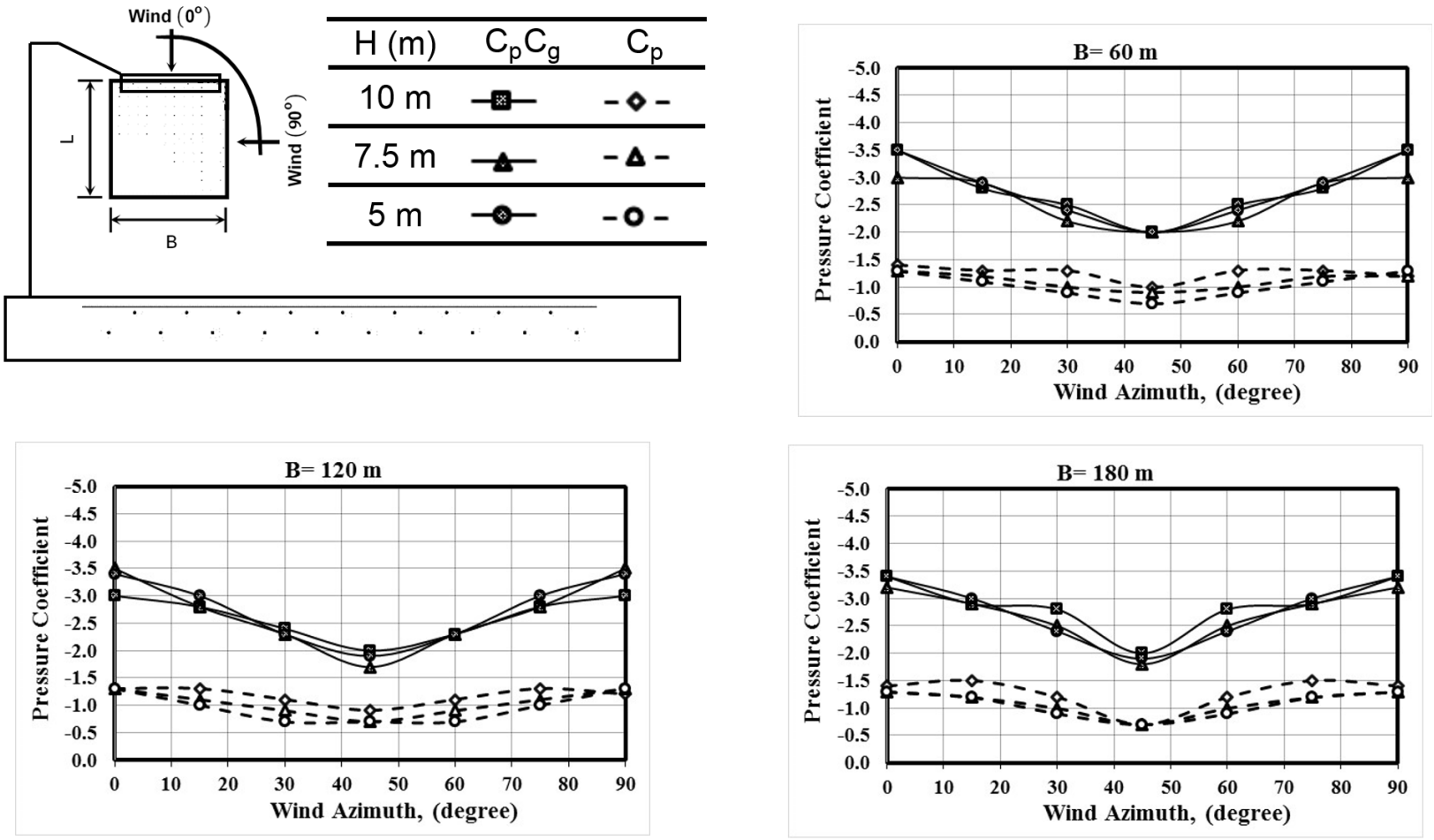

Figure 5.15: Extreme negative peak and mean pressure coefficients on windward edge of the building versus wind direction.

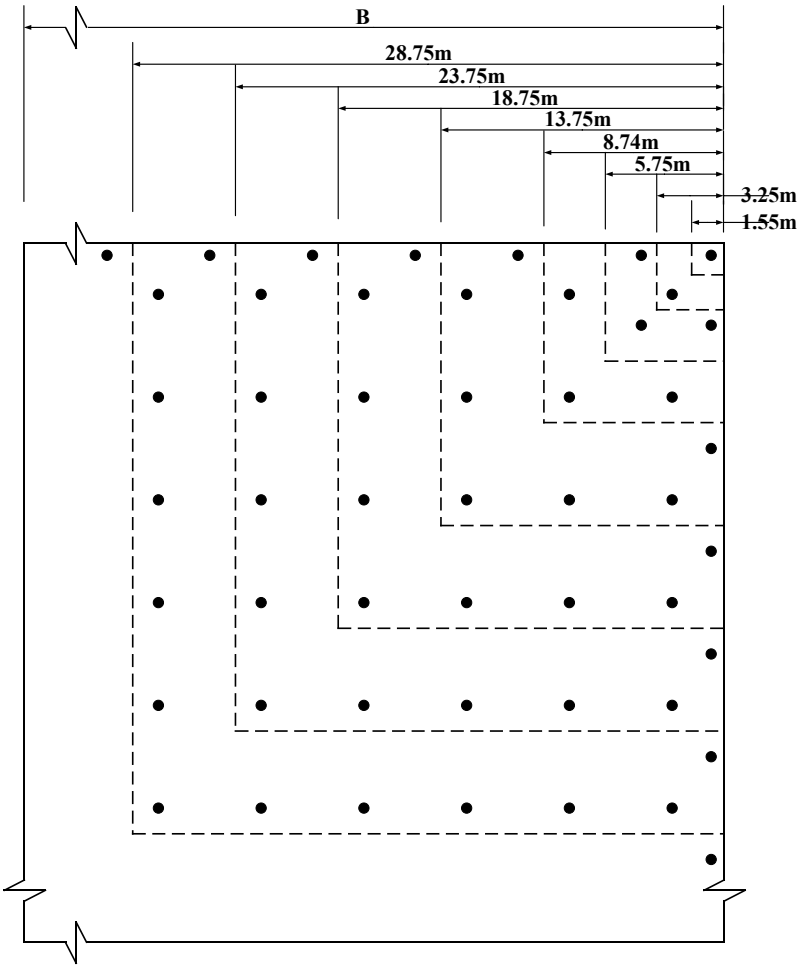

Figure 5.16: Illustration of the tributary areas and pressure taps covering the area.

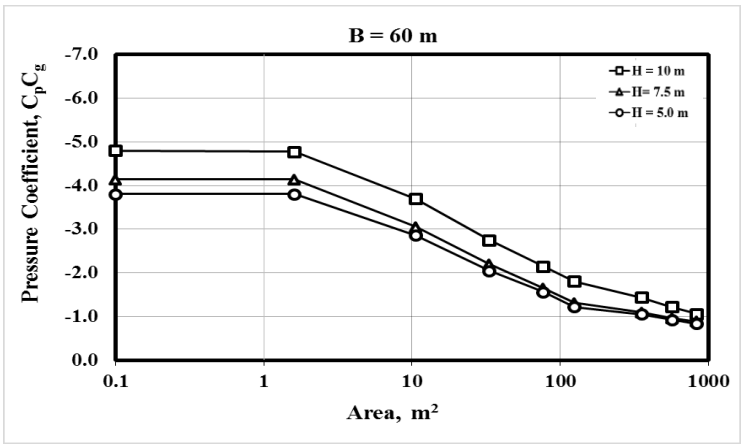

a)

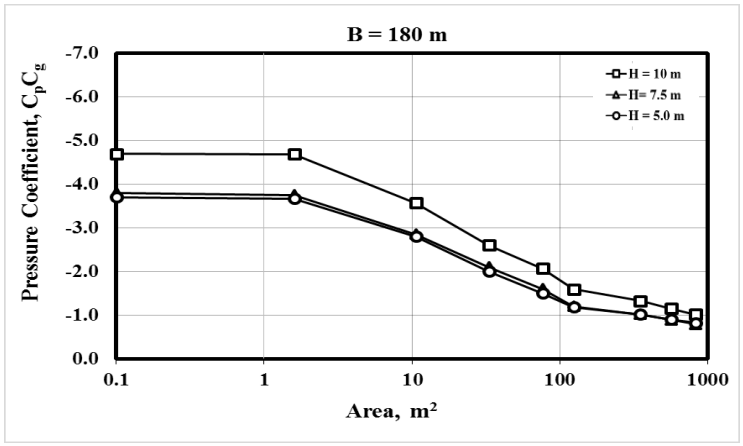

b)

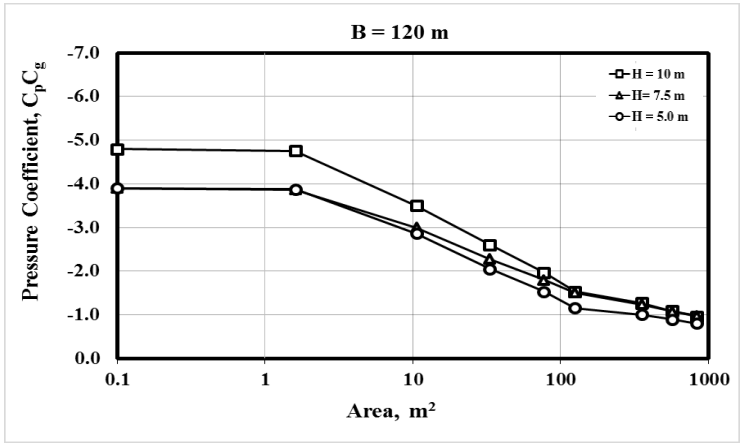

c)

Figure 5.17: Variation of the most critical area-averaged pressure coefficients, CpCg, for the roof corner zone with tributary area for buildings with horizontal plan width of: (a) 60 m, (b) 120 m and (c) 180 m.

5.3 Size of Corner and Edge Zones

The same methodology implemented for the ASCE 7-10 and NBCC 2010 has been applied to this study to generate the roof zones of the tested models by using the patterns shown in Figure 4.3. This approach starts from finding the maximum negative peak wind pressure on the entire model roof for each wind direction. Then, it is required to determine how far it will take to reduce the maximum pressure to the 0.7 level; the generated distance represents the edge zone width.

Therefore, the width Z of the edge/corner zone has been established for all tested roofs and wind directions considered in this study. Roof zone sizes of the tested buildings for all wind directions are summarized in Table 5.1. Roof zones for wind directions from 0° to 45° are only presented because of the symmetric shape of the square building plans. The envelope values for edge/corner zone width occur mainly at normal wind directions; thus for oblique wind directions, the pressure distributions are steeper than in case of normal wind direction. This makes getting the 70% of Cp,worst in shorter distances for oblique wind direction.

Furthermore, Table 5.1 shows clearly that the lower the building height, the more significant the reduction of the edge zone width becomes. Indeed, the lowest building height shows the narrowest edge/corner zone, i.e. the minimum Z.

Table 5.1: Size of corner and edge zone of building models of current study.

Building Dimensions (m)	Corner and Edge Zone Width Z, (m)				
	Experimental Results				
	0°	15°	30°	45°	Envelope
B1: 60X60X10	5.3	5.3	5.3	5.3	5.3
B2: 120X120X10	6.0	5.9	5.7	5.4	6.0
B3: 180X180X10	6.9	6.9	5.9	5.4	6.9
B4: 60X60X7.5	5.2	4.7	4.6	4.0	5.2
B5: 120X120X7.5	5.3	5.0	4.5	4.0	5.3
B6: 180X180X7.5	5.4	5.4	4.5	3.8	5.4
B7: 60X60X5	3.3	3.3	2.9	1.9	3.3
B8: 120X120X5	3.4	3.4	3.0	2.5	3.4
B9: 180X180X5	3.4	3.4	3.4	3.0	3.4

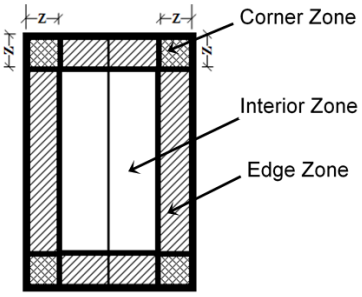

CHAPTER 6

COMPARISON OF THE EXPERIMENTAL RESULTS WITH CURRENT STANDARDS AND CODES OF PRACTICE

This chapter includes the comparison of the experimental results of the present study with respective values from the current wind codes/standards in order to stand on their adequacy in predicting design wind loads for corner and edge zones of large roofs. The findings from this comparison will provide solid information to assess the efficiency of the current building code/standard provisions as to their applicability to very large buildings.

6.1 Edge and Corner Zones

6.1.1 Comparison with North American Standard/Code (ASCE7-10 and NBCC 2010)

Comparison of the roof zone sizes of the experimental results with those created by the current guidelines of ASCE 7-10 and NBCC 2010 are presented in Table 6.1. Roof zones of ASCE 7-10 and NBCC 2010 for most tested roofs in this study are created by the design criterion 4% of the least horizontal dimension (0.04Ds).

Table 6.1 shows that for buildings with low height and large roofs ($B \geq 120$ m and $H \leq 7.5$ m), the sizes of the edge and corner zones of this study are considerably smaller than the sizes created by the ASCE 7-10 (NBCC 2010) guidelines. The disagreements between the experimental results and the respective code values are due to the zoning parameter 4% of the least horizontal dimension (0.04Ds). For instance, the edge zone size of ASCE 7-10 (NBCC 2010) for building (B9) is found to be twice as large as the actual (experimental)

size. On the contrary, for relatively high and large roof buildings (B3), the sizes of the edge and corner zones created by this investigation are comparable to the current ASCE 7-10 (NBCC 2010) guidelines.

Table 6.1: Size of corner and edge zones of present study compared with ASCE 7-10 and NBCC 2010.

Building Dimensions (m)	Corner and Edge Zone Width Z, (m)	
	Experimental Results	Current Provisions
B1: 60X60X10	5.3	4.0
B2: 120X120X10	6.0	4.8
B3: 180X180X10	6.9	7.2
B4: 60X60X7.5	5.2	3.0
B5: 120X120X7.5	5.3	4.8
B6: 180X180X7.5	5.4	7.2
B7: 60X60X5	3.3	2.4
B8: 120X120X5	3.4	4.8
B9: 180X180X5	3.4	7.2

Moreover, the current roof zones of ASCE 7-10 (NBCC 2010) and experimental roof pressure distributions have been investigated together. For illustration purposes, the contour distribution of most critical peak pressure coefficients over the perimeters of roofs of the models B7: 60X60X5 m and B9: 180X180X5 m are respectively drawn in Figures 6.1 and 6.2 with roof zones of current provisions of ASCE 7-10 and NBCC 2010. Since the roof models are square, these contours of pressure coefficients take advantage of the symmetry of the roof models, thus the contours on a quarter of the roof reflect the pressure distribution on the entire roof perimeter. The summary of this investigation is presented in Table 6.2, in which the minimum values (in absolute sense) of most critical pressure coefficients captured by each corner and edge zone of current provisions are provided. These are the values at the boundaries with the roof interior zone.

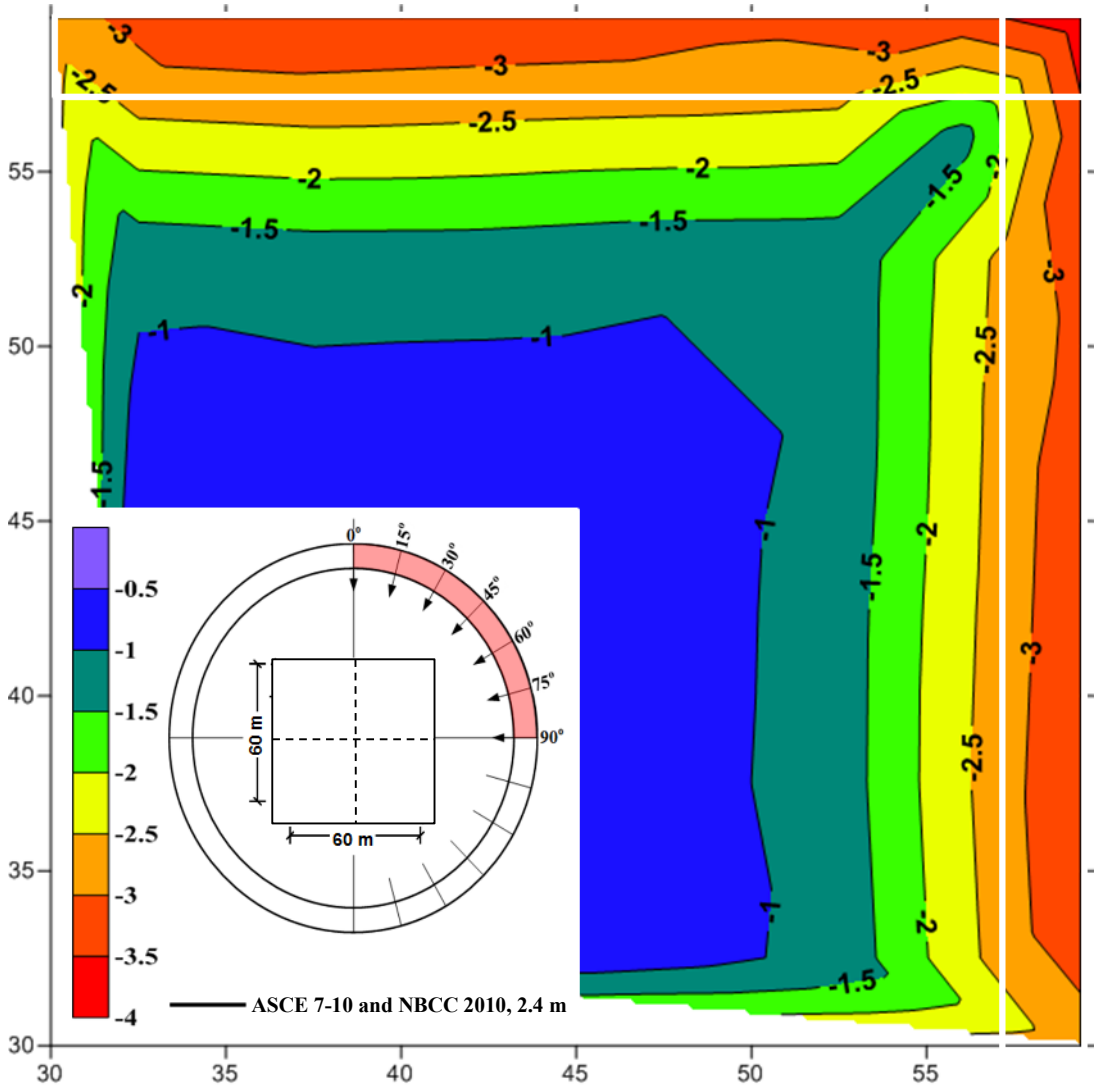

Figure 6.1: Most critical negative peak pressure coefficient contours (envelope for all wind directions) with roof zones of the current provisions of ASCE 7-10 (NBCC 2010) for building B7: 60X60X5 m.

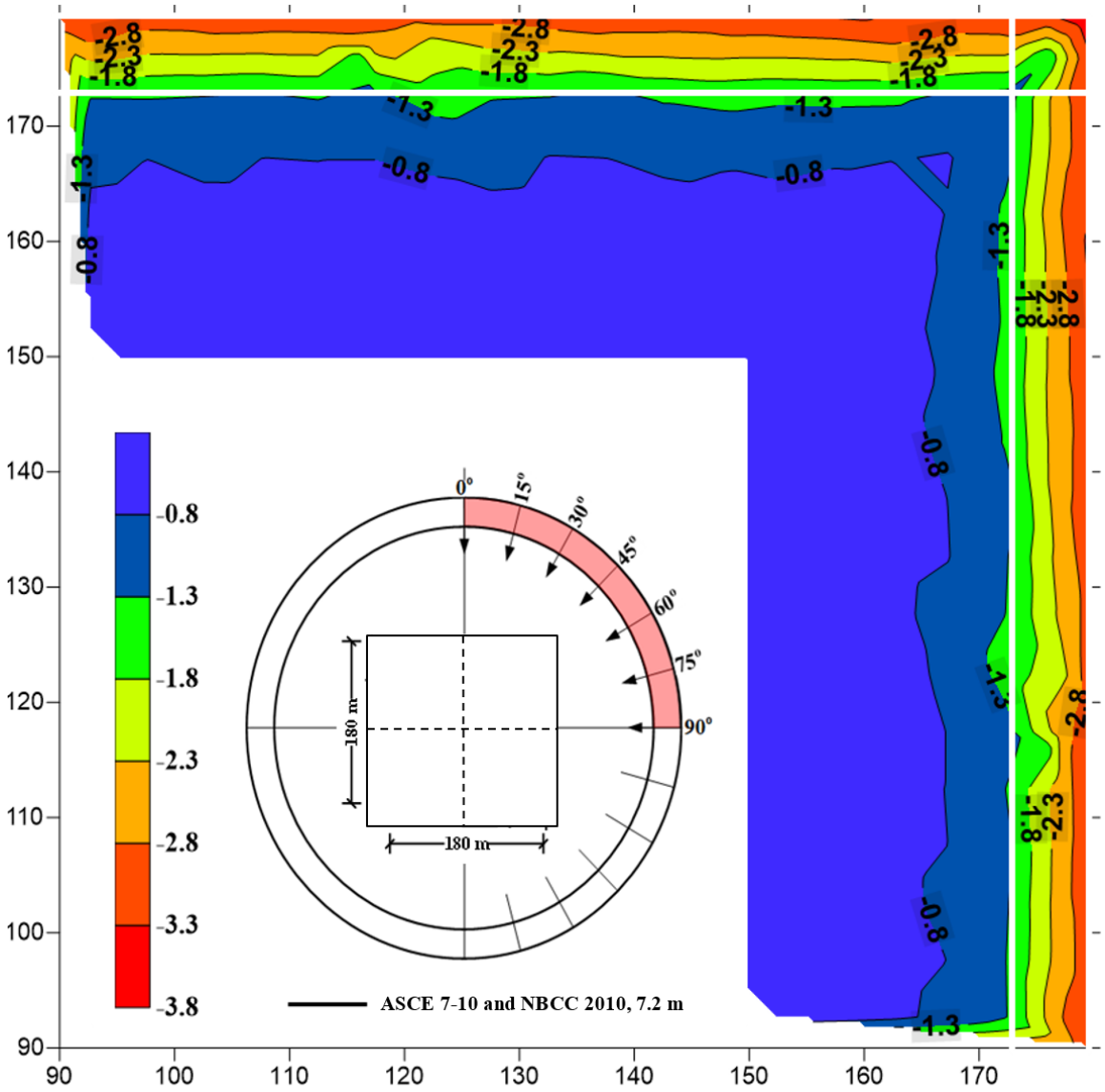

Figure 6.2: Most critical negative peak pressure coefficient contours (envelope for all wind directions) with roof zones of the current provisions of ASCE 7-10 (NBCC 2010) for building B9: 180X180X5 m.

Table 6.2 shows that for buildings with large roofs (B ≥ 120 m) and relatively low heights (H ≤ 7.5 m) the current provisions of ASCE 7-10 and NBCC 2010 have a tendency to provide very conservative corner and edge zones of unjustified size increases - with attention to values of the design local pressure coefficient of the interior zones recommended by ASCE 7-10 and NBCC 2010 for local areas (Figure 4.2) – it is observed that very low values of pressure coefficients, even lower than the code design local pressure of interior zones, are held by edge and corner zones of these buildings (B ≥ 20 m and H ≤ 7.5 m). For instance, for building model (B7: 60X60X5 m) the current code/standard edge and corner zones capture all peak pressure coefficients higher (in absolute sense) than -2.5 and -2.0, respectively; whereas the code corner and edge zones of the building model (B9: 180X180X5 m) capture the local peak pressure coefficients to a very conservative degree; thus, CpCg values much higher than -1.3.

Table 6.2: Minimum values (in absolute sense) of most critical pressure coefficients captured by current ASCE 7-10 and NBCC 2010 roof zones – see Figures 6.1 and 6.2 for B7 and B9.

Building Dimensions (m)	Value of minimum pressure coefficient	
	Edge Zone	Corner Zone
B1: 60X60X10	-2.5	-2.5
B2: 120X120X10	-2.3	-2.0
B3: 180X180X10	-2.0	-2.0
B4: 60X60X7.5	-2.5	-2.2
B5: 120X120X7.5	-2.3	-1.9
B6: 180X180X7.5	-1.8	-1.3
B7: 60X60X5	-2.5	-2.0
B8: 120X120X5	-1.5	-1.5
B9: 180X180X5	-1.3	-1.3

6.1.2 Comparison with European Standard (EN 1991-1-4:2005)

As mentioned in Chapter 4, the European standard recommends the use of L-shape corner zones. According to the European standard, the zones of large roofs are mainly dominated by the building height. Thus, width of the roof zones of the European standard for the tested roofs in this study are covered by the design criterion 20% eave height (0.2H), whereas the length of the corner zones are covered by the design criterion 50% of the eave height (0.5H).

Corner and edge zones of EN 1991-1-4:2005 capture all pressure coefficients higher than -3.0 for all tested buildings. Thus, roof zones of EN 1991-1-4:2005 capture the highest values of pressure coefficient. This may indicate that the length of the corner ~~and edge~~ zones of large roofs (being 20% of the eave height (0.2H)) provides very small length for areas with high wind fluctuations

Figures 6.3 and 6.4, respectively, represent the contours of worst peak pressure coefficient distribution over the roofs of relatively small and large dimensions with the zonal system of EN 1991-1-4:2005 figured on the contours. Generally, the actual edge and corner zones generated in this study are found to be in the range of 2.5 to 3.5 of those provided by the European Standard.

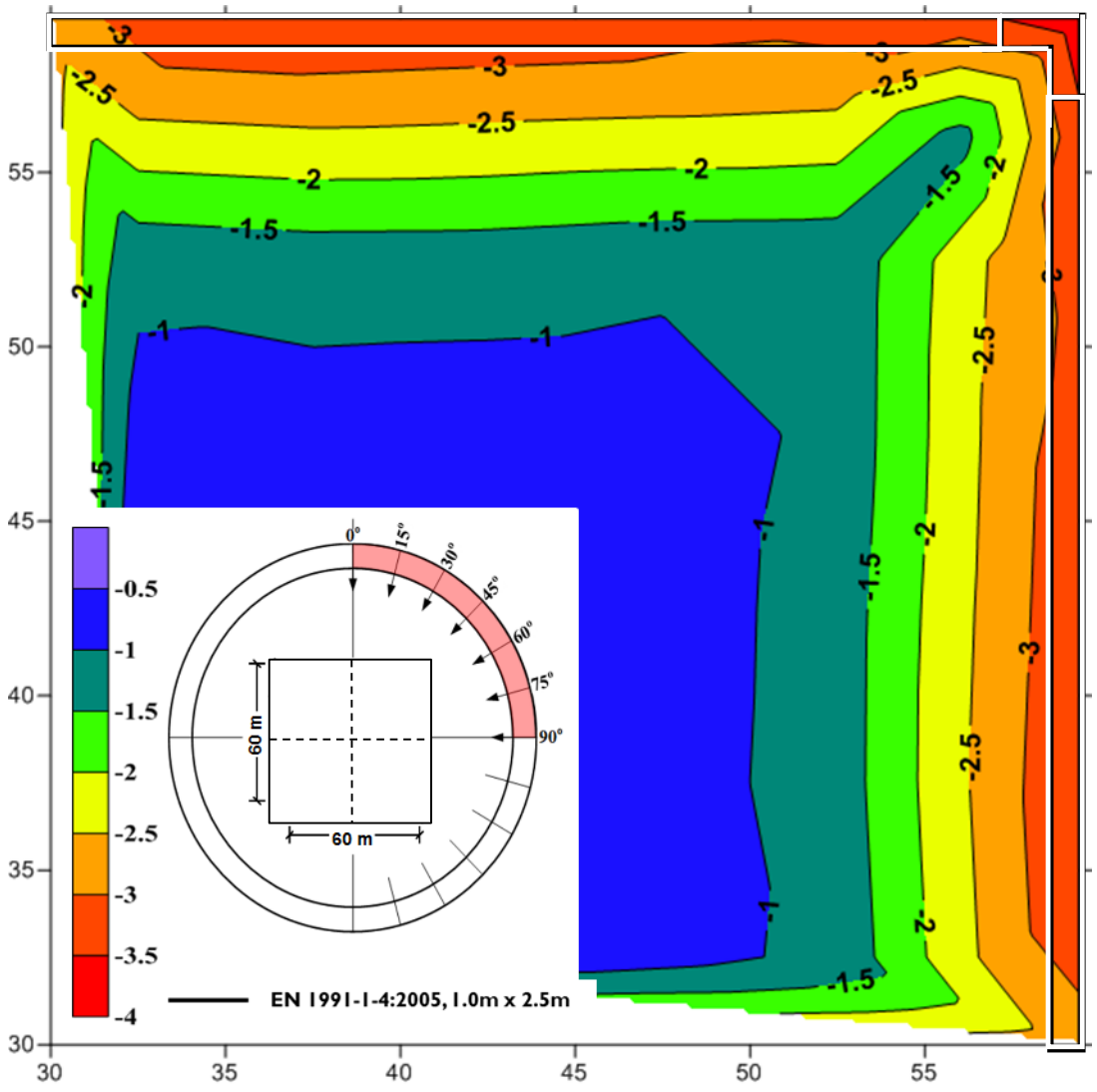

Figure 6.3: Most critical negative peak pressure coefficient contours (envelope for all wind directions) with roof zones of the current provisions of EN 1991-1-4:2005 for building B7: 60X60X5 m

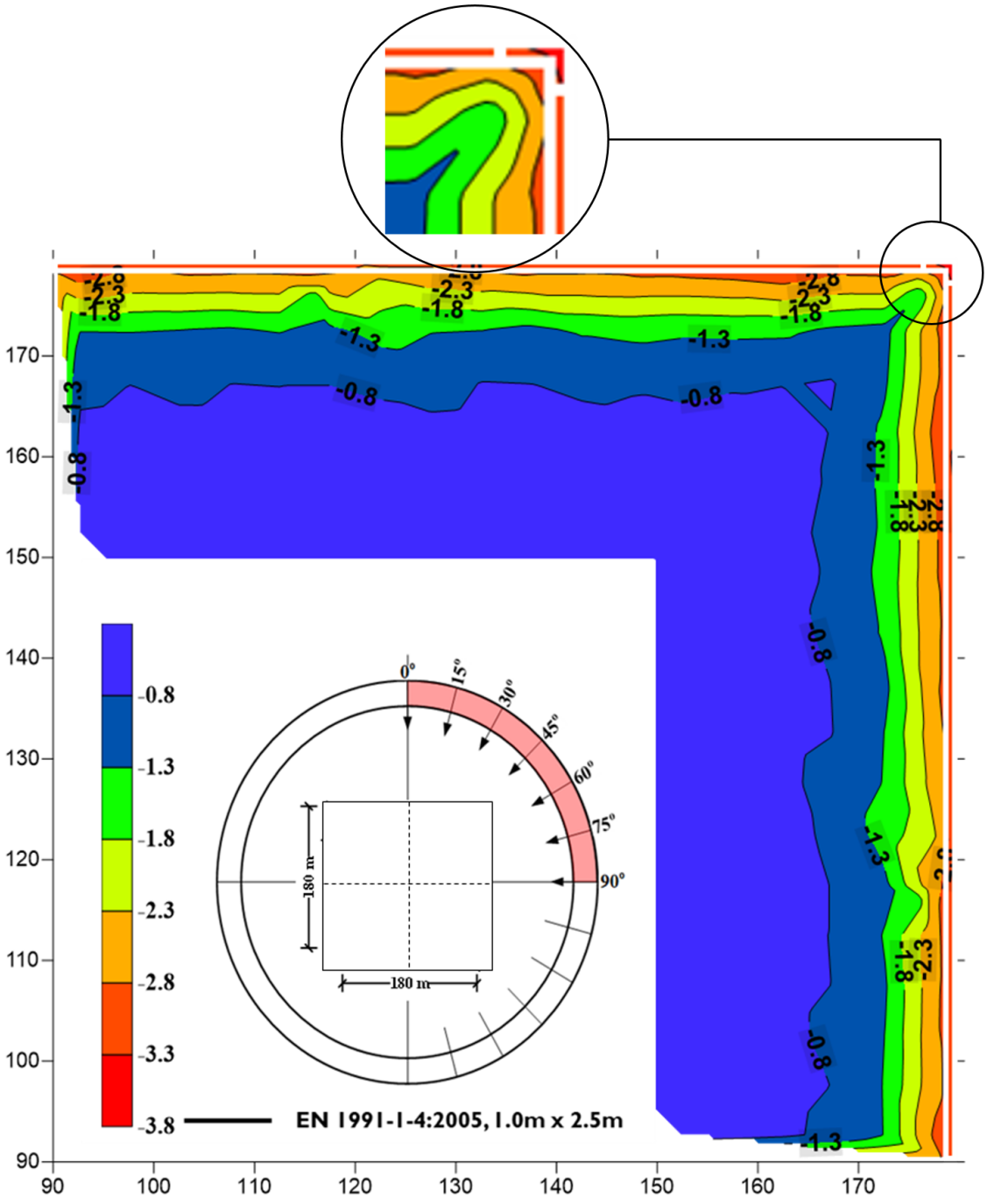

Figure 6.4: Most critical negative peak pressure coefficient contours (envelope for all wind directions) with roof zones of the current provisions of EN 1991-1-4:2005 for building B9: 180X180X5 m

6.1.3 Comparison with Australian/New Zealand Standard (AS-NZS 1170-2, 2011)

As discussed in Chapter 4, the Australian Standard recommends the use of square corner zones. Moreover, the edge and corner zones are divided into additional sub-sections.

Corner zones of AS-NZS 1170-2, 2011 capture all local pressure coefficients higher than -1.8, -1.7, and -1.5 for all roofs of heights 10, 7.5 and 5m, respectively. Edge zones of AS-NZS 1170-2, 2011 capture all local peak pressure coefficients higher than -2.4 by the exterior edge zones and all pressure coefficients between -1.8 and -2.4 for all buildings.

Figures 6.5 and 6.6 represent, respectively, the contours of worst peak pressure coefficients distribution over the roofs of relatively small and large dimensions with the zonal system of AS-NZS 1170-2, 2011 figured on the contours. Regarding the size of the roof zones, comparison of the experimental corners and edges zones of this investigation with those created by the current AS-NZS 1170-2, 2011guidelines shows that the edge zone sizes of experimental results are found to be approximately three quarters of those created by AS-NZS 1170-2, 2011 guidelines for buildings with large roofs and relatively low height. Thus, the design criterion concerning the mean roof height (h) dominated the size of the roof zones and provides unnecessarily large areas for corner zones of large roofs.

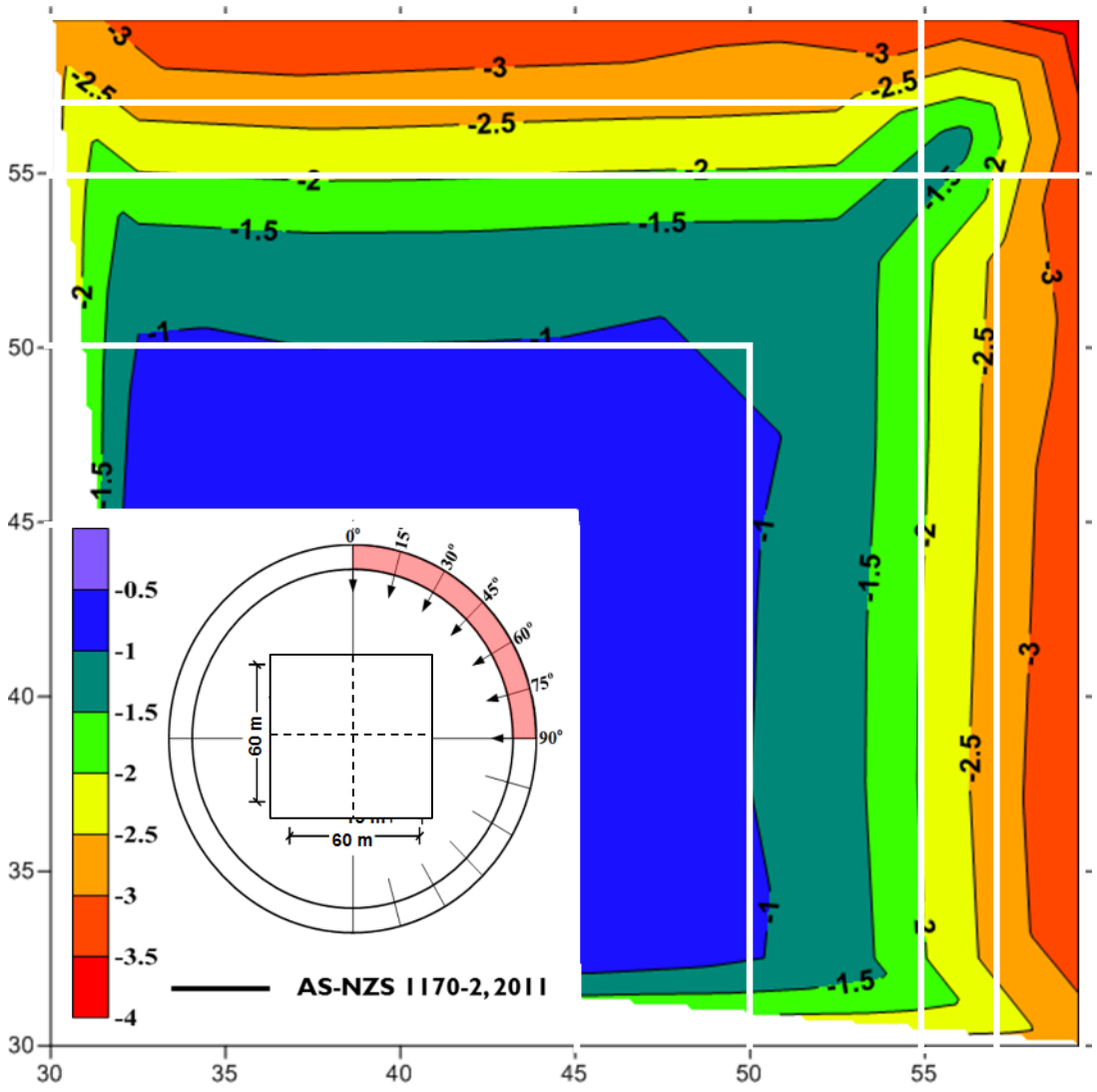

Figure 6.5: Most critical negative peak pressure coefficient contour (envelope for all wind directions) with roof zones of the current provisions of AS-NZS 1170-2, 2011 for building B7: 60X60X5 m

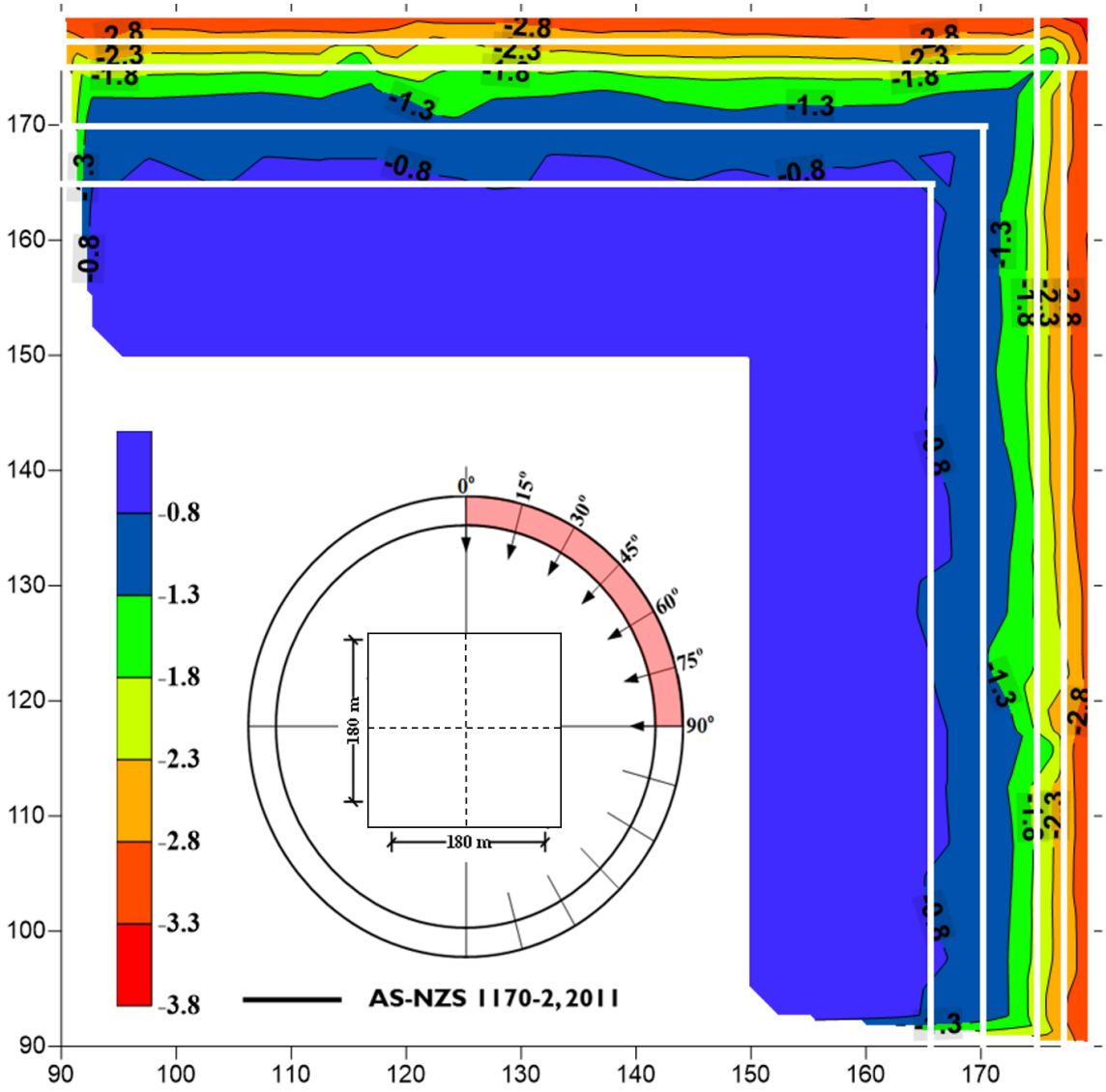

Figure 6.6: Most critical negative peak pressure coefficient contours (envelope for all wind directions) with roof zones of the current provisions of AS-NZS 1170-2, 2011 for building B9: 180X180X5 m

6.2 Roof Corner Pressure Coefficients

The comparison of the current experimental wind tunnel results with the current code and standard provisions is necessary to check their adequacy in predicting the design wind loads on roofs of buildings with large dimensions. As mentioned in Chapter 5, eight square tributary areas of sizes ranging between 2.4 m^2 and 827 m^2 were selected at the windward roof corner to calculate area-averaged pressure coefficients, since the experimental wind pressures are consistent with the provisions of ASCE 7-10 and NBCC 2010.

It should be noted that the pressure coefficients of ASCE 7-10 that will be incorporated into the comparisons with the wind tunnel results and the corresponding NBCC 2010 values have been multiplied by the reduction factor of 0.85 to account for directionality; further information concerning this factor is provided by Davenport (1983).

The most critical area-averaged peak wind pressures for the corner zones are compared with the design values recommended by ASCE 7-10 and NBCC 2010. The comparisons are presented in Figure 6.6. The experimental values of Figure 6.6 are the most critical (envelope) values from all wind directions and tested buildings. The values on non-marker lines represent the external design wind pressure coefficients of ASCE 7-10 and NBCC 2010 on roof components and cladding.

Figure 6.6 shows that the design values recommended by ASCE 7-10 and NBCC 2010 are generally good for buildings of large size, although for loading areas between 2.5 and 30 m^2 the ASCE 7-10 and NBCC 2010 underestimate the wind loads.

Also, the values of the most critical negative peak pressure coefficients (local loads) measured over the leading edges of the roofs are found to be in the range of -3.0 to -3.5 for all tested buildings. These values are comparable to the respective design values of ASCE 7-10 and NBCC 2010 – see Figure 4.2. Furthermore, the tested roofs have experienced positive wind pressures (downward pressures) - see Figure 5.1. Generally, the local positive

pressures (instantaneous values) are found to be in the range of 0 and +0.5 on the large roofs tested in this study. The positive pressures are comparable to the respective values of ASCE 7-10 (+0.6) and NBCC 2010 (+0.5).

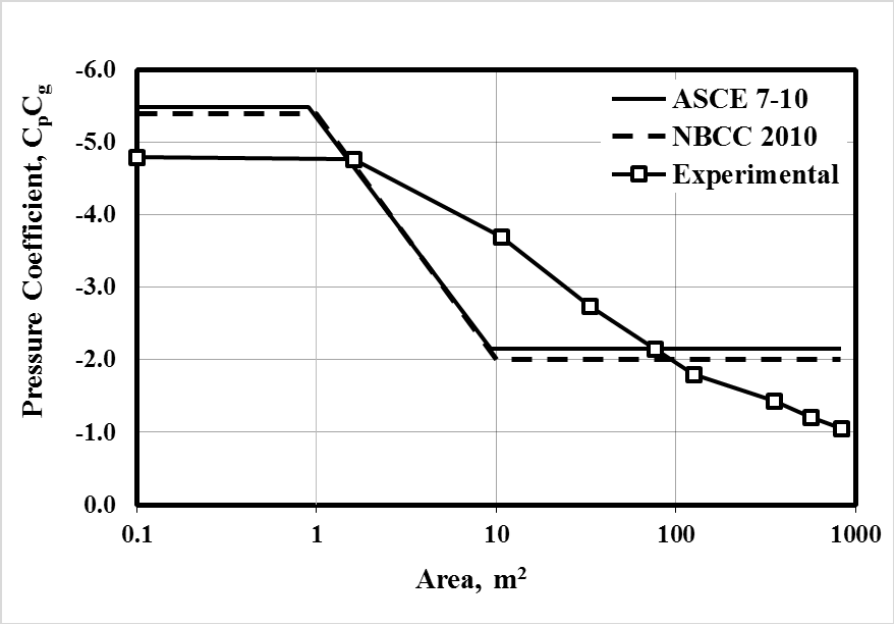

Figure 6.7: Comparison of most critical pressure coefficients, C_pC_g, between the present study results and the recommended code values for the roof corner zone.

CHAPTER 7

TOWARD BETTER EVALUATION OF EDGE AND CORNER ZONES

The applicability of the current wind provisions for large flat roofs of low-rise buildings has been verified experimentally. The GCp or CpCg values recommended by ASCE 7-10 and NBCC 2010 for edge and corner zones of flat roofs were applied successfully to buildings with large dimensions. The experimental results of the roof zones of large buildings were produced following the same pattern adopted by ASCE 7-10 and NBCC 2010 and then compared with the respective code values. Although the maximum values measured were similar with those provided by the codes and standards, the corner/edge zones were found to be excessive for large roofs of low buildings due the unnecessary restriction of the 0.04Ds criterion. Therefore, it was suggested to carry out some work to modify the provisions for such buildings without altering the current provisions for the majority of the common-size residential and industrial low buildings.

7.1 Modifying the Current Provisions of ASCE 7-10 and NBCC 2010

As already noted, current guidelines of ASCE 7-10 and NBCC 2010 overestimate the roof zones of large roofs (width $\geq$ 120 m) and low heights (height $\leq$ 7.5 m) by applying conservative zones of areas larger than required. These zones are produced by the design criterion of 4% of the least horizontal plan dimension (0.04Ds), while for this kind of geometries, the values of roof pressure coefficients have mainly been affected by the building height. For the roof zones of ASCE 7-10 and NBCC 2010 to hold most wind pressures of high values close to the windward roof edge, economy dictates to narrow the width of this zone as much as it is necessary.

Under these circumstances, the results lend support to the idea that a suggestion can be proposed to make an exception to the current low building provisions for very large buildings. This exception may be added to the current guidelines defining the width of the edge zone. The current roof pattern and the current guidelines specified in ASCE 7-10 and NBCC 2010 are presented in Figure 7.1 with the proposed exception:

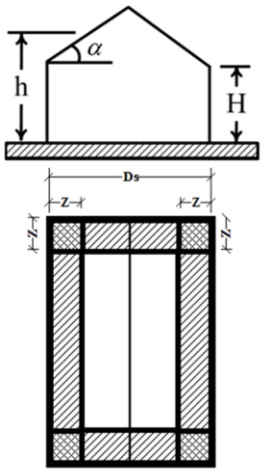

"*End- zone width z is the lesser of 10% of the least horizontal dimension and 40% of the height, h, but not less than 4% of the least horizontal dimension or 1m*". (NBCC 2010).

Exception: for roofs of buildings with α = 0° to 7°, h less than 8 m and a least horizontal dimension greater than 90 m the edge zone width shall be limited to a maximum of (0.8h).

Figure 7.1: The current roof system specified in ASCE 7-10 and NBCC 2010 with the proposed exception.

According to Table 5.1 which shows the experimental roof zones sizes, it seems better to define the edge and corner zone by the ratio 0.72H which represents the envelope value for all ratios of Zexp/H. However, it was decided to propose 0.8H in order to be more conservative due to the limited configurations tested and the possible measurement error. It was indeed observed that the pressure gradients close to the windward areas of the roofs are very steep. Therefore, the envelope value has an inherent increased error. Finally, buildings with roof mean height less than 8 m and least horizontal dimension greater than 90 m have been included in this exception. The author believes that application of this exception to current wind provisions will lead to more economic but adequate design for roofs cladding of low-rise buildings with large roofs.

7.2 Assessment of the Efficiency of the Proposed Exception To the Current Provisions

The roof zones of the current ASCE 7-10 and NBCC 2010 are compared with the modified provisions by applying the proposed exception. The comparison of the roof zones (experimental, current and modified) is presented in Table 7.1. Undoubtedly, the final outcomes of these code/standard provisions become more reliable against wind loading for low-rise buildings. As an illustration, for building model (B9: 180X180X5 m), based on the modified guidelines, the size of the edge/corner zones is decreased from 7.2 m to 4.0 m.

Table 7.1: Size of corner/edge zones of present study and the current zones of ASCE 7-10 and NBCC 2010 compared with the proposed exception.

Building Dimensions (m)	Corner and Edge Zone Width Z, (m)		
	Experimental Results	Current Provisions	Modified Provisions
B1: 60X60X10	5.3	4.0	4.0
B2: 120X120X10	6.0	4.8	4.8
B3: 180X180X10	6.9	7.2	7.2
B4: 60X60X7.5	5.2	3.0	3.0
B5: 120X120X7.5	5.3	4.8	4.8
B6: 180X180X7.5	5.4	7.2	**6.0**
B7: 60X60X5	3.3	2.4	2.4
B8: 120X120X5	3.4	4.8	**4.0**
B9: 180X180X5	3.4	7.2	**4.0**

The proposed roof zones are figured on the contours of most critical peak pressure coefficient distribution over the roof perimeter of the models B8: 120X120X5 m and B9: 180X180X5 m of Figure 7.2.

Clearly, the areas of the edge and corner zones of building model (B9) are reduced. This reduction in the size goes to the conservative portion of the roof zones created by the current provisions of ASCE 7-10 and NBCC 2010. Thus, the corner zones of the modified provisions hold all local peak pressure coefficients higher than -1.8, whereas the corner zones of the current provisions hold all peak pressure coefficients higher than -1.3. In the same way, the edge zones of the modified provisions hold all local peak pressure coefficients higher than -2.0 in comparison with the edge zones of the current provisions that hold all peak pressure coefficients higher than -1.3.

Moreover, the design wind pressure coefficients provided by ASCE 7-10 and NBCC 2010 become more consistent with the actual pressure distribution on large roofs with the modified zonal system. For instance, the maximum factored local peak pressure coefficients measured on the modified interior zone are found to be ranging from -1.5 to -1.7, which are consistent with the respective design values -2.0 and -1.9 of ASCE 7-10 and NBCC 2010, respectively.

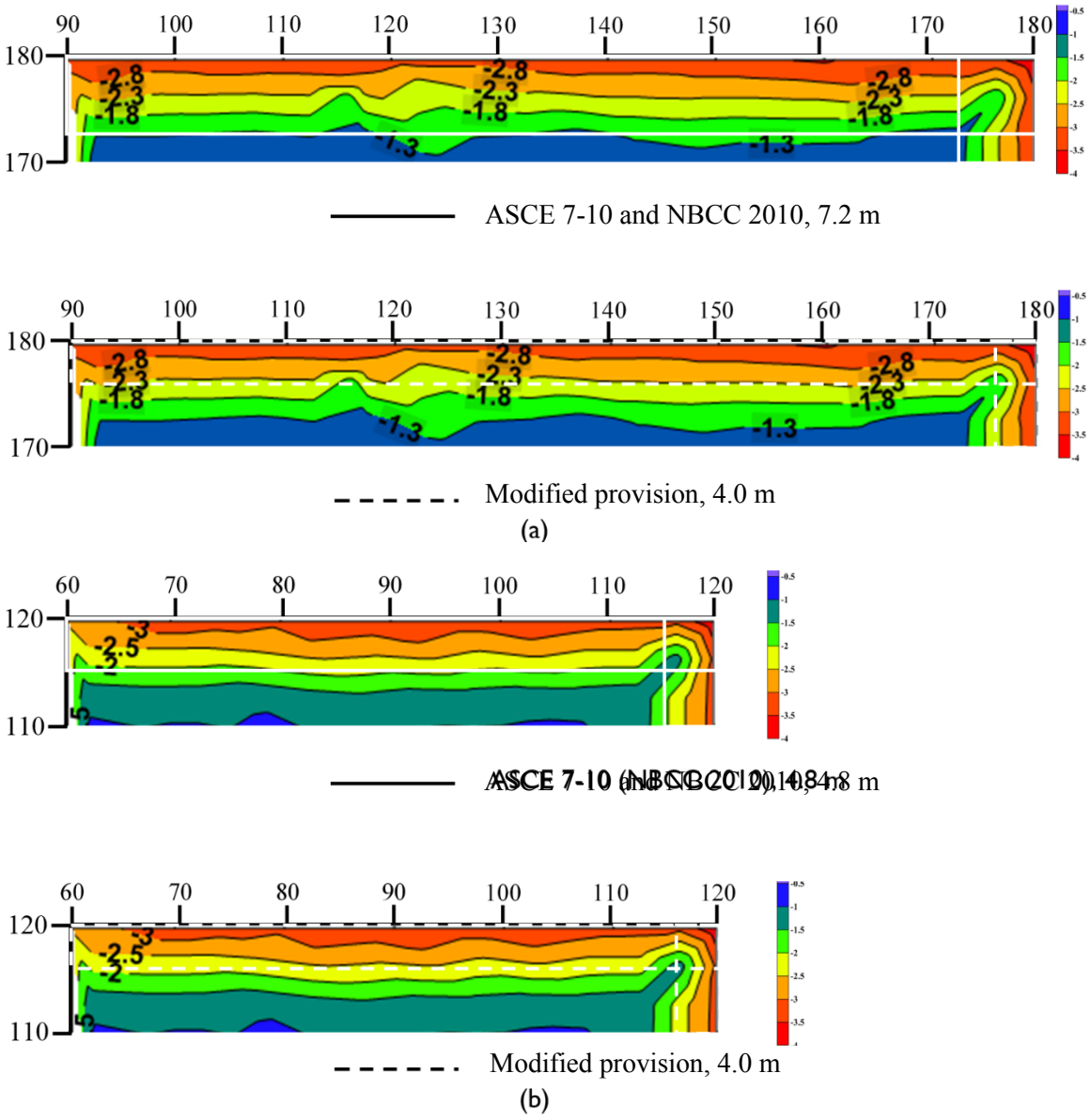

Figure 7.2: Most critical negative peak pressure coefficient contours (envelope for all wind directions) with roof zones of current and modified provisions for buildings: (a) B9: 180X180X5 and (b) B8: 120X120X5

CHAPTER 8
CONCLUSIONS AND RECOMMENDATIONS

8.1 Summary and Conclusions

A series of wind tunnel model tests have been carried out to investigate wind-induced suctions on flat roofs of large dimensions with emphasis on the generated wind loads on corner and edge zones and to examine the suitability of the current building code and standard provisions as to their applicability for very large buildings. Wind provisions of four national codes and standards have been discussed in this study, namely: the American Society of Civil Engineers Standard (ASCE7-10), the National Building Code of Canada (NBCC 2010), the European Standard (EN 1991-1-4:2005) and the Australian/New Zealand Standard (AS-NZS 1170-2, 2011). The scope of this discussion included the guidelines of the previous codes/standards to create the roof zones for buildings with large and flat roofs.

The present wind tunnel study has examined nine low-rise buildings 5, 7.5 and 10 m high. All buildings were assumed in open terrain exposure and tested for several wind directions from 0° to 90° at wind azimuth increments of 15°. The models have square plan and flat roofs with full-scale horizontal dimensions ranging from 60 to 180 m. An intensive set of experimental results has been acquired and applied for code comparisons and codifications. Most of the results have been provided in form similar to that specified in ASCE 7-10 and NBCC 2010.

The efficiency of the current wind provisions in the codes and standards and the code definitions of the roof zones along with the design zonal wind pressure coefficients have been discussed. The results and findings can be summarized as follows:

1. There are significant differences in the definition of edge and corner roof zones among current wind codes and standards.

2. External wind pressure coefficients of ASCE 7-10 and NBCC 2010 are generally applicable for designing corner and edge zones of large flat roofs. This holds true of both local and area-averaged pressure coefficients. However, the distribution patterns of roof wind pressures are mainly affected by building plan dimensions. This is more pronounced for buildings with lower heights.

3. The actual size of the edge and corner zones of buildings with large roofs and low heights are considerably smaller than the sizes created by ASCE 7-10 (NBCC 2010) guidelines. Thus, the ASCE 7-10 and NBCC 2010 restriction (0.04Ds) may lead to oversized edge and corner zones for such buildings.

Ultimately, the present wind tunnel experimental study confirms that the ASCE 7-10 and NBCC 2010 wind pressure coefficients can be used for flat roof zones of low-rise buildings with large dimensions. However, an exception to the general definition of the width of edge and corner zones was formulated for buildings with least horizontal dimension of 90 m and height less than 8 m. This exception addresses the current problem without altering all other cases in the North American wind codes and standards.

8.2 Limitations and Recommendations for Further Work

The major concern of the current research study was to assess the suitability of the current national wind code/standard provisions, mainly ASCE 7-10 and NBCC 2010, for the design of large flat roofs.

Several factors affecting the roof wind pressures have not been taken into consideration during the tests. For example, the building could have a different shape; could be located in suburban exposure. Could be in grouping or surrounded by other obstacles to measure surrounding effects etc. These limitations can be addressed in future studies.

REFERENCES

ASCE/SEI 7-10, 2010. Minimum Design Loads for Buildings and Other Structures. Structural Engineering Institute of ASCE, Reston, VA.

ASCE, 1999. Wind Tunnel Studies of Buildings and Structures. Manual of Practice No. 67, American Society of Civil Engineers, Reston, VA, 20191-4400, USA.

ASCE, 2012. Wind Tunnel Testing for Buildings and Other Structures. ASCE Standard (ASCE/SEI 49-12), American Society of Civil Engineers, Reston, VA, 20191, USA.

AS/NZS 1170.2 (2011). Australian/New Zealand Standard for Structural Design Actions, part 2: Wind Actions. Sydney, New South Wales, Australia: Standards Australia and Standards New Zealand.

Blackmore, P. A., 1988. Load Reduction on Flat Roofs – The Effect of Edge Profile. Journal of Wind Engineering and Industrial Aerodynamics, 29, 1-3, 89–98.

Barnaud, G., Gandemer, J., 1974. Determination en Soufflerie Simulant le Vent Naturel des Coefficients de Pression sur les Structures Basses. Section Aerodynamique des Constructions ADYM-12.74, Centre Scientifique et Technique du Batiment, Etablissement de Nantes.

Baskaran, A., Stathopoulos, T., 1988. Roof Corner Wind Loads and Parapet Configurations, Journal of Wind Engineering and Industrial Aerodynamics, 29, 1-3, 79–88.

Cermak, J.E, 1975. Applications of Fluid Mechanics to Wind Engineering – A Freeman Scholar Lecture. Journal of fluids Engineering, March. Pp. 9-38.

Cochran, L.S., Cermak, J.E., 1992. Full- and Model-Scale Cladding Pressures on the Texas Tech Experimental Building. Journal of Wind Engineering and Industrial Aerodynamics, 43, 1589–1600.

Cook, N.J., 1990. The Designer's Guide to Wind Loading of Buildings Structures, Part 2: Static Structures, BRE, Gariston.

Davenport A.G., 1983. On the Assessment of the Reliability of Wind Loading on Low Buildings. Journal of Wind Engineering and Industrial Aerodynamics, 11, 21-37.

Davenport, A. G., Surry, D., 1974. Pressures on Low Rise Structures in Turbulent Wind. Presented at the Canadian Structural Engineering Conference, Toronto.

Davenport, A.G., Surry, D., Stathopoulos, T, 1977. Wind Loads on Low-Rise Buildings, Final Report on Phases I and II. BLWT-SS7, The University of Western Ontario, London, Ontario, Canada.

Davenport, A.G., Surry, D., Stathopoulos, T, 1978. Wind Loads on Low-Rise Buildings, Final Report on Phase III. BLWT-SS8, The University of Western Ontario, London, Ontario, Canada.

Durst, C.S, 1960. Wind Speeds Over Short Periods of Time. Meteor. Magazine, 89, 181-187.

Eaton, K.J., Mayne, J.R., 1975. The Measurements of Wind Pressures on Two-Story Houses at Aylesbury. Journal of Wind Engineering and Industrial Aerodynamics, 1(1), 67-109.

Elsharawy, M., Galal, K., Stathopoulos, T., 2014. Comparison of Wind Tunnel Measurements with NBCC 2010 Wind-induced Torsion Provisions for Low- and Medium-rise Buildings. Canadian Journal of Civil Engineering, 41(5), 409-420.

Evans, B. H., 1957. Natural Air Flow Around Buildings. Texas Engineering Experimental Station Research Report 59, College Station, Texas.

EN 1991-1-4, 2005. Eurocode 1, 2005: Actions on Structures-General actions-Part 1-4: Wind Actions, European Standard.

Garret, J.R., 1994. The Atmospheric Boundary Layer, Cambridge University Press (Cambridge).

Gerhardt, H. J., Kramer, C., 1992. Effect of Building Geometry on Roof Wind Loading. Journal of Wind Engineering and Industrial Aerodynamics, 43, 1765–1773.

Geurts, C.P.W, Bentum, C.V., 2007. Wind Loading on Buildings: Eurocode and Experimental Approach, in T. Stathopoulos and C.C. Baniotopoulos, Wind Effects on Buildings and Design of Wind-Sensitive Structures, New York, pp. 31-65, Springer.

Geurts, C.P.W., Kopp, G.A., Morrison, M.J., 2013. A Review of the Wind Loading Zones for Flat Roofs in Code Provisions. Conference Paper: 6th European and African Conference on Wind Engineering, (EACWE 2013), Cambridge, (pp. 1-9).

Ginger, J.D., Reardon, G.F., Whitbread, B.J., 2000. Wind Load Effects and Equivalent Pressures on Low-Rise House Roofs. Engineering Structures, 22(6), 638-646.

Hee, J., Bienkiewicz, B., 1998. Wind Tunnel Simulation of TTU Flow and Building Roof Pressure. Journal of Wind Engineering and Industrial Aerodynamics. 77-78, 119-133.

Hellers, G., Lundgren, S., 1974. Wind Loads on Generally Shaped House Bodies-Model Tests. Report R22: 1974, National Swedish Building Research Summaries.

Hillier, R., 1973. An Investigation of the Cladding Wind Loads on Model of Hartlepool Switch House. CERL Report RDL/N227/73, Central Electricity Research Laboratories, Surrey, England.

Ho, T.C.E., Surry, D., Morrish, D., Kopp, G.A., 2005. The UWO Contribution to the NIST Aerodynamic Database for Wind on Low Buildings: Part 1. Archiving Format and Basic Aerodynamic Data. Journal of Wind Engineering and Industrial Aerodynamics, 93, 1-30.

Holmes, J. D., 1986. Wind Pressures on Tropical Housing. Journal of Wind Engineering and Industrial Aerodynamics, 53, 1-2, 105–123.

Holmes, J.D., 1993.Wind Loads on Low-rise Buildings - A Review. CSIRO, Division of Building Research, Highett, Victoria, Australia.

Holmes, J.D., 2001. Wind Loading of Structures, Spon Press London, New York.

Holmes, J. D., Best, R.J., 1978. Wind Pressures on an Isolated High-Set House. James Cook University of North Queensland, Australia, Wind Engineering Report 3/78, Qeensland, Australia.

Jensen, M., 1958. The model Law for Phenomena in Natural Wind. Ingenioren (international edition), 2, 4, 121-128.

Jensen, M., Franck, N., 1965. Model-Scale Tests in Turbulent Wind, Parts I and II. The Danish Technical Press, Copenhagen.

Kasperski, M., 1996. Design Wind Loads for Low-rise Buildings: A Critical Review of Wind Load Specifications for Industrial Buildings. Journal of Wind Engineering and Industrial Aerodynamics, 61,169-179.

Kind, R. J., 1988.Worst Suctions Near Edges of Flat Rooftops with Parapets. Journal of Wind Engineering and Industrial Aerodynamics, 31, 2-3, 251–264.

Kramer, C., Gerhardt, H. J., 1975. Windbelastung auf Flachdachern. Published in Das Dechdeckerhandwerk, Koln. 96, 16.

Krishna, P., 1995. Wind Loads on Low Rise Buildings - A Review. Journal of Wind Engineering and Industrial Aerodynamics, 54-55, 383-396.

Leutheusser, H. J.,1964 .The Effects of Wall Parapets on the Roof Pressure Coefficient of Block-Type and Cylindrical Structures, Univ. Toronto, Dept. Mech. Eng., 1964, TP 6404.

Lin, J.X., Surry, D., 1998. The Variation of Peak Loads With Tributary Area Near Corners on Flat Low Building Roofs. Journal of Wind Engineering and Industrial Aerodynamics, 77-78, 185-196

Lin, J.X., Surry, D., Tieleman, H.W., 1995. The Distribution of Pressure Near Roof Corners of Flat Roof Low Buildings. Journal of Wind Engineering and Industrial Aerodynamics, 56, 235–265.

Marshall, R. D., 1974. A Study of Wind Pressures on a Single-Family Dwelling in Model and Full Scale. Proceedings of the Invitational Symposium on Full Scale Measurements of Wind Effects on Tall Buildings and Other Structures. Boundary Layer Wind Tunnel Laboratory, The University of Western Ontario, Canada, June 23-29.

Marshall, R.D., 1977. The Measurement of Wind Loads on a Full-Scale Mobile Home. National Bureau of Standards, U.S. Dep. of Commerce, Washington, D.C., NBSIR 77-1289.

Milford, R.V., Goliger, A.M., Waldech, J.L., 1992. Jan Smuts Experiment: Comparison of Full-Scale and Wind-Tunnel Results. Journal of Wind Engineering and Industrial Aerodynamics, 43, 1693-1704.

Minor, J.E., and Mehta K.C., 1979. Wind Damage Observations and Implications. Journal of the Structural Division. ASCE, November, pp 2279-2291.

Morrison, M.J., Kopp, G.A., 2007. Evaluation of the ASCE 7-05 Definition of Edge and Corner Zones for Low-Rise Buildings. The Boundary Layer Wind Tunnel Laboratory, The University of Western Ontario, Faculty of Engineering, London, Ontario, Canada N6A 5B9.

NBC2010, 2010. User's Guide-NBC 2010, Structural Commentaries (Part 4). Issued by the Canadian Commission on Buildings and Fire Codes, National Research Council of Canada.

Prandtl, L., 1905. Verhandlungen des dritten internationalen Mathematiker-Kongresses in Heidel berg 1904, Krazer, A. (ed.), Leipzig: Teubner, p. 484. English trans. Ackroyd, J. A. K., Axcell, B. P., Ruban, A. I. (eds.) 2001. Early Developments of Modern Aerodynamics. Oxford: Butterworth-Heinemann, p. 77.

Simiu, E., Scanlan, R.H., 1996. Wind Effects on Structures: Fundamentals and Applications to Design, third edition Wiley and Sons, New York.

Shoemaker, W.L., 2014. Insights into Wind Loads for Low-Rise Buildings. Structure Magazine.

Stathopoulos, T., 1975. Wind Pressure Loads on Flat Roofs. BLWT Report 3-1975, The University of Western Ontario, London, Ontario, Canada.

Stathopoulos, T., 1979. Turbulent Wind Action on Low-rise Buildings. Ph.D. Thesis, The University of Western Ontario, London, Ontario, Canada.

Stathopoulos, T., 1981. Wind Loads on Eaves of Low Buildings. Journal of the Structural Division, ASCE, 107(10), 1921-1934.

Stathopoulos, T., (1982). Techniques and Modeling Criteria for Measuring Area Averaged Pressures. International Workshop on Wind Tunnel Modeling Criteria and Techniques in Civil Engineering Applications, Gaithersburg, MD, p. 257 – 274, Cambridge University Press.

Stathopoulos, T., 1984-A. Design and Fabrication of a Wind Tunnel for Building Aerodynamics. Journal of Wind Engineering and Industrial Aerodynamics, 16, 361-376.

Stathopoulos, T., 1984-B. Wind Loads on Low-rise Buildings - A Review of the State of the Art, Engineering Structures, 6, 119–135.

Stathopoulos, T., Baniotopoulos, C.C., (2007). Wind Effects on Buildings and Design of Wind-Sensitive Structures. SpringerWeinNewYork, ISBN 978-3-211-73075-1.

Stathopoulos, T., Dumitrescu-Brulotte, M., 1989. Design Recommendations for Wind Loading on Buildings of Intermediate Height. Canadian Journal of Civil Engineering, 16, 910-916.

Stathopoulos, T., Luchian, H.D., 1990. Wind Pressures on Buildings Configurations with Stepped Roofs. Canadian Journal of Civil Engineering, 17(4), 569-577.

Stathopoulos, T., Luchian, H., 1992. Wind-Induced Forces on Eaves of Low Buildings. Wind Engineering Society Inaugural Conference, Cambridge, England.

Stathopoulos, T., Saathoff, P., 1991. Wind Pressures on Roofs of Various Geometries. Journal of Wind Engineering and Industrial Aerodynamics, 38, 273-284.

Stathopoulos, T., Surry, D., 1983. Scale Effects in Wind Tunnel Testing of Low Buildings. Journal of Wind Engineering and Industrial Aerodynamics, 13, 313-326.

Stathopoulos, T., Marathe, R., Wu, H., 1999. Mean Wind Pressures on Flat Roof Corners Affected by Parapets: Field and Wind Tunnel Studies. Engineering Structures, 21, 629–638.

Stathopoulos, T., Surray, D., Davenport, A. G., 1985. A Simplified Model of Wind Pressure Coefficients for Low-Rise Buildings. In Proc. ICOSSAR'85.

Stathopoulos, T., Zhu, X., 1988. Wind Pressures on Buildings with Appurtenances. Journal of Wind Engineering and Industrial Aerodynamics, 31, 265-281.

Stathopoulos, T., Kumar, K.S., Mohammadiam, A.R., 1996. Design Wind Pressure Coefficients for Monoslope Roofs: A Time Series Approach. Journal of Wind Engineering and Industrial Aerodynamics, 65, 143-153.

St. Pierre, L.M., Kopp, G.A., Surry, D., Ho, T.C.E., 2005. The UWO Contribution to the NIST Aerodynamic Database for Wind on Low Buildings: Part 2. Comparison of Data with Wind Load Provisions. Journal of Wind Engineering and Industrial Aerodynamics, 93, 31-59.

Surry, D., Kitchen, R. B., Davenport, A. G., 1977. Wind Loading of Two Hangars Proposed for Jeddah Airport, Saudi Arabia - A Rigid Model Study. Report unpublished, Boundary Layer Wind Tunnel Laboratory, The University of Western Ontario, London, Ontario, Canada.

Surry, D., Stathopoulos, T., 1978. An Experimental Approach to the Economical Measurements of Spatially Averaged Wind Loads. Journal of Wind Engineering and Industrial Aerodynamics, 2 (4), 385-97.

Uematsu, Y., Isyumov, N., 1999. Wind Pressures Acting on Low-Rise Buildings. Journal of Wind Engineering and Industrial Aerodynamics, 82, 1-25.

Uematsu, Y., Suzuya, J. and Nozawa, T., 1992. Building Damage in Aomori and Akita Prefectures Die to Typhoon No.19 of 1991, Journal of Wind Engineering, Japan Association for Wind Engineering, 51, 35-47.

Vickery, B. J., 1976. Wind Loads on Low-Rise Buildings. Presented at D.R.C Seminar, Darwin, March 30, Unpublished.

Wiren, B., 1971. Wind Tunnel Investigation of the Pressure Distribution on a Flat Roof with Different Edge Profiles. Translated From the Swedish, Library Communication 1606, Building Research Station.

APPENDIX A

Figures from wind codes and standards

Appendix A1: ASCE 7-10.

Appendix A2: ASCE 7-10.

Appendix: NBCC 2010.

Appendix A4: EN 1991-1-4:2005.

Appendix A5: AS/NZS 1170.2 (2011).

Appendix A6: AS/NZS 1170.2 (2011).

Appendix A7: AS/NZS 1170.2 (2011).

Appendix A1 Ratio of maximum wind speed averaged over a period "t" to the maximum wind speed averaged over one hour provided by ASCE 7-10.

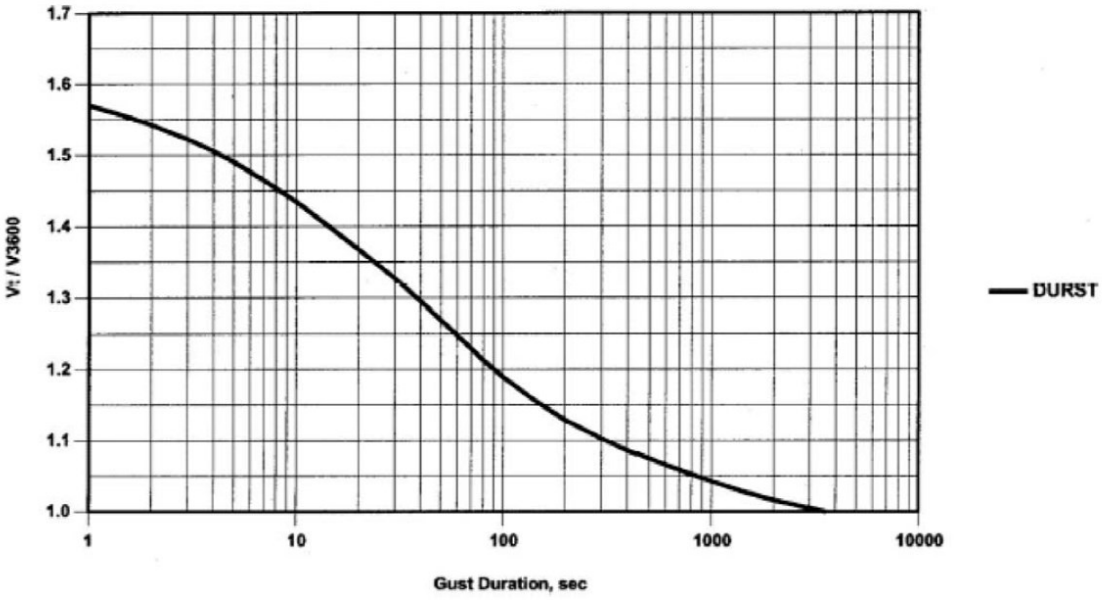

Appendix A2 Roof zones and external peak pressure coefficients, CpCg, on edge, corner, and interior zones of building roofs with a slope of 7° or less in ASCE 7-10.

Components and Cladding		h ≤ 60 ft.
Figure 30.4-2A	External Pressure Coefficients, GC_p	Gable Roofs θ ≤ 7°
Enclosed, Partially Enclosed Buildings		

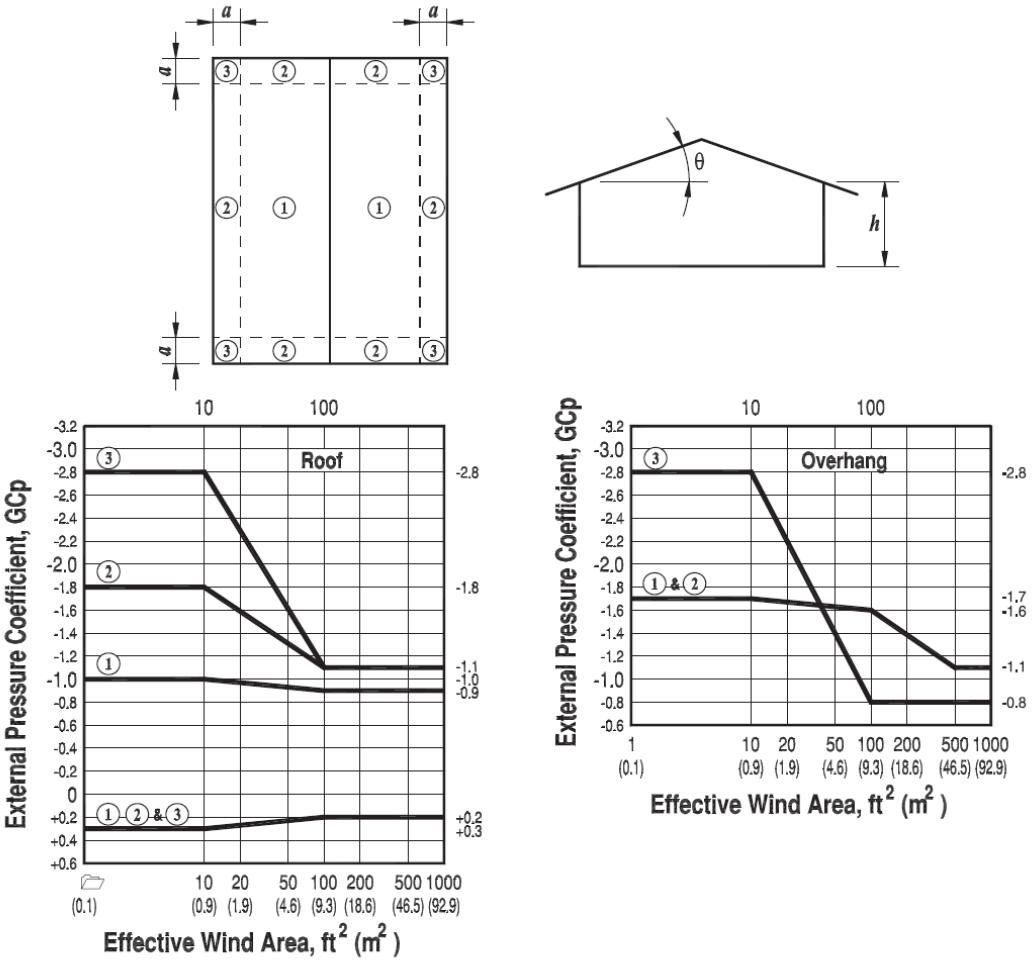

Notes:

1. Vertical scale denotes GC_p to be used with q_h.
2. Horizontal scale denotes effective wind area, in square feet (square meters).
3. Plus and minus signs signify pressures acting toward and away from the surfaces, respectively.
4. Each component shall be designed for maximum positive and negative pressures.
5. If a parapet equal to or higher than 3 ft (0.9m) is provided around the perimeter of the roof with θ ≤ 7°, the negative values of GC_p in Zone 3 shall be equal to those for Zone 2 and positive values of GC_p in Zones 2 and 3 shall be set equal to those for wall Zones 4 and 5 respectively in Figure 30.4-1.
6. Values of GC_p for roof overhangs include pressure contributions from both upper and lower surfaces.
7. Notation:
   - *a*: 10 percent of least horizontal dimension or 0.4h, whichever is smaller, but not less than either 4% of least horizontal dimension or 3 ft (0.9 m).
   - *h*: Eave height shall be used for θ ≤ 10°.
   - θ: Angle of plane of roof from horizontal, in degrees.

Appendix A3 Roof zones and external peak pressure coefficients, CpCg, on edge, corner, and interior zones of building roofs with a slope of 7° or less in NBCC 2010.

Commentary

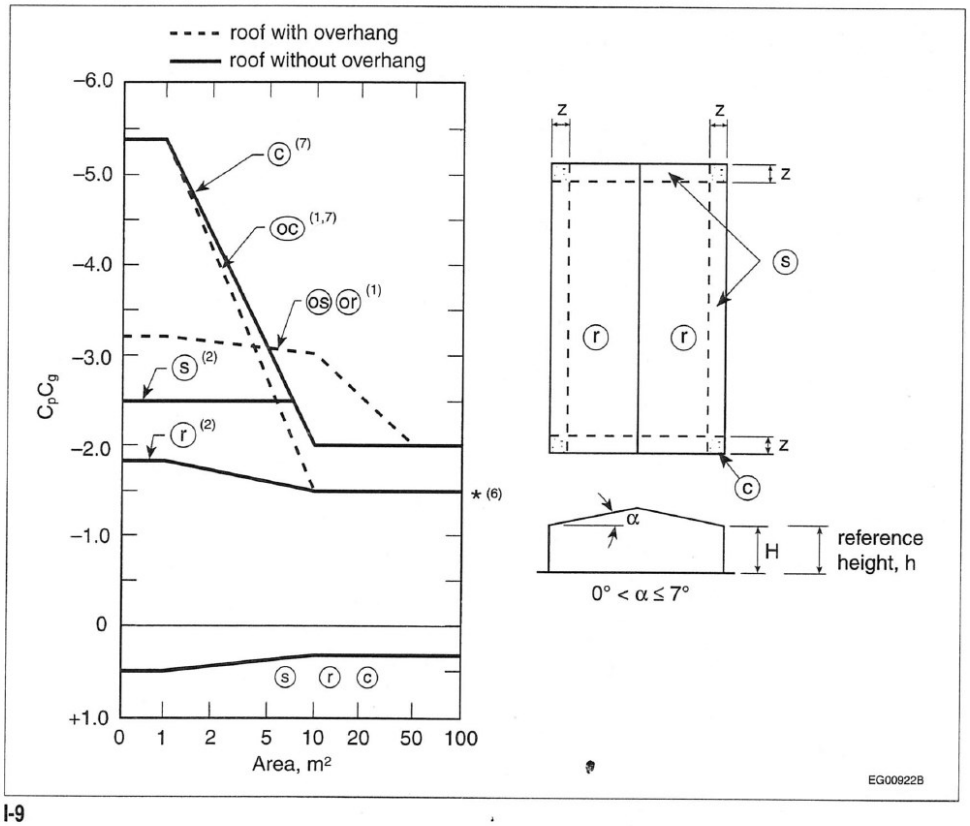

Figure I-9

External peak composite pressure-gust coefficients, C_pC_g, on roofs with a slope of 7° or less for the design of structural components and cladding

Notes to Figure I-9:

(1) Coefficients for overhung roofs have the prefix "o" and refer to the same roof areas as referred to by the corresponding symbol without a prefix. They include contributions from both upper and lower surfaces. In the case of overhangs, the walls are inboard of the roof outline.[38]

(2) s and r apply to both roofs and upper surfaces of canopies.

(3) The abscissa area in the graph is the design tributary area within the specified zone.

(4) End-zone width z is the lesser of 10% of the least horizontal dimension and 40% of height, H, but not less than 4% of the least horizontal dimension or 1 m.

(5) Combinations of exterior and interior pressures must be evaluated to obtain the most severe loading.

(6) Positive coefficients denote forces toward the surface, whereas negative coefficients denote forces away from the surface. Each structural element must be designed to withstand the forces of both signs.

(7) For calculating the uplift forces on tributary areas larger than 100 m² on unobstructed nearly-flat roofs with low parapets, and where the centre of the tributary area is at least two building heights from the nearest edge, the value of C_pC_g may be reduced to -1.1 at x/H = 2 and further reduced linearly to -0.6 at x/H= 5, where x is distance to the nearest edge and H is building height.[40]

(8) For roofs having a perimeter parapet that is 1 m high or greater, the corner coefficients C_pC_g for small tributary areas can be reduced from -5.4 to -4.4. [41][42]

Appendix A4 External pressure coefficients, C_{pe}, for buildings with a loaded areas between 1 m^2 and 10 m^2 in EN 1991-1-4:2005.

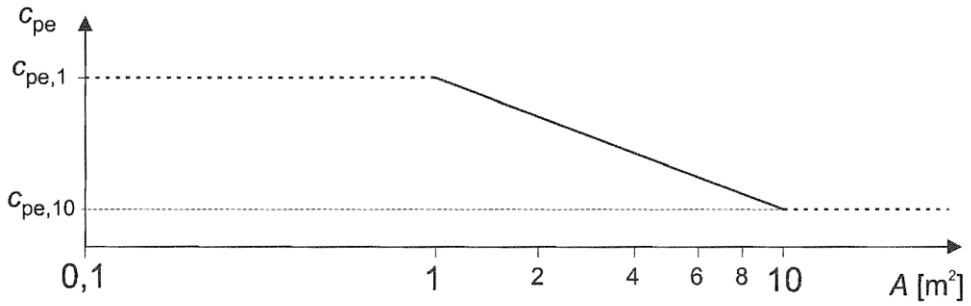

The figure is based on the following:
for 1 $m^2 < A < 10$ m^2 $\quad c_{pe} = c_{pe,1} - (c_{pe,1} - c_{pe,10}) \log_{10} A$

Appendix A5 Values of local pressure factor, K_l, recommended by AS/NZS 1170.2 (2011).

LOCAL PRESSURE FACTOR (K_ℓ)

Design case	Figure 5.3 reference number	Building aspect ratio (r)	Area (A) m^2	Proximity to edge	K_ℓ
Positive pressures					
Windward wall	WA1	All	$A \le 0.25a^2$	Anywhere	1.5
All other areas	—	All	—	—	1.0
Negative pressures					
Upwind corners of roofs with pitch <10°	RC1	All	$A \le 0.25a^2$	$<a$ from two edges	3.0
Upwind roof edges	RA1	All	$A \le a^2$	$< a$	1.5
	RA2	All	$A \le 0.25a^2$	$< 0.5a$	2.0
Downwind side of hips and ridges of roofs with pitch ≥10°	RA3	All	$A \le a^2$	$< a$	1.5
	RA4	All	$A \le 0.25a^2$	$< 0.5a$	2.0
Side walls near windward wall edges	SA1	≤ 1	$A \le a^2$	$< a$	1.5
	SA2	≤ 1	$A \le 0.25a^2$	$< 0.5a$	2.0
	SA3	>1	$A \le 0.25a^2$	$>a$	1.5
	SA4	>1	$A \le a^2$	$<a$	2.0
	SA5	>1	$A \le 0.25a^2$	$\le 0.5a$	3.0
All other areas	—	All	—	—	1.0

NOTES:

1 Figure reference numbers and dimension a are defined in Figure 5.3.

2 If an area of cladding is covered by more than one case in Table 5.6, use the largest value of K_ℓ obtained for any case.

3 The building aspect ratio (r) is defined as the average roof height (h) divided by the smaller of b or d.

Appendix A6 Loading areas locations for values of local pressure factor, K_l, in AS/NZS 1170.2 (2011).

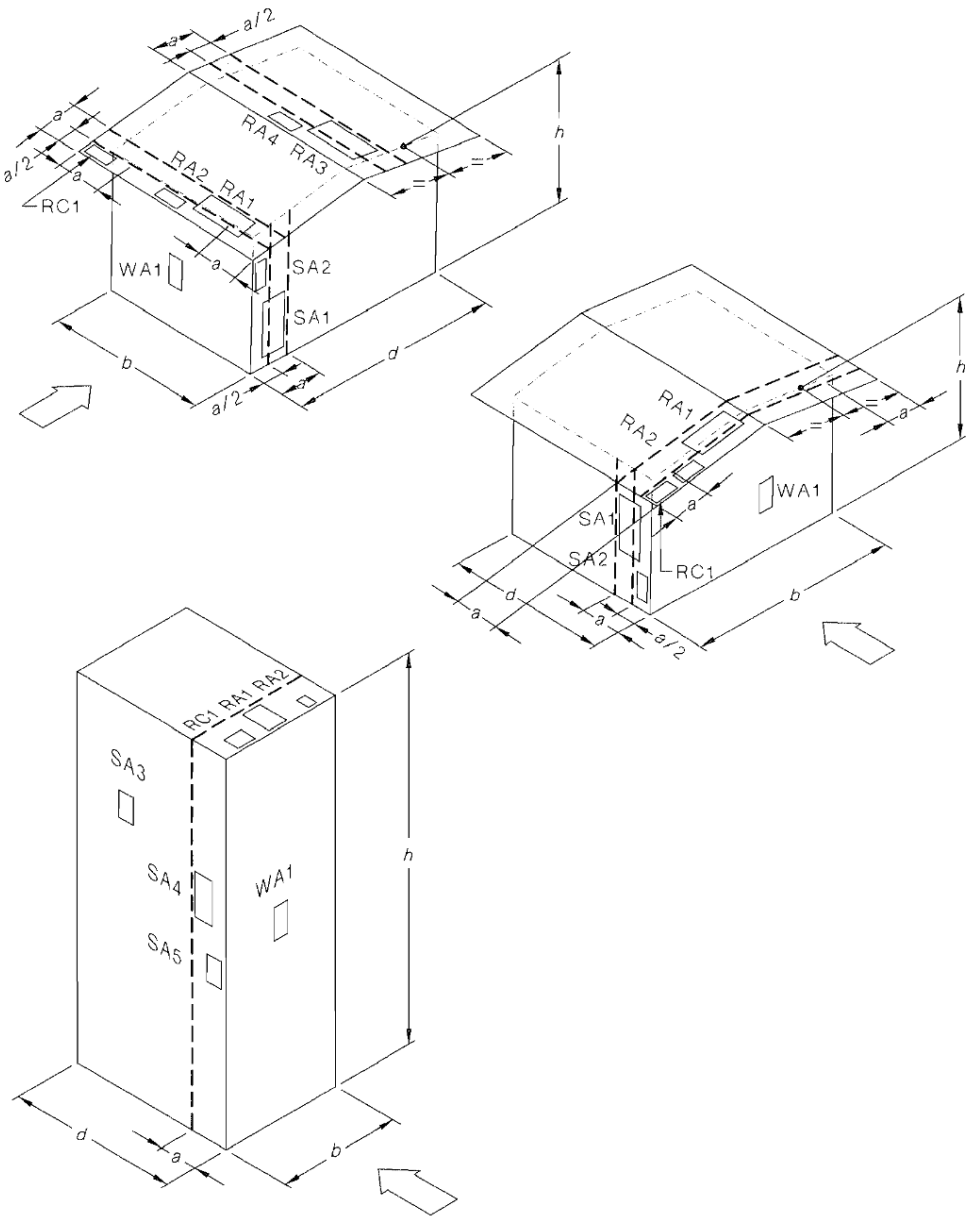

NOTES:

1 The value of dimension a is the minimum of $0.2b$, $0.2d$ and h.

2 The side ratio of any local pressure factor area on the roof shall not exceed 4.

Appendix A7 External pressure coefficients, Cpe, for enclosed low-rise buildings in AS/NZS 1170.2 (2011).

ROOFS—EXTERNAL PRESSURE COEFFICIENTS ($C_{p,e}$) FOR RECTANGULAR ENCLOSED BUILDINGS—FOR UPWIND SLOPE (U), AND DOWNWIND SLOPE (D) AND (R) FOR GABLE ROOFS, FOR $\alpha < 10°$

Roof type and slope		Horizontal distance from windward edge of roof	External pressure coefficient ($C_{p,e}$)	
Crosswind slopes for gable roofs, (R)	Upwind slope, (U), Downwind slope, (D)		$h/d \leq 0.5$ (see Note 1)	$h/d \geq 1.0$ (see Note 1)
All α	$\alpha < 10°$	0 to $0.5h$	−0.9, −0.4	−1.3, −0.6
		0.5 to $1h$	−0.9, −0.4	−0.7, −0.3
		$1h$ to $2h$	−0.5, 0	(−0.7), (−0.3)
		$2h$ to $3h$	−0.3, 0.1	see Note 2
		$>3h$	−0.2, 0.2	

NOTES:

1 For intermediate values of roof slopes and h/d ratios, linear interpolation shall be used. Interpolation shall only be carried out on values of the same sign.

2 The values given in parentheses are provided for interpolation purposes.

APPENDIX B

Contours of local peak pressure coefficients at normal and diagonal wind directions for all tested buildings

Appendix B1: buildings plan dimension (60 m), all heights and normal wind.

Appendix B2: buildings plan dimension (60 m), all heights and diagonal wind.

Appendix B3: buildings plan dimension (120 m), all heights and normal wind.

Appendix B4: building plan dimension (120 m), height (5 m) and diagonal wind.

Appendix B5: building plan dimension (120 m), height (7.5 m) and diagonal wind.

Appendix B6: building plan dimension (120 m), height (10 m) and diagonal wind.

Appendix B7: building plan dimension (180 m), height (5 m) and normal wind.

Appendix B8: building plan dimension (180 m), height (5 m) and diagonal wind.

Appendix B9: building plan dimension (180 m), height (7.5 m) and normal wind.

Appendix B10: building plan dimension (180 m), height (7.5 m) and diagonal wind.

Appendix B11: building plan dimension (180 m), height (10 m) and normal wind.

Appendix B12: building plan dimension (180 m), height (10 m) and diagonal wind.

Appendix B1 Peak pressure coefficients contours (normal wind).

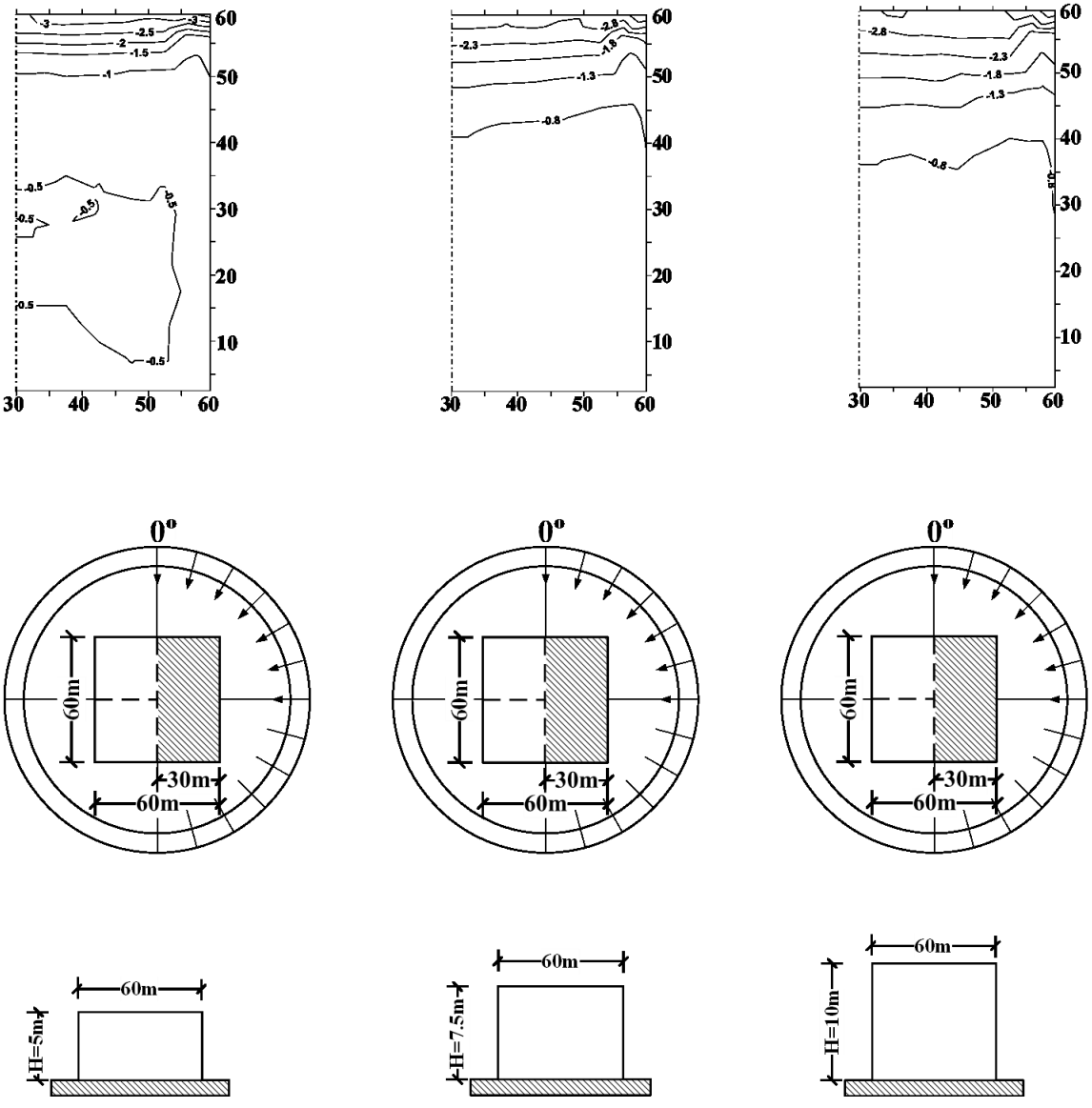

Appendix B2 Peak pressure coefficients contours (diagonal wind).

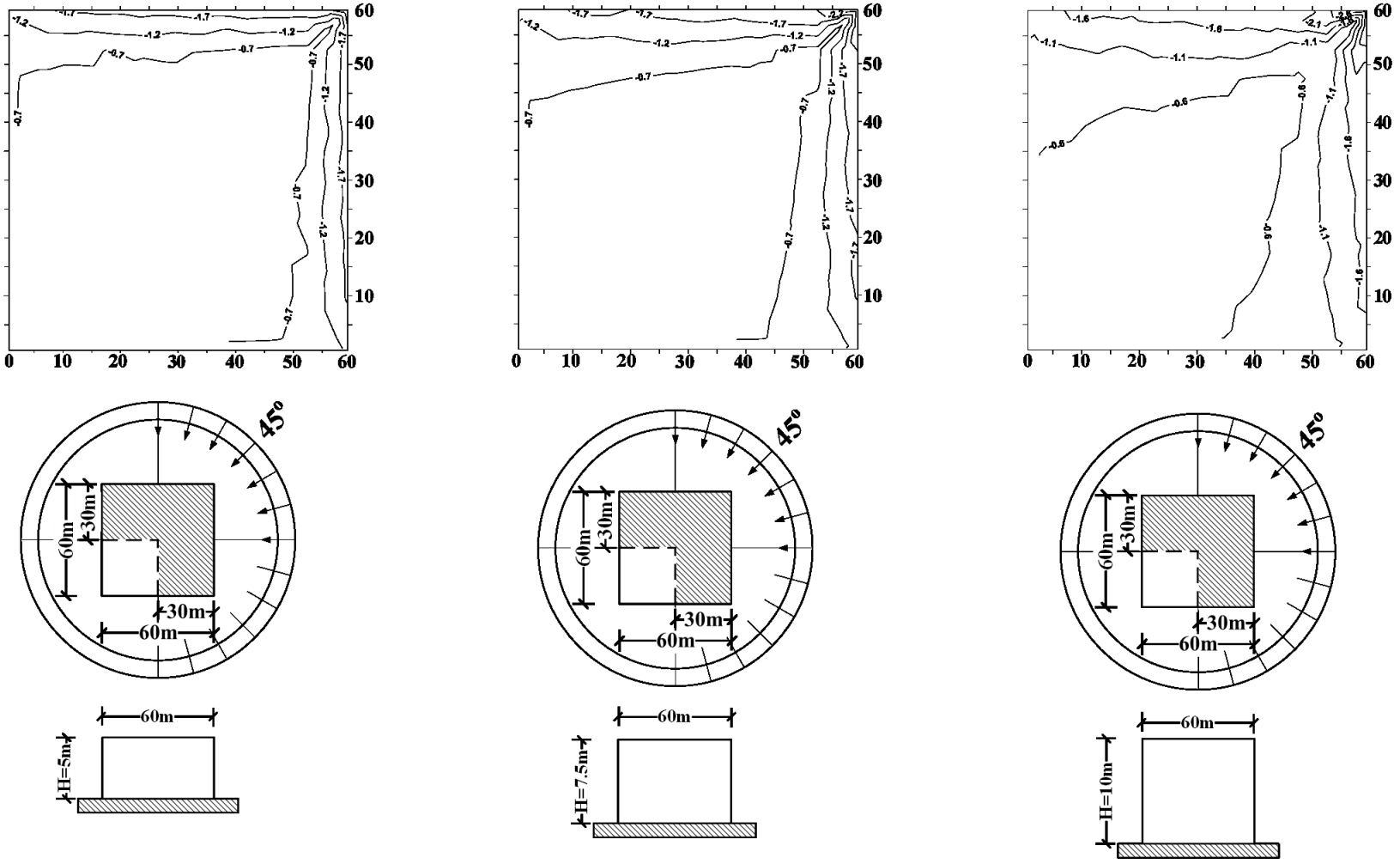

Appendix B3 Peak pressure coefficients contours (normal wind).

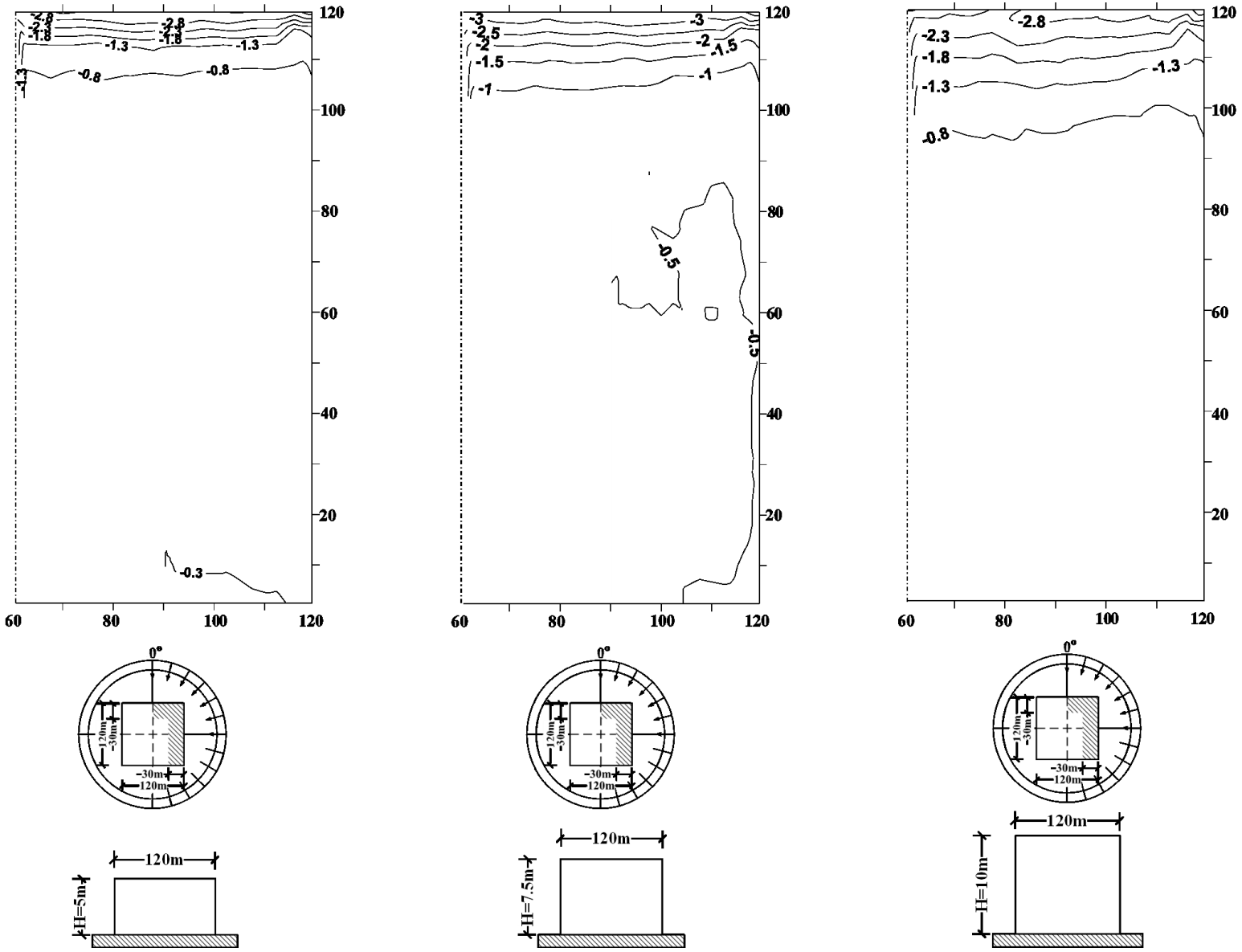

Appendix B4 Peak pressure coefficients contours (diagonal wind).

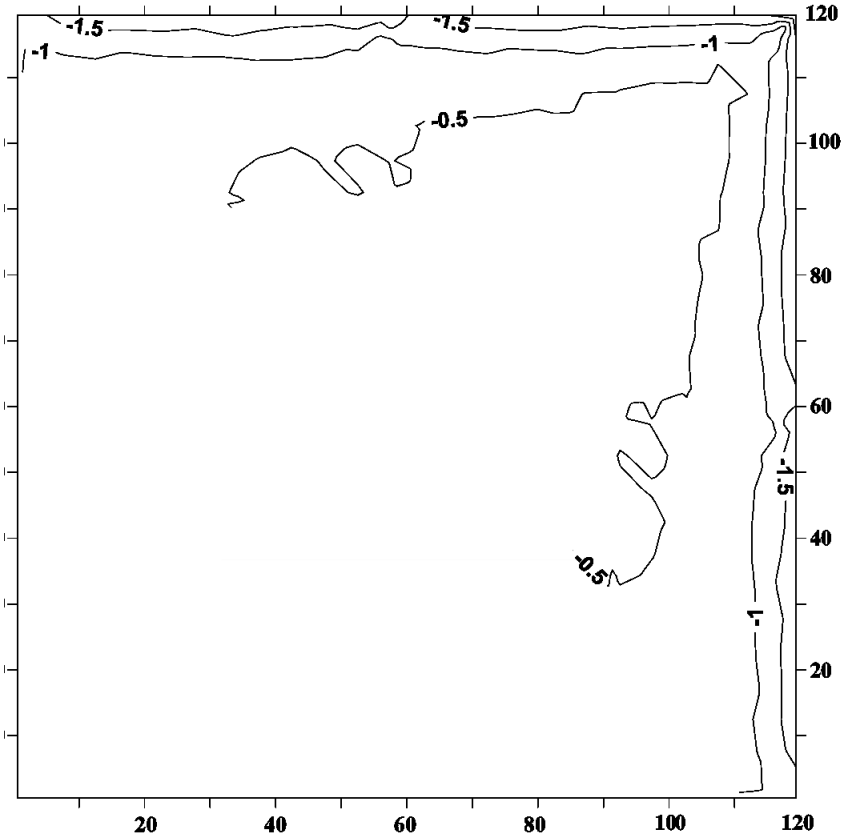

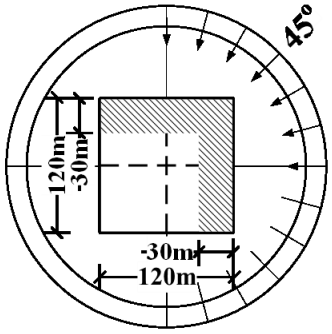

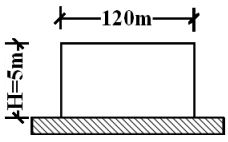

Appendix B5 Peak pressure coefficients contours (diagonal wind).

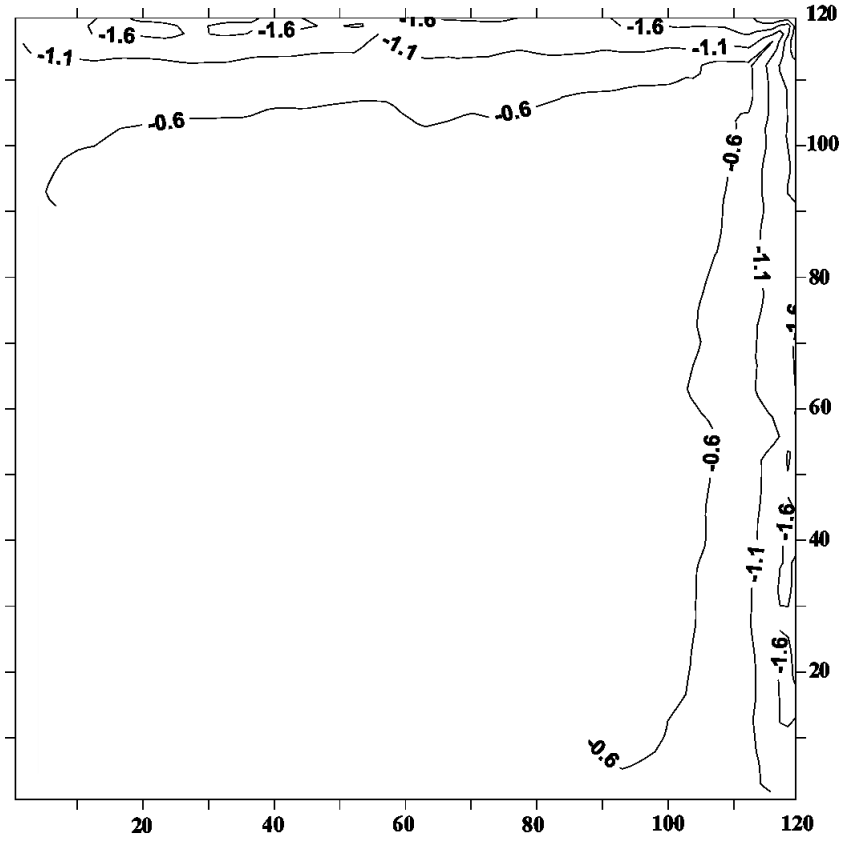

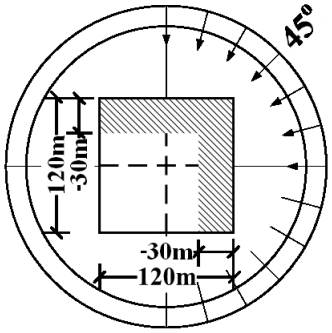

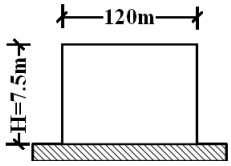

Appendix B6 Peak pressure coefficients contours (diagonal wind).

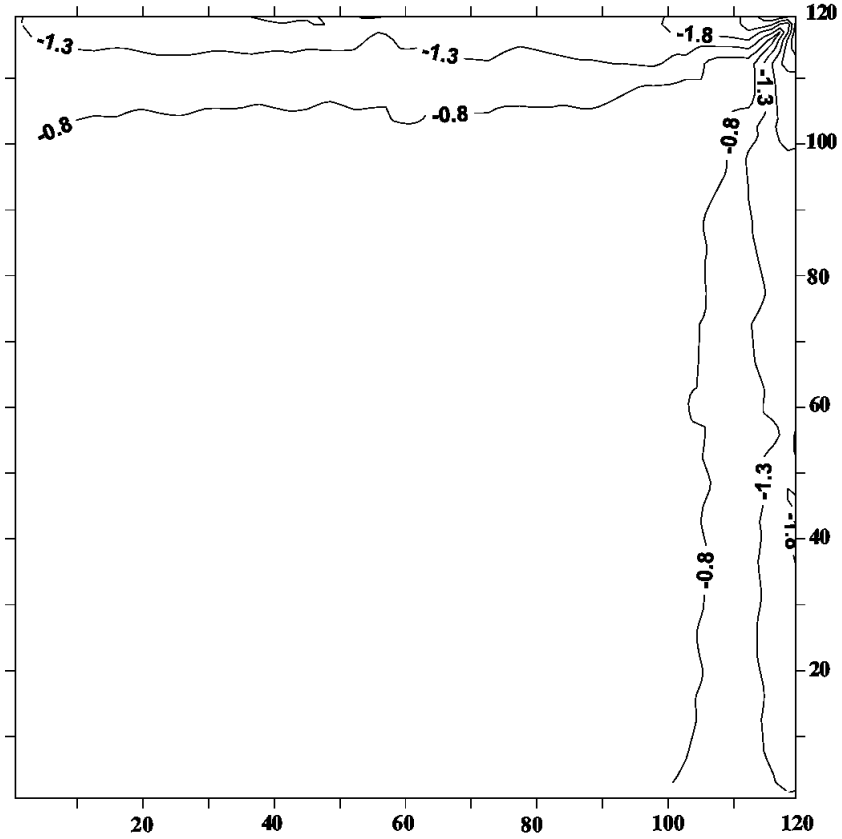

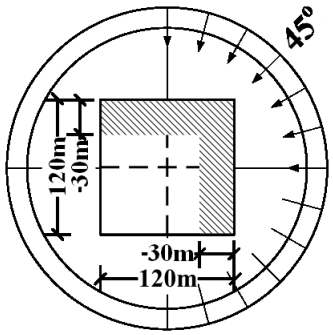

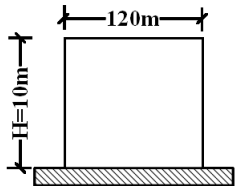

Appendix B7 Peak pressure coefficients contours (normal wind).

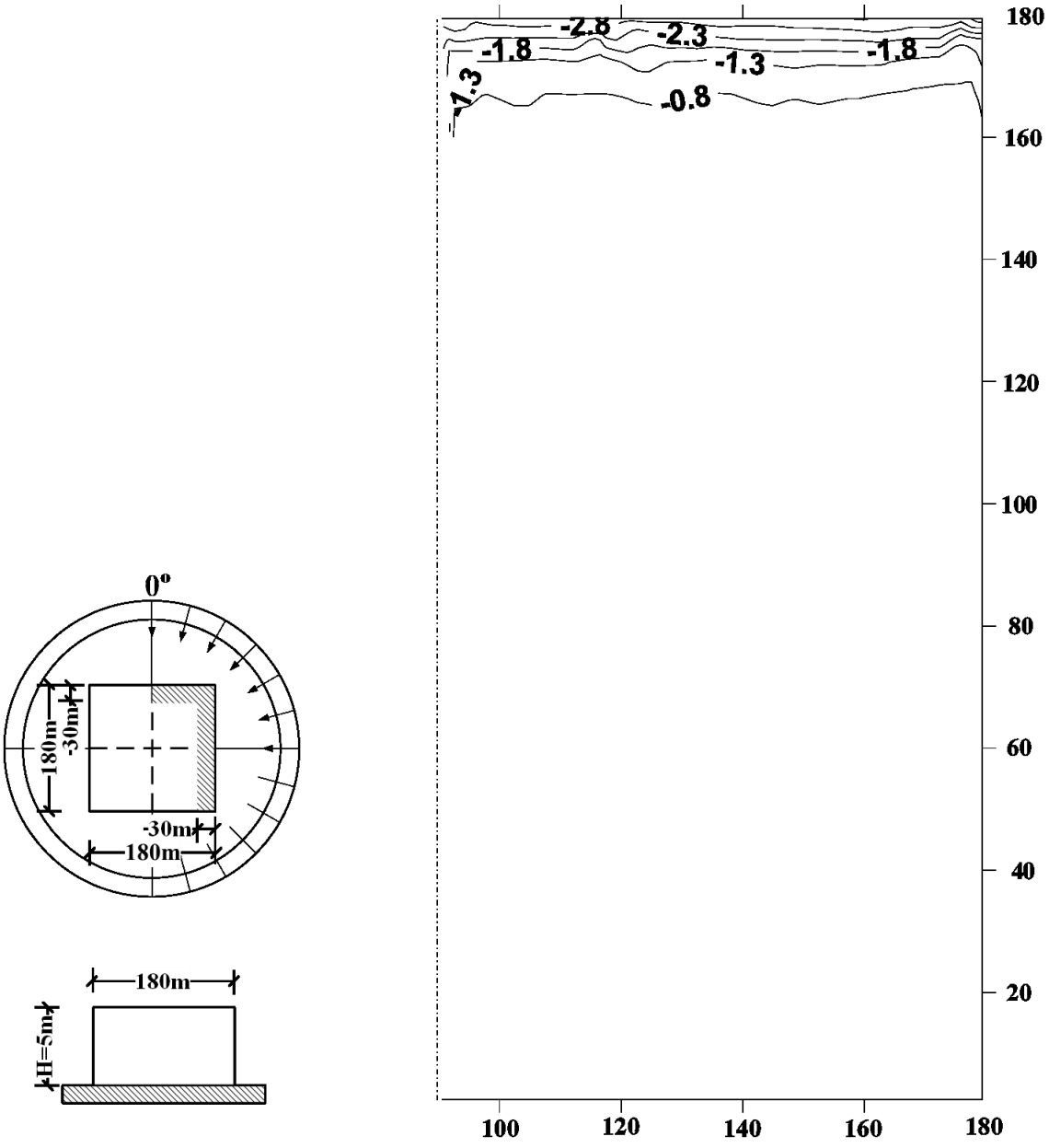

Appendix B8 Peak pressure coefficients contours (diagonal wind).

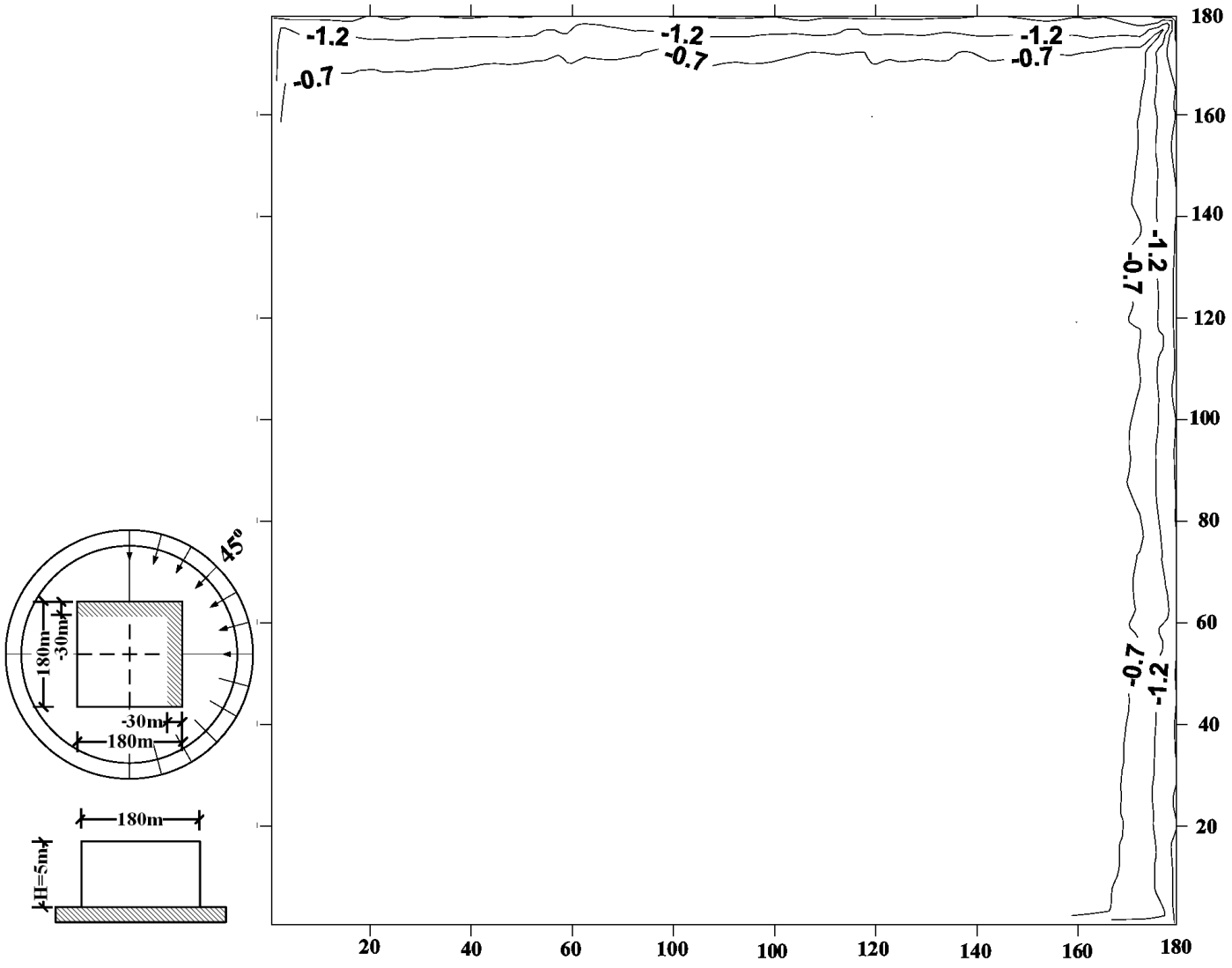

Appendix B9 Peak pressure coefficients contours (normal wind).

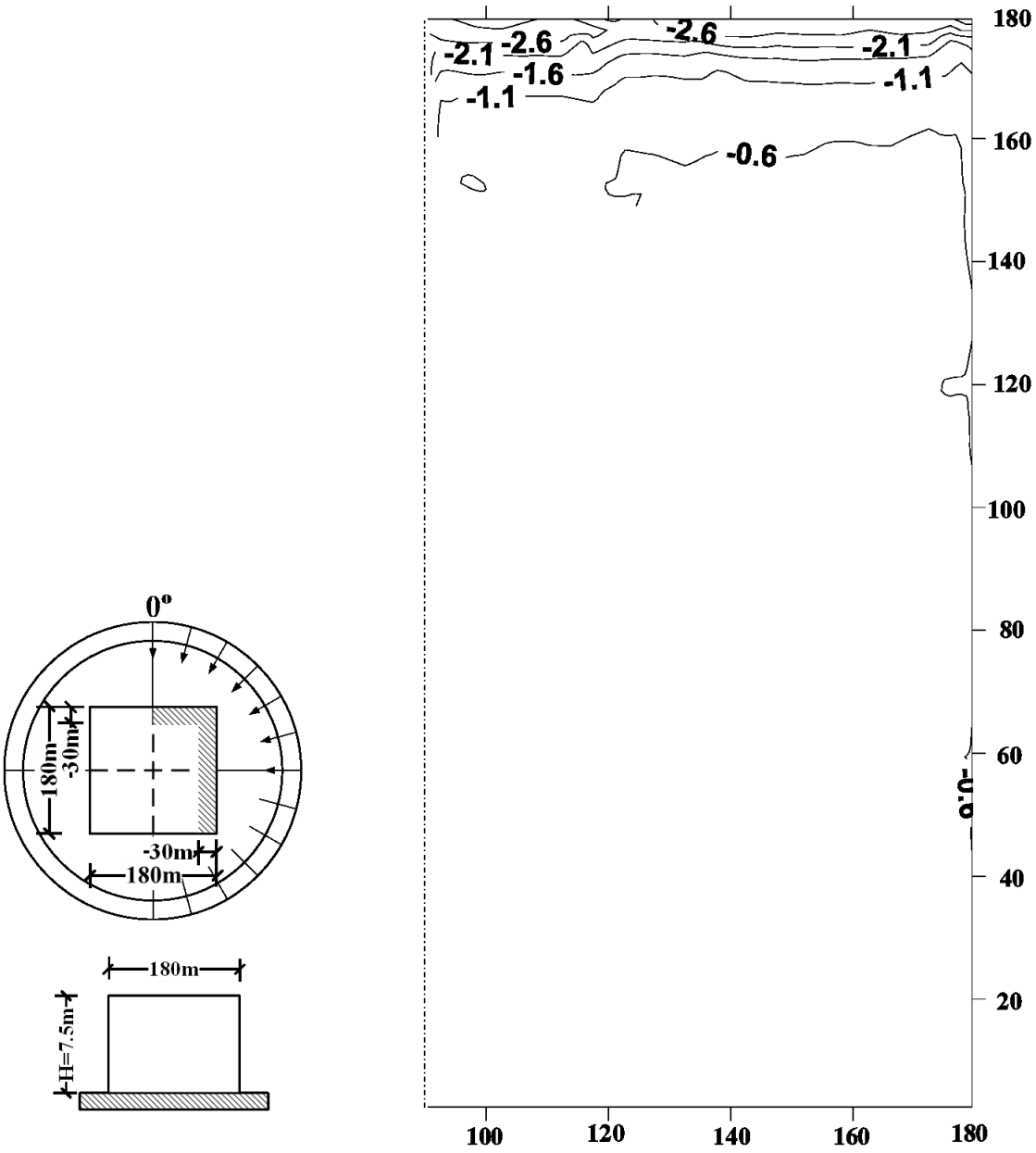

Appendix B10 Peak pressure coefficients contours (diagonal wind).

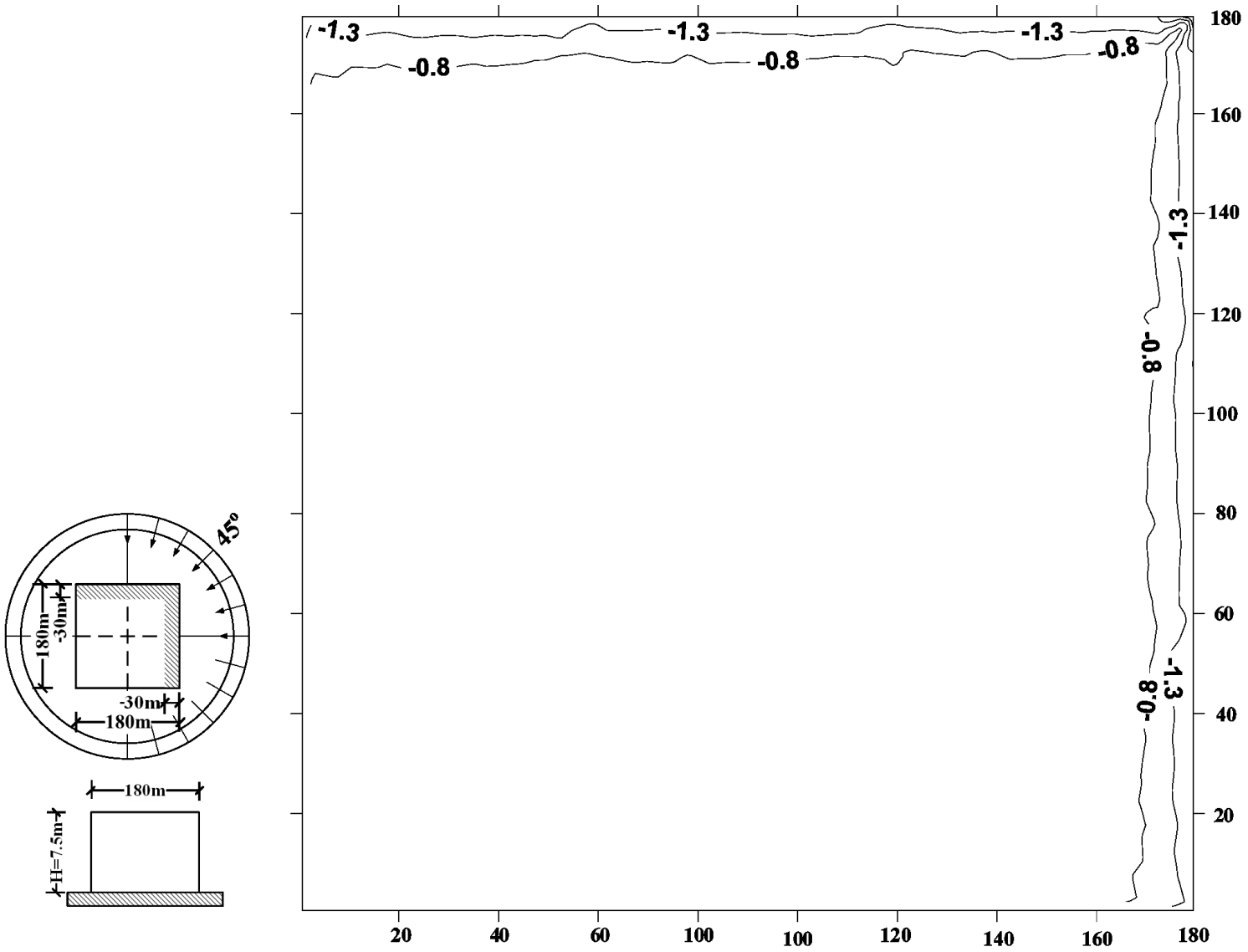

Appendix B11 Peak pressure coefficients contours (normal wind).

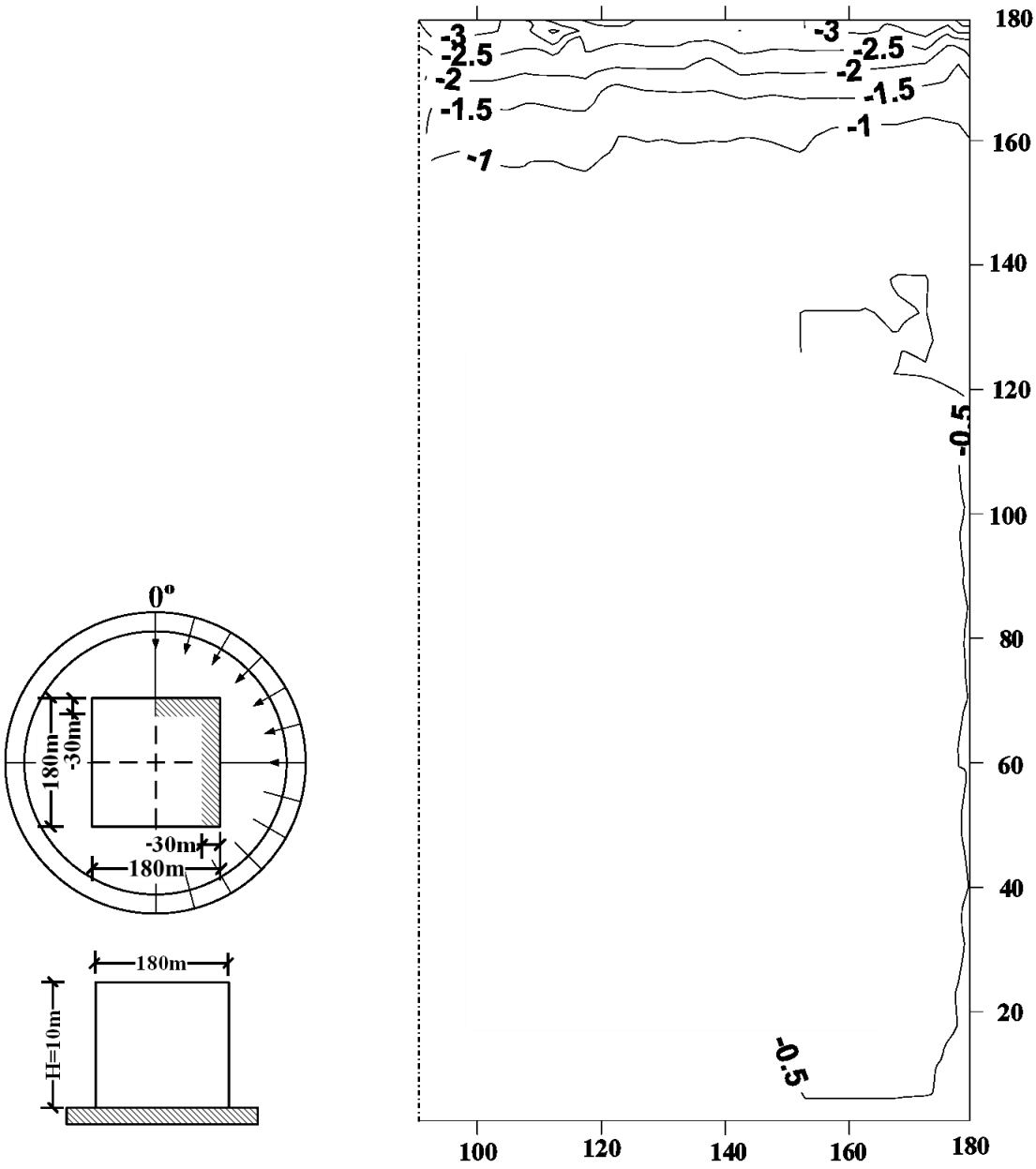

Appendix B12 Peak pressure coefficients contours (oblique wind).

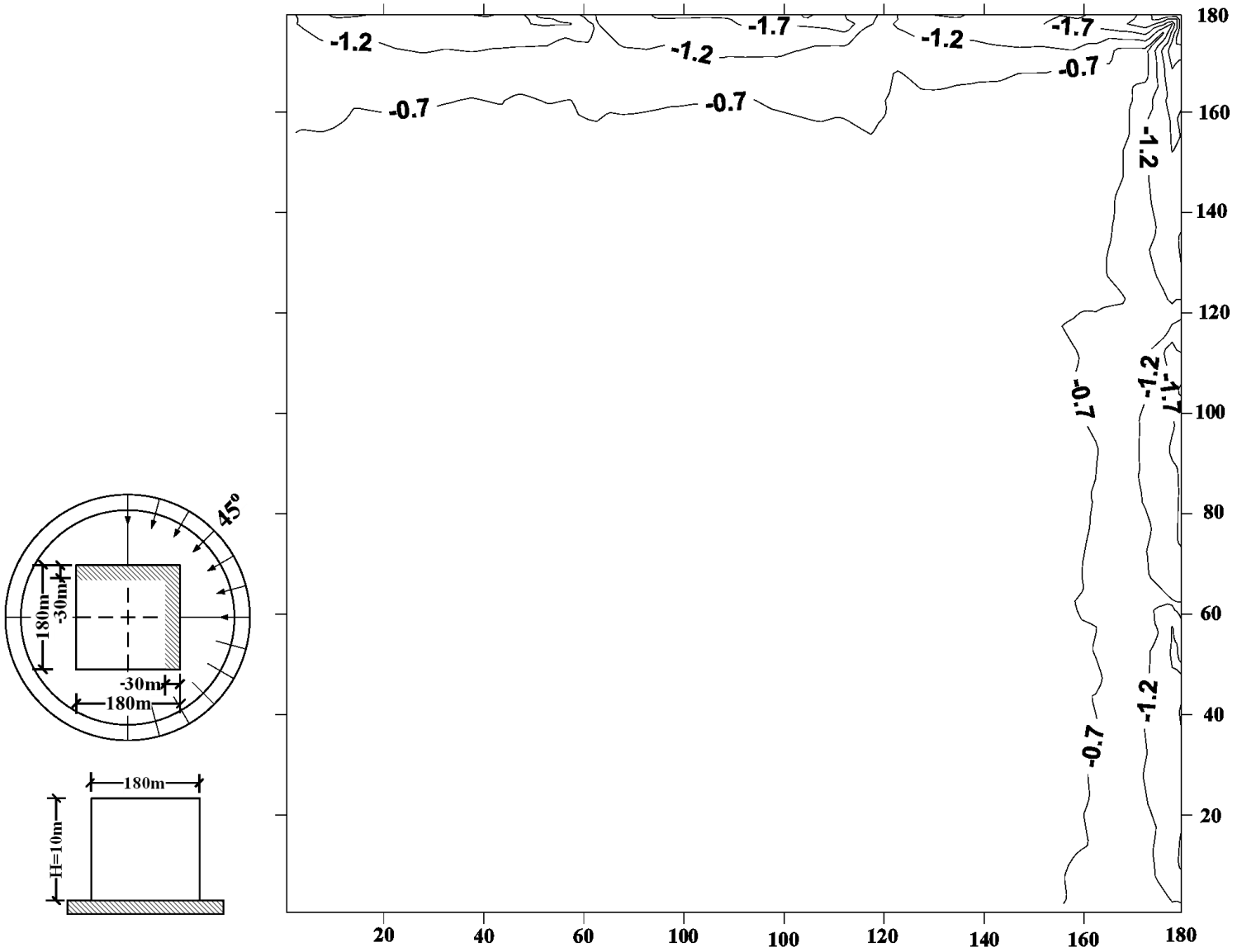

APPENDIX C

Area-averaged peak pressure coefficients for roof corner zones with tributary area for 0^o, 15^o, 30^o and 45^o wind directions

Appendix C1: buildings plan dimension (60 m) and all heights.

Appendix C2: buildings plan dimension (120 m) and all heights.

Appendix C3: buildings plan dimension (180 m) and all heights.

Appendix C1 Area- averaged pressure coefficients for buildings of plan dimension B = 60 m.

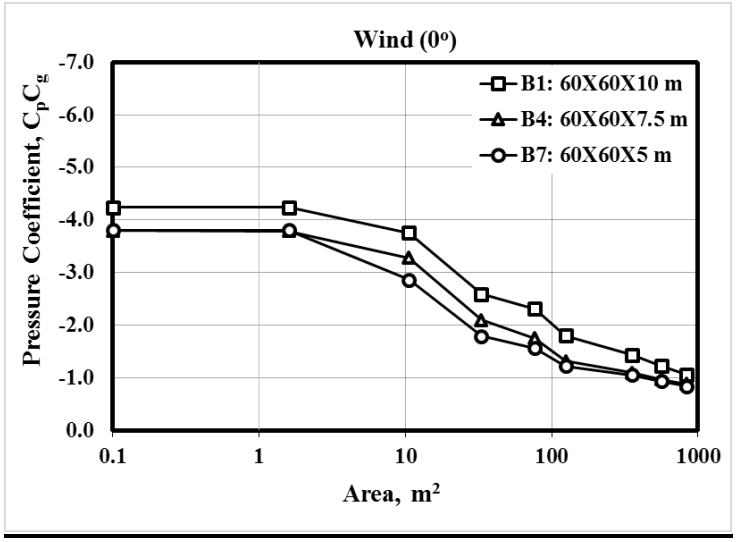

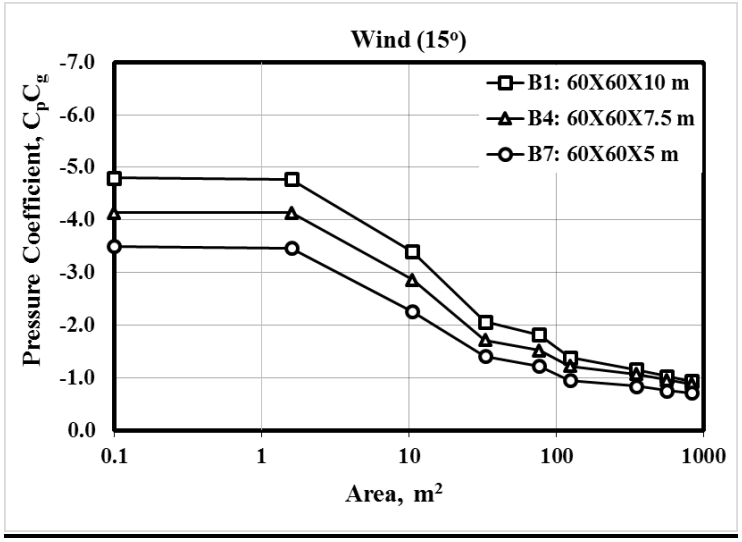

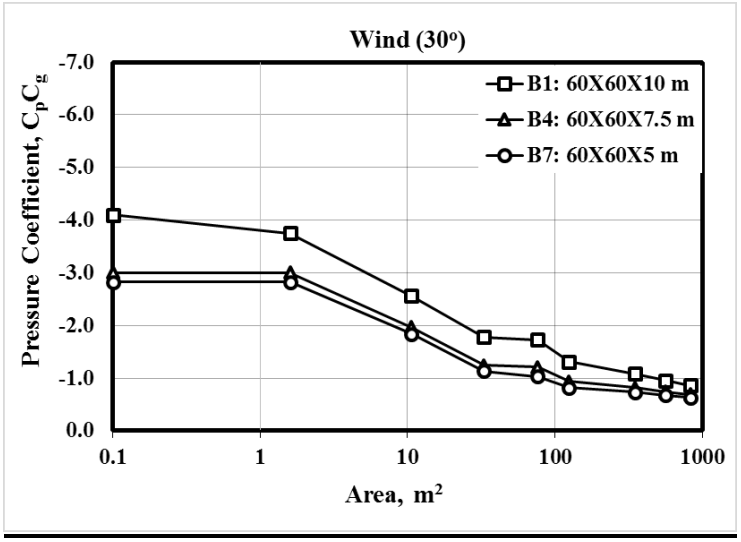

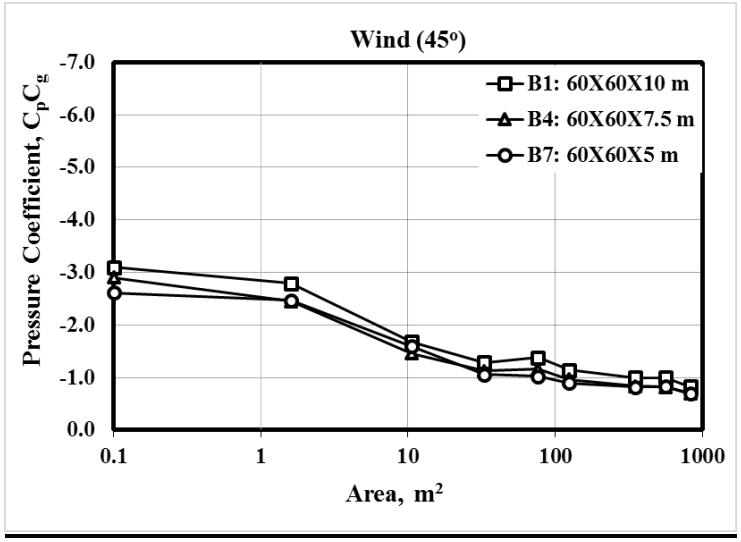

Appendix C2 Area- averaged pressure coefficients for buildings of plan dimension B = 120 m.

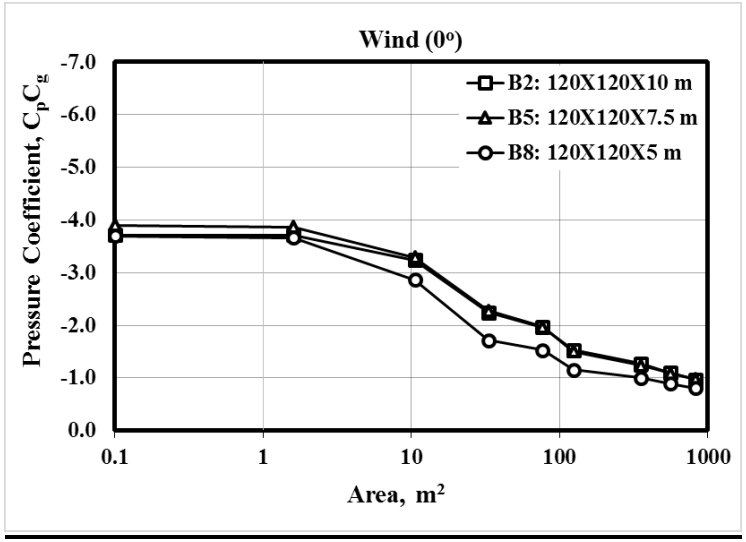

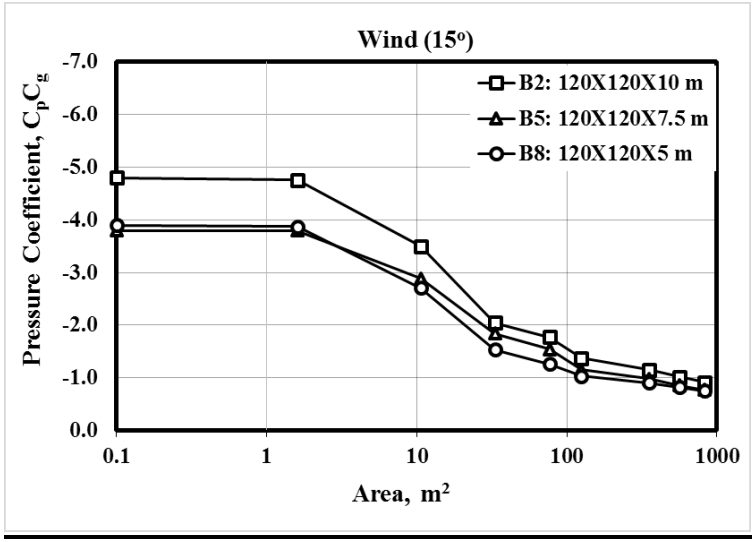

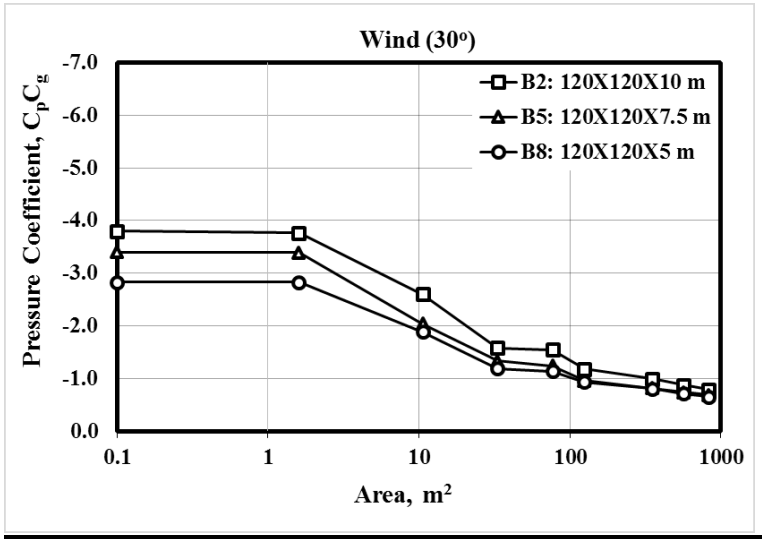

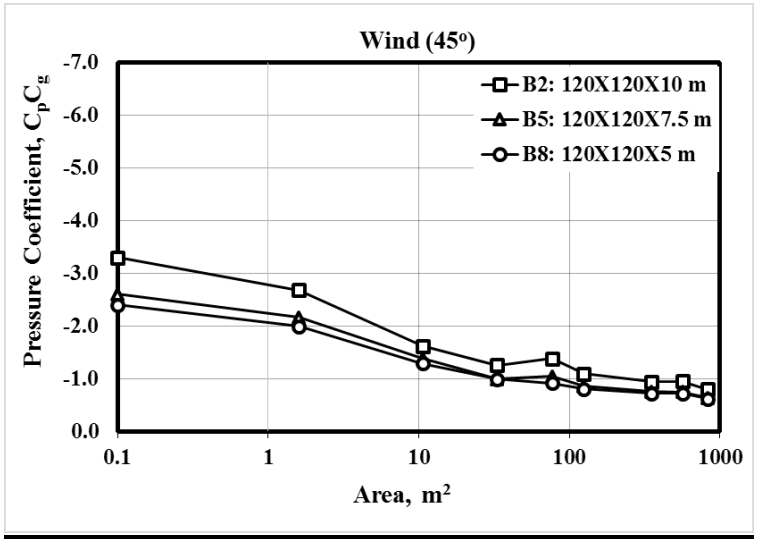

Appendix C3 Area- averaged pressure coefficients for buildings of plan dimension B = 180 m